UNIVERSIDAD DE BARCELONA

FACULTAD DE FARMACIA

DEPARTAMENTO DE BIOQUÍMICA Y BIOLOGÍA MOLECULAR

ESTUDIO DE LOS MECANISMOS DE INHIBICIÓN DE LA ACTIVIDAD CARNITINA PALMITOILTRANSFERASA 1

ASSIA BENTEBIBEL

Barcelona, 2009

PUBLICACIONES

THE JOURNAL OF BIOLOGICAL CHEMISTRY
Vol. 278, No. 11, Issue of March 14, pp. 9058–9063, 2003
© 2003 by The American Society for Biochemistry and Molecular Biology, Inc.
Printed in U.S.A.

Identification of Conserved Amino Acid Residues in Rat Liver Carnitine Palmitoyltransferase I Critical for Malonyl-CoA Inhibition

MUTATION OF METHIONINE 593 ABOLISHES MALONYL-CoA INHIBITION*

Received for publication, September 30, 2002, and in revised form, December 17, 2002
Published, JBC Papers in Press, December 23, 2002, DOI 10.1074/jbc.M209999200

Montserrat Morillas‡§, Paulino Gómez-Puertas§¶, Assia Bentebibel‡‖, Eva Sellés‡, Nuria Casals, Alfonso Valencia¶, Fausto G. Hegardt‡ ‡‡, Guillermina Asins‡, and Dolors Serra‡**

*From the ‡Department of Biochemistry and Molecular Biology, University of Barcelona, School of Pharmacy, E-08028 Barcelona, Spain, the ¶Protein Design Group, National Center for Biotechnology, Consejo Superior de Investigaciones Científicas, Cantoblanco, E-28049 Madrid, Spain, and the **Department of Biochemistry and Molecular Biology, International University of Catalonia, 08190 Sant Cugat, Spain*

Carnitine palmitoyltransferase (CPT) I, which catalyzes the conversion of palmitoyl-CoA to palmitoylcarnitine facilitating its transport through the mitochondrial membranes, is inhibited by malonyl-CoA. By using the SequenceSpace algorithm program to identify amino acids that participate in malonyl-CoA inhibition in all carnitine acyltransferases, we found 5 conserved amino acids (Thr^{314}, Asn^{464}, Ala^{478}, Met^{593}, and Cys^{608}, rat liver CPT I coordinates) common to inhibitable malonyl-CoA acyltransferases (carnitine octanoyltransferase and CPT I), and absent in noninhibitable malonyl-CoA acyltransferases (CPT II, carnitine acetyltransferase (CAT) and choline acetyltransferase (ChAT)). To determine the role of these amino acid residues in malonyl-CoA inhibition, we prepared the quintuple mutant CPT I T314S/N464D/A478G/M593S/C608A as well as five single mutants CPT I T314S, N464D, A478G, M593S, and C608A. In each case the CPT I amino acid selected was mutated to that present in the same homologous position in CPT II, CAT, and ChAT. Because mutant M593S nearly abolished the sensitivity to malonyl-CoA, two other Met^{593} mutants were prepared: M593A and M593E. The catalytic efficiency (V_{max}/K_m) of CPT I in mutants A478G and C608A and all Met^{593} mutants toward carnitine as substrate was clearly increased. In those CPT I proteins in which Met^{593} had been mutated, the malonyl-CoA sensitivity was nearly abolished. Mutations in Ala^{478}, Cys^{608}, and Thr^{314} to their homologous amino acid residues in CPT II, CAT, and ChAT caused various decreases in malonyl-CoA sensitivity. Ala^{478} is located in the structural model of CPT I near the catalytic site and participates in the binding of malonyl-CoA in the low affinity site (Morillas, M., Gómez-Puertas, P., Rubí, B., Clotet, J., Ariño, J., Valencia, A., Hegardt, F. G., Serra, D., and Asins, G. (2002) *J. Biol. Chem.* 277, 11473–11480). Met^{593} may participate in the interaction of malonyl-CoA in the second affinity site, whose location has not been reported.

The enzyme carnitine palmitoyltransferase (CPT)[1] I catalyzes the conversion of long chain fatty acyl-CoAs to acylcarnitines, which is the first step in the transport of fatty acyl-CoA groups from the cytosol to mitochondria where they undergo β-oxidation. This reaction is inhibited by malonyl-CoA, and so this enzyme could be the most physiologically important regulatory step in mitochondrial fatty acid oxidation (1). This process allows the cell to signal the relative availability of lipid and carbohydrate fuels in liver, heart, skeletal muscle, and pancreatic β-cell (2). The mechanism of malonyl-CoA inhibition can be potentially mimicked by pharmacological malonyl-CoA-related agents for the treatment of metabolic disorders such as diabetes, insulin resistance, and coronary heart disease (3).

Mammals express two isoforms of CPT I, a liver isoform (L-CPT I) and a heart/skeletal muscle isoform (M-CPT I), which are the products of two different genes (4, 5). The identity in amino acids residues is high (62%) but they are differentially regulated by malonyl-CoA. The L-CPT I isoform is inhibited by malonyl-CoA to a much lesser extent than the M-CPT I isoform (the IC_{50} value for M-CPT I is about 2 orders of magnitude lower than for L-CPT I) (6). This property is probably involved in the finer regulation of fatty acid oxidation in heart and skeletal muscle in comparison to liver.

From studies on the pH dependence of the affinity of CPT I for its substrate and from the ability of palmitoyl-CoA to displace [^{14}C]malonyl-CoA bound to skeletal muscle mitochondria it was hypothesized (7) that the palmitoyl-CoA and malonyl-CoA bind at different sites. A number of studies have shown that in rat liver CPT I there are two malonyl-CoA binding sites: one with greater capacity for binding and regulation of the inhibitor and not susceptible to competition from acyl-CoA, which behaves as an allosteric component (8–12); and a second acyl-CoA binding site, which is located near the catalytic site (13).

Various groups have attempted to establish the basis of the L-CPT I/malonyl-CoA interactions. The probable binding sites of malonyl-CoA in L-CPT I were deduced to be at the C terminus after preparation of several L-CPT I chimeras whose IC_{50} values for malonyl-CoA corresponded to the C-terminal region (14) of the chimera. However, the N terminus of L-CPT I was also shown to influence the enzyme/inhibitor interaction. Mutation of Glu^3, His^5, or His^{140} produced a loss of malonyl-CoA

* This work was supported in part by Dirección General de Investigación Científica y Técnica, Spain, Grant BMC2001-3048 and Ajuts de Suport als Grups de Recerca de Catalunya Grant 2001SGR-00129 (to F. G. H.) and the Marató de TV3. The costs of publication of this article were defrayed in part by the payment of page charges. This article must therefore be hereby marked "*advertisement*" in accordance with 18 U.S.C. Section 1734 solely to indicate this fact.

§ Contributed equally to the results of this study.

‖ Recipient of a fellowship from the Ministerio de Ciencia y Tecnología, Spain.

‡‡ To whom correspondence should be addressed: Dept. of Biochemistry and Molecular Biology, School of Pharmacy, Diagonal 643, E-08028 Barcelona, Spain. Tel.: 34-93-402-4523; Fax: 34-93-402-4520; E-mail: hegardt@farmacia.far.ub.es.

[1] The abbreviations used are: CPT, carnitine palmitoyltransferase; L-CPT I, liver isoform of carnitine palmitoyltransferase I; M-CPT I, muscle isoform of carnitine palmitoyltransferase I; CAT, carnitine acetyltransferase; COT, carnitine octanoyltransferase; ChAT, choline acetyltransferase.

This paper is available on line at http://www.jbc.org

sensitivity (15, 16). In addition, the removal of the segment comprised between amino acids 1 and 18 in L-CPT I and 1–28 in M-CPT I produced a decrease in malonyl-CoA sensitivity, which emphasizes the importance of the N terminus before the first transmembrane region as a modulator of the malonyl-CoA inhibition (17, 18). On the basis of these results, it was proposed that the two malonyl-CoA inhibitable domains might be located at the C terminus as suggested by several kinetic studies. The development of a CPT I catalytic core model (19) allowed us to assign the low affinity binding site to a domain near the catalytic channel in which palmitoyl-CoA is bound containing the catalytic acyl-CoA binding domain (20)

Here we used the SequenceSpace algorithm program to identify five amino acid residues (Thr^{314}, Asn^{464}, Ala^{478}, Met^{593}, and Cys^{608}), which may contribute to the sensitivity of CPT I to malonyl-CoA. The proposal is based on the finding that they are present in malonyl-CoA-inhibitable CPT I ((isoforms L- and M-) and COT from various organisms and absent in noninhibitable acyltransferases (CPT II, CAT, and ChAT). Mutation of these amino acids to their counterparts in CPT II showed that mutation of Met^{593} by itself, M593S, or the quintuple mutant containing the M593S mutation, T314S/N464D/A478G/M593S/C608A, or other Met^{593} point mutants such as M593A and M593E nearly abolished malonyl-CoA sensitivity of L-CPT I. The remaining mutated amino acids showed slight, varied sensitivity to malonyl-CoA inhibition.

EXPERIMENTAL PROCEDURES

Tree-determinants Analysis—Sequences of proteins from the carnitine-choline acyltransferase family were obtained using BLAST (21). Multiple alignment was performed using ClustalW (22). The analysis of conserved differences (tree-determinants) between malonyl-CoA-regulated (L-CPT I, M-CPT I, and COT) and nonregulated (CPT II, CAT, and ChAT) acyltransferases, using multivariate statistics for low-dimensional representation, was done using the SequenceSpace algorithm (23, 24). Graphics of vectors representing protein sequences and individual residues from the multiple alignment were performed using the Sequence Space Java-based viewer (www.industry.ebi.ac.uk/SeqSpace).

Construction of Site-directed Mutants—Plasmids $pYESLCPTI^{wt}$ and $pYESLCPT^{A478G}$ were obtained as previously described (20). Plasmids $pYESLCPT^{T314S}$, $pYESLCPT^{N464D}$, $pYESLCPT^{M593S}$, $pYESLCPT^{M593A}$, $pYESLCPT^{M593E}$, and $pYESLCPT^{C608A}$ were constructed using the QuikChange polymerase chain reaction-based mutagenesis procedure (Stratagene) with the $pYESLCPT^{wt}$ plasmid as template. The following primers were used: primer T314S.for 5′-GGGAGCGACTCTTCAATAG-TTCCCGGATCCCTGGG-3′, primer T314A.rev 5′-CCCAGGGATCCG-GGAA*C*TATTGAAGAGTCGCTCCC-3′, primer N464D.for 5′-CACCTT-TGTTGTCTTCAAAGACAGCAAGATAGGC-3′, primer N464D.rev 5′-GCCTATCTTGCTGTCTTTGAAGACACCAAAGGTG-3′, primer M593S.for 5′-CCTCACATATGAGGCCTCCAGTACCCGGCTCTTCCG AGAAGG-3′, primer M593S.rev 5′-CCTTCTCGGAAGAGCCGGGTAC-TGGAGGCCTCATATGTGAGG-3′, primer M593A.for 5′-CCTCAC-ATATGAGGCCTCCGCGACCCGGCTCTTCCGAGAAGG-3′, primer M593A.rev 5′-CCTTCTCGGAAGAGCCGGGTCGCGGAGGCCTCATA TGTGAGG-3′, primer M593E.for 5′-CCTCACATATGAGGCCTCCGA-GACCCGGCTCTTCCGAGAAGG-3′, primer M593E.rev 5′-CCTTCTC-GGAAGAGCCGGGTCTCGGAGGCCTCATATGTGAGG-3′, primer C608A.for 5′-GAGACTGTACGCTCCGCCACTATGGAGTCCTGC-3′, and C608A.rev 5′-GCAGGACTCCATAGTGGCGGAGCGTACAGTCT-C-3′ (the mutated nucleotides are underlined). The plasmid $pYESLCPTI^{T314S/N464D/A478G/M593S/C608A}$ was obtained by the same method, but performing each new mutation stepwise starting on plasmid $pYESLCPT^{T314S}$. The appropriate substitutions as well as the absence of unwanted mutations were confirmed by sequencing the inserts in both directions with an Applied Biosystems 373 automated DNA sequencer.

Expression of L-CPT I in Saccharomyces cerevisiae—The expression of the constructs containing L-CPT I wild type and mutants (see above) in yeast cells and the preparation of the cell extracts were performed as described in Ref. 19. *S. cerevisiae* was chosen as an expression system for L-CPT I wild type and the mutants because it does not have endogenous CPT I activity.

Determination of Carnitine Acyltransferase Activity—Carnitine palmitoyltransferase activity was determined by the radiometric method as described in Ref. 19 with minor modifications. The substrates were L-[*methyl*-^{3}H]carnitine and palmitoyl-CoA. Enzyme activity was assayed for 4 min at 30 °C in a total volume of 200 μl.

For determination of the K_m for carnitine, palmitoyl-CoA was fixed at 135 μM (for L-CPT I). For determination of the K_m for acyl-CoA, carnitine concentration was fixed at 400 μM. When malonyl-CoA inhibition was assayed, increasing concentrations of malonyl-CoA were included. The IC_{50}, defined as the malonyl-CoA concentration that produces 50% inhibition of enzyme activity, was determined using 50 μM palmitoyl-CoA and 400 μM carnitine. K_m was estimated by analyzing the data from three experiments using the program Enzifit (Biosoft), and IC_{50} was calculated by Excel software using linear regression analysis.

Values reported in the text are the means and standard deviations of three to five determinations. Curve fitting was carried out using Excel software. All protein concentrations were determined using the Bio-Rad protein assay with bovine albumin as standard.

Immunological Techniques—Western blot analysis was performed as described (19). The antibody for rat L-CPT I was kindly given by Dr. V. A. Zammit (Hannah Research Institute, Ayr, Scotland, United Kingdom) and was directed against peptide 428–441, in the cytosolic catalytic C-terminal domain.

RESULTS

Residues Conserved in Malonyl-CoA Inhibited Versus Noninhibited Carnitine-Choline Acyltransferases—An exhaustive analysis of the presence of residues shared by all the malonyl-CoA-regulated enzymes of the carnitine-choline acyltransferase family *versus* the malonyl-CoA nonregulated members of the same family was performed using the algorithm SequenceSpace (23, 24). This method uses a vectorial representation of each protein sequence as a point in a multidimensional space (SequenceSpace) and multivariate statistics, principal component analysis, to allow reduction of the number of dimensions. This representation allows us not only to define clusters of proteins according to specific properties by choosing the appropriate axes defined by the highest corresponding eigenvalues (also known as proper values), but also to project the individual residues on the same axes, and thus trace the positions conserved in the subfamilies defined. The main advantage of this method is the possibility of predicting which residues may be responsible for the specific characteristics of each protein subfamily or group of subfamilies as has been reported previously for short- and medium-long substrate specificity for the carnitine-choline acyltransferases protein family (19, 20) or effector recognition by some members of the Ras superfamily (25).

The two-dimensional projection of sequence vectors on the plane defined by the axes corresponding to eigenvalues 2 and 4 showed clustering of the enzyme subfamilies according to their malonyl-CoA inhibition properties (Fig. 1*A*). Proteins whose activity is not regulated by malonyl-CoA (CPT II, CAT, and ChAT subfamilies) were grouped, whereas the sequences of the proteins regulated by malonyl-CoA (COT, L-CPT I, and M-CPT I) occupy separate, and opposite, zones. The projection of the individual amino acid residues on the same plane (Fig. 1*B*) revealed the amino acids responsible for this segregation might be responsible for the susceptibility to malonyl-CoA of the corresponding enzymes. Five of these amino acids (Thr^{314}, Asn^{464}, Ala^{478}, Met^{593}, and Cys^{608}) were present in all malonyl-CoA inhibitable carnitine acyltransferases and absent in the nonmalonyl-CoA inhibitable acyltransferases (CPT II, CAT, and ChAT from several species). Fig. 2 shows the sequence alignment of three fragments of the C-terminal region of various acyltransferases. We can also observe that those enzymes that are not inhibitable by malonyl-CoA (CPT II, CAT, and ChAT) show the same amino acids in these positions, which are different from those observed in inhibitable malonyl-CoA acylcarnitines. As an example the positions and amino acids of CPT II are given: Ser^{223}, Asp^{363}, Gly^{377}, Ser^{490}, and Ala^{505} (Fig. 2).

Expression of Wild Type and Mutants in S. cerevisiae—We

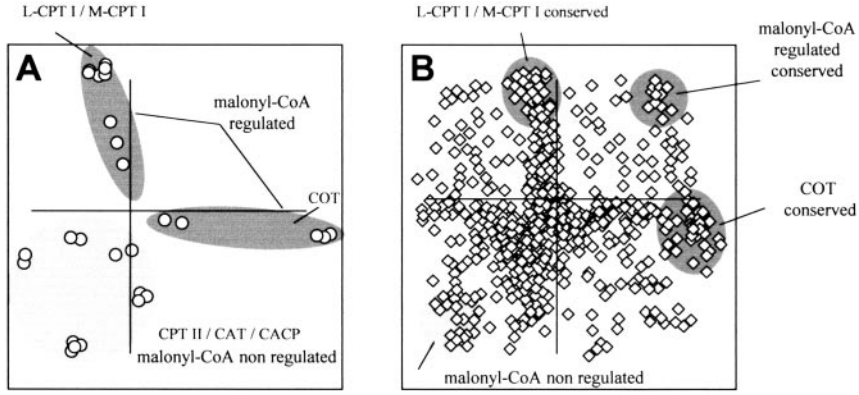

FIG. 1. **Sequence space analysis of the carnitine-choline acyltransferase family.** *A*, protein sequences projected onto the plane defined by principle axes 2 and 4. This two-dimensional space allows separation of protein subfamilies according to their malonyl-CoA regulatory characteristics; CPT II, CAT, and ChAT (*CACP*) enzymes (malonyl-CoA insensitive) are clustered to the *lower left corner* of the panel, whereas CPT I (L- and M-isoforms) and COT (malonyl-CoA inhibitable enzymes) are projected on the *upper* and *right* areas of the vertical and horizontal axes, respectively. *B*, the sequence of each subfamily is represented as a vector point in a multidimensional space (sequence space), with residue positions and types as the basic dimensions. Single residues completely conserved in CPT I or COT subfamilies are projected in the same position as their corresponding protein sequences. Residues conserved in both groups of malonyl-CoA-regulated enzymes occupy the *upper right corner*, whereas the residues conserved in the nonregulated cluster of acyltransferases (CPT II, CAT, and ChAT) occupy the *opposite* one. Residues located in alignment positions present in both opposite corners of the two-dimensional plot are responsible for protein cluster segregation and are predicted to be involved in malonyl-CoA sensitivity.

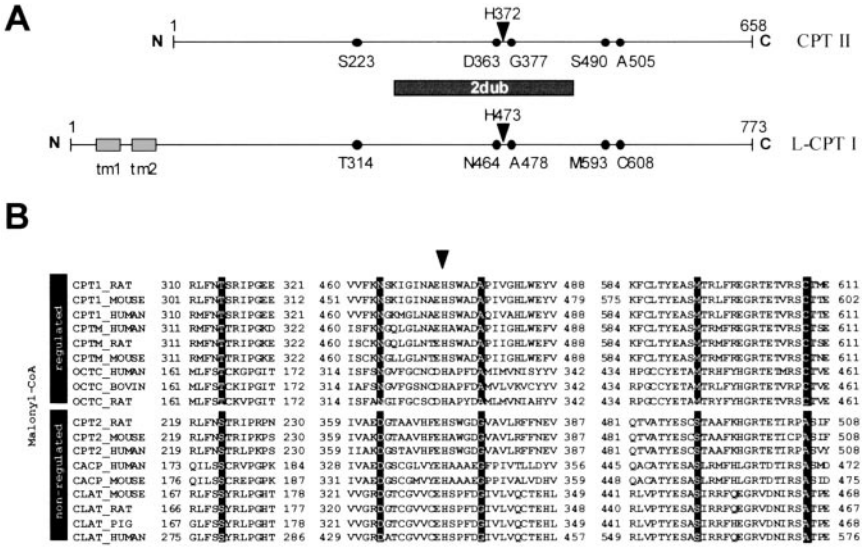

FIG. 2. **Alignment of representative sequences of mammalian carnitine-choline acyltransferases.** Amino acid sequence of 18 representative members of the malonyl-CoA-insensitive enzymes, CPT II (CPT2) from rat, mouse, and human; CAT (*CACP*) from human and mouse; ChAT (*CLAT*) from human, pig, rat, and mouse; and malonyl-CoA inhibitable enzymes L-CPT I (CPT1) from rat, mouse, and human; M-CPT I (CPTM) from human, rat, and mouse; and COT (*OCTC*) from human, rat, and bovine, were obtained from the SwissProt data bank and aligned using ClustalW (22). *A*, schematic representation of the position of the tree-determinant residues obtained using the SequenceSpace algorithm (23, 24) on the rat CPT II and L-CPTI proteins: Ser^{223}/Thr^{314}, Asp^{363}/Asn^{464}, Gly^{377}/Ala^{478}, Ser^{490}/Met^{593}, Ala^{505}/Cys^{608}. Transmembrane regions of L-CPT I are also represented (*tm1* and *tm2*). Position of the catalytic histidine (His^{372}/His^{473}) as well as the previously three-dimensional modeled core of the proteins, 2dub, (amino acids 368–567 of L-CPT I) (19, 20), are indicated. *B*, selected regions of the multiple alignment of the protein family. Subfamily conserved residues according to malonyl-CoA regulation are *shadowed*. Position of catalytic histidine (*arrowhead*) is also indicated.

prepared a quintuple mutant, T314S/N464D/A478G/M593S/C608A, and separately, the point mutants T314S, N464D, A478G, M593S, and C608A and all were expressed in *S. cerevisiae*. After we observed that mutant M593S nearly abolished the sensitivity to malonyl-CoA (see below), new point Met mutants were prepared: M593A and M593E. All transformed yeast cells expressed a protein with the same molecular mass (88 kDa) and the mutant enzymes were expressed in roughly the same proportion per milligram of protein as the wild type L-CPT I as deduced from immunoblot analysis (data not shown).

Kinetic Properties of CPT I Wild Type and Mutants—L-CPT I activities of the wild type, quintuple mutant variant T314S/N464D/A478G/M593S/C608S, and point mutants were similar (values ranged between 14 and 20 nmol min^{-1} mg $protein^{-1}$) when the protein was overexpressed 20 h after galactose induction, showing that the various mutations assayed produce small changes in L-CPT I activity (Table I).

All mutants exhibited standard saturation kinetics when the carnitine concentration was varied relative to a constant concentration of the second substrate, palmitoyl-CoA, and when palmitoyl-CoA concentration was varied relative to a constant carnitine concentration, a property identical to that of the wild type L-CPT I (Fig. 3). The quintuple mutant produced small changes in the kinetic constants for carnitine and palmitoyl-CoA as substrates (Table I). Catalytic efficiency (V_{max}/K_m) was increased by a factor of 2.6 (carnitine) and 2.2 (palmitoyl-CoA). The catalytic efficiency for carnitine as substrate of those point

TABLE I

Enzyme activity, malonyl-CoA sensitivity and kinetic parameters of carnitine palmitoyltransferase I in Saccharomyces cerevisiac cells expressing CPI I wild type and point mutants, T314S, N464D, A478G, C608A, M593S, M593A, M593E and quintuple mutant T314S/N464D/A478G/M593S/C608A (QM)

Extracts from yeast expressing wild type and several mutants of L-CPT I were assayed for activity, malonyl-CoA sensitivity, and kinetics as described under "Experimental Procedures." The results are the mean ± S.D. of at least three independent experiments with different preparations. In parentheses are shown the increase (in-fold number) of the catalytic efficiency (V_{max}/K_m) versus to that of the wild type.

L-CPT I	Activity	IC_{50} malonyl-CoA	K_m		V_{max}		Catalytic efficiency	
			Carnitine	Palmitoyl-CoA	Carnitine	Palmitoyl-CoA	Carnitine	Palmitoyl-CoA
	nmol min^{-1} mg protein^{-1}		*μm*		*nmol min^{-1} mg protein^{-1}*		V_{max}/K_m	
Wild-type	17.7 ± 0.9	12.3	127 ± 4.5	4.9 ± 0.3	6.6 ± 0.8	6.3 ± 0.4	0.05 (× 1)	1.28 (× 1)
T314S	14.4 ± 2.1	15.0	88.2 ± 2.4	1.7 ± 0.5	12.8 ± 0.1	6.8 ± 0.1	0.15 (× 2.8)	3.98 (× 3.1)
N464D	20.1 ± 3.1	8.7	69.5 ± 8.2	4.1 ± 0.4	19.4 ± 1.4	18.9 ± 3.6	0.28 (× 5.6)	4.63 (× 3.6)
A478G	16.7 ± 0.7	39.5	327 ± 41	15.1 ± 4.0	69.8 ± 9.3	50.4 ± 17	0.21 (× 4.1)	3.34 (× 2.6)
C608A	17.3 ± 1.7	27.5	51.6 ± 4.0	24.3 ± 2.0	23.7 ± 5.0	67.5 ± 9.0	0.46 (× 8.8)	2.78 (× 2.2)
M593S	17.0 ± 0.8	319	124 ± 0.8	7.4 ± 1.2	133 ± 18	20.9 ± 1.6	1.07 (× 21)	2.84 (× 2.2)
M593A	17.2 ± 0.9	155	56.3 ± 2.1	6.1 ± 0.2	32.5 ± 4.6	30.3 ± 4.7	0.58 (× 12)	4.81 (× 3.7)
M593E	14.1 ± 1.8	220	150 ± 3.4	6.3 ± 0.5	31.3 ± 2.6	27.5 ± 1.8	0.21 (× 4.2)	4.37 (× 3.4)
QM	13.6 ± 1.6	258	95.7 ± 2.8	4.6 ± 1.5	13.1 ± 4.7	13.0 ± 6.3	0.14 (× 2.6)	2.84 (× 2.2)

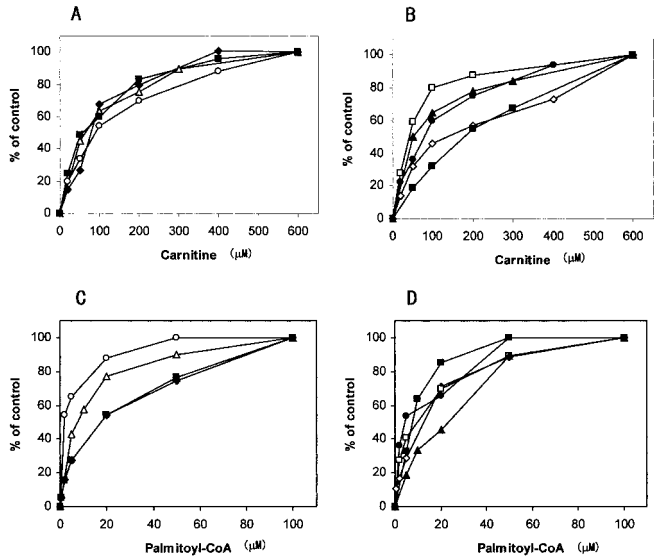

FIG. 3. **Kinetic analysis of wild type and different mutants of L-CPT I.** Yeast extracts (10 μg of protein) of (*A* and *C*) wild type (*open circles*) and mutants M593S (*open triangles*), M593A (*black rhombus*), M593E (*black squares*), and (*C* and *D*) T314S (*open rhombus*), N464D (*open squares*), A478G (*black squares*), C608A (*black triangles*), and quintuple mutant T314S/N464D/A478G/M593S/C608A (*black circles*) were incubated at increasing concentrations of carnitine (*A* and *B*) and palmitoyl-CoA (*C* and *D*).

mutants that altered the sensitivity to malonyl-CoA increased (see below). The catalytic efficiency of the methionine mutants increased between 4.2- and 21-fold, C608A increased 8.8-fold, and A478G increased 4.1-fold. T314S, which produced a small change in malonyl-CoA sensitivity (see below), increased the V_{max}/K_m value by only 2.8, whereas in N464D, in which the sensitivity to malonyl-CoA was unchanged (see below), the catalytic efficiency was modified by a factor of 5.6.

An analogous tendency was also observed in K_m for palmitoyl-CoA but the changes were smaller. K_m values for palmitoyl-CoA were 24.3, 15.1, 7.4, 6.1, and 6.3 for mutants C608A, A478G, M593S, M593A, and M593E, respectively (K_m value for the wild type was 4.9) (Table I). Catalytic efficiencies for palmitoyl-CoA as substrate increased in all mutants, the values ranging between 2.78 and 4.81 (Table I).

Inhibition of CPT I Wild Type and Mutants by Malonyl-CoA—When inhibitory kinetics *versus* increasing concentrations of malonyl-CoA was performed, the quintuple mutant practically abolished the sensitivity toward malonyl-CoA (IC_{50} of 258 *versus* 12.3 μM of the wild type) (Fig. 4*B* and Table I). Even at concentrations as high as 100 μM malonyl-CoA the CPT I quintuple mutant maintained 80% of the activity of the control without malonyl-CoA.

We then addressed the individual responsibility of the separate CPT I mutants for the malonyl-CoA sensitivity. Mutants T314S, N464D, M593S, and C608A expressed in *S. cerevisiae* were incubated with increasing amounts of malonyl-CoA, and CPT I activity was determined. Mutant A478G had been previously studied in Ref. 20 and showed decreased sensitivity to malonyl-CoA (IC_{50} of 39.5 *versus* 12.3 μM of the wild type).

The kinetics of inhibition by malonyl-CoA depended on the mutant considered. Whereas mutant M593S (Fig. 4*A*) showed very low sensitivity at malonyl-CoA inhibition (IC_{50} of 319 μM), the other mutations produced varied changes in malonyl-CoA sensitivity. L-CPT I C608A slightly modified the sensitivity to malonyl-CoA (IC_{50} is 27.5 μM), the change in IC_{50} of mutant T314S was small, whereas N464D showed similar sensitivity to malonyl-CoA to the wild type (Fig. 4*B* and Table I). Because the highest changes in sensitivity to malonyl-CoA and K_m values for carnitine were observed in the methionine mutants (point and quintuple mutants), we additionally prepared two new mutants: M593A and M593E to examine whether Met^{593} was essential to the malonyl-CoA interaction in L-CPT I. Results show that the sensitivity to malonyl-CoA was also nearly abolished in these mutants (Fig. 4*A*) (IC_{50} values of 155 and 220 μM, respectively) as in the M593S mutant, confirming the essential role of Met^{593} in this interaction.

DISCUSSION

We attempted to identify the amino acids in the C-terminal domain of L-CPT I that are responsible for the inhibition of the catalytic activity by malonyl-CoA. Over many years much work has been done to identify the domains in L-CPT I that may bind malonyl-CoA. Different groups have tested different empirical hypotheses and mutated amino acids, mostly in the amino-terminal region of L-CPT I. The results have shown that this domain plays a role in the regulation of CPT I by malonyl-CoA, because in some cases the sensitivity to the inhibitor is impaired.

A different approach was employed by our group very recently. This was based on the conservation of two histidine residues, which are present in the inhibitable malonyl-CoA carnitine acyltransferases (CPT I and COT) and absent in noninhibitable enzymes (CPT II and CAT). Mutation of both histidines resulted in the abolition of malonyl-CoA sensitivity in COT (26). Analogous results were observed in CPT I when its concentration at the mitochondrial membranes was not high. Mutation of other amino acids in the domain proximal to the catalytic site (Ala^{478} and Pro^{479}) indicated that a malonyl-CoA-

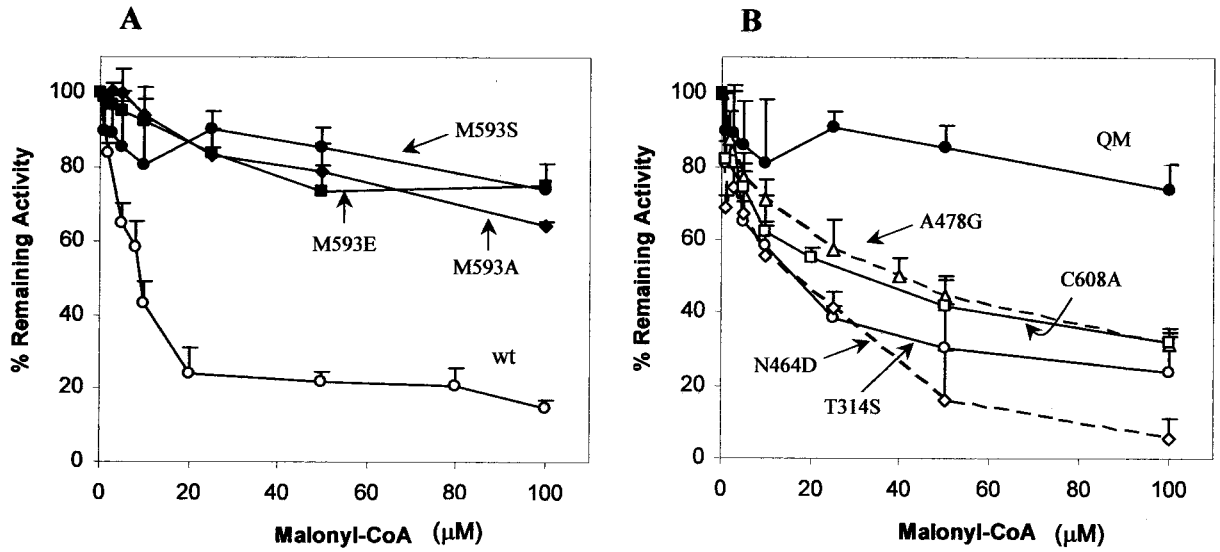

FIG. 4. **Effect of malonyl-CoA on the activity of yeast overexpressed L-CPT I (wild type) and several mutants.** *A*, L-CPT I wild type (*open circles*) and point methionine mutants M593S (*black circles*), M593A (*black rhombus*), M593E (*black squares*), and *B*, quintuple mutant (*QM*) (*black circles*) and point mutants T314S (*open circles*), N464D (*open rhombus*, *broken line*), A478G (*open triangles*, *broken line*), and C608A (*open squares*) overexpressed in yeast were incubated with increasing concentrations of malonyl-CoA and the enzyme activity was measured. Data are expressed relative to control values in the absence of inhibitor (100%) as the mean of three independent measurements.

inhibitable domain was probably the low-affinity malonyl-CoA binding site. Our previous studies showed that the location of malonyl-CoA in the structural model was compatible with competition of the inhibitor *versus* the substrate in the malonyl-CoA low affinity binding site (20).

The site-directed mutagenesis study used here to identify amino acids responsible for malonyl-CoA inhibition is based on the comparison of the sequences in a range of carnitine and choline acyltransferases, taking the positive or negative sensitivity to malonyl-CoA as a discriminatory criterion. The biocomputing study has shown that five amino acids are present in all CPT I (isoforms L- and M-) and in COT from various organisms and that they are absent not only in other nonmalonyl-CoA-inhibitable carnitine acyltransferases but also in ChAT. In rat L-CPT I these amino acids are Thr^{314}, Asn^{464}, Ala^{478}, Met^{593}, and Cys^{608}. The corresponding positional amino acids in CPT II, CAT, and ChAT are Ser^{223}, Asp^{363}, Gly^{377}, Ser^{490}, and Ala^{505}, respectively (coordinates of rat CPT II). Therefore, we considered it highly probable that these amino acids were involved in the interaction of malonyl-CoA. Results confirmed in part this supposition. The quintuple mutant reduced malonyl-CoA sensitivity almost completely (80% activity at 100 μM malonyl-CoA (which is outside the physiological range)), supporting the initial hypothesis. The results obtained using separate single mutants indicate that not all of these amino acids have the same role in malonyl-CoA inhibition. Whereas M593S nearly abolished the sensitivity to malonyl-CoA like the quintuple mutant, A478G increased the IC_{50} from 12 to 39.5 μM (20). The other amino acids are less responsible for the inhibition.

The relevance of Met^{593} as a critical amino acid for malonyl-CoA sensitivity was confirmed by the results of mutation to other two amino acids, Ala and Glu. The mutants equally showed diminished sensitivity to malonyl-CoA like mutant M593S. Met^{593}, when mutated to Ser as it appears in CPT II and CAT, decreased the sensitivity to malonyl-CoA in a stronger fashion than when it was mutated to other amino acids like Ala and Glu, which were unrelated to this position in other carnitine acyltransferases. Therefore, we conclude that the occurrence of Ser in this position has probably been evolutionary conserved in nonmalonyl-CoA-sensitive carnitine acyltransferases because it prevents sensitivity to malonyl-CoA. In any case, it appears that Met^{593} is critical in the interaction of malonyl-CoA with L-CPT I.

It was of interest to measure the kinetic constants of all CPT I mutants. Several authors reported the competition between malonyl-CoA and carnitine (27, 28). The tissues in which the sensitivity of CPT I to malonyl-CoA is highest are those that require the highest concentration of carnitine to drive the reaction and the requirement for carnitine and sensitivity to malonyl-CoA appears to be inversely related. The authors concluded that the sites to which the two metabolites bind are closely associated (27, 7). Studies by Bird and Saggerson (28) showed on the one hand that malonyl-CoA reduced the effectiveness of carnitine as substrate, and on the other hand, that carnitine might diminish the regulatory effect of malonyl-CoA (29). Although a clear mechanism for this competition could not be established, the data strongly supported this idea. In the present study the various CPT I mutants have altered K_m or V_{max} for carnitine. Whereas the K_m for C608A was half of the wild type, its V_{max} was 3.6-fold higher. The mutant M593S had the same K_m value for carnitine as the wild type but its V_{max} increased 20-fold. The mutant A478G increased both the K_m value and the V_{max} with respect to the wild type values. The relationship between these values and catalysis is best revealed in the term catalytic efficiency. This term as calculated by the V_{max}/K_m ratio varies considerably among different mutants. Carnitine catalytic efficiencies for mutants M593S, M593A, M593E, C608A, and A478G increased 21-, 12-, 4.2-, 8.8-, and 4.1-fold with respect to the wild type. This means that mutations designed to decrease malonyl-CoA sensitivity strongly modified the catalytic efficiency of CPT I mutants measured in the absence of malonyl-CoA. Interestingly, the increase in catalytic efficiency appears to be roughly proportional to the extent of the alteration in malonyl-CoA sensitivity. The IC_{50} values for malonyl-CoA run in the same direction to the catalytic efficiency of the mutants. This indicates that those mutants that can locate carnitine better at the catalytic site might displace malonyl-CoA from its site, preventing the binding of the metabolite and thus the inhibition of CPT I.

Because L-CPT I has not been crystallized, we do not know the proximity of Met^{593} to the site of carnitine binding to perform the catalytic event. However, Met^{593} is very near the tripeptide $TET^{602-604}$, which has been reported to play an

important role in the accommodation of carnitine in catalysis. Cronin (30) showed that mutation of the homologous tripeptide VDN in choline acetyltransferases to TET greatly increased the catalytic efficiency of the reaction (137-fold) using carnitine as substrate. This proximity between Met^{593} and $TET^{602-604}$ would explain the inverse correlation observed between the catalytic efficiency for carnitine and the IC_{50} for malonyl-CoA values of the mutants assayed. A new scenario appears in the mutual interaction between carnitine and malonyl-CoA in CPT I. The domain comprised, at least, between amino acid residues 593 and 604 is probably the site of interaction between carnitine and malonyl-CoA, which exclude each other. Higher catalytic efficiencies for carnitine in the mutants are followed by decreases in the inhibitory sensitivity to malonyl-CoA.

It is equally interesting to note that all mutants tested show higher catalytic efficiency for palmitoyl-CoA as substrate than the wild type. The increase in V_{max}/K_m ranges from 2- to 3-fold. Previous work with a partially purified preparation of CPT I had indicated that the kinetics of the reaction with respect to carnitine concentration could be highly dependent on the concentration of the second substrate, palmitoyl-CoA (29). Experiments carried out by Bird and Saggerson (28) showed that in fasted animals, in which carnitine concentration was decreased, the IC_{50} values for malonyl-CoA increased up to 17-fold and the binding of [2-^{14}-C]malonyl-CoA was reduced by 35% at 50 μM palmitoyl-CoA and to even lower values at increasing palmitoyl-CoA concentrations.

Only two of these mutated amino acids are located in the three-dimensional CPT I structural model. Ala^{478} is one of the amino acids present in the low affinity site of malonyl-CoA interaction. This amino acid together with Pro^{479} and His^{483} conform a domain to which malonyl-CoA appears to bind (20). Mutation of this amino acid would explain a decrease in sensitivity to malonyl-CoA, and therefore it would also explain the increase in catalytic efficiency. On the other hand, Asn^{464} is also present in the catalytic core of the structural model of CPT I (20), but its location does not permit any conclusions about a participation in the malonyl-CoA inhibitory effect. In fact it is located on the opposite site to malonyl-CoA (data not shown). Therefore, it is not surprising that its mutation from Asn^{464} to Asp^{464} does not alter sensitivity to the inhibitor. As a corollary of this study, we conclude that the occurrence of the five other amino acids (Ser^{223}, Asp^{363}, Gly^{377}, Ser^{490}, and Ala^{505}) at the positions, respectively, identical to those amino acids seen in CPT I may be sufficient to prevent the sensitivity to malonyl-CoA not only to carnitine acyltransferases such as CPT II and CAT but also to ChAT.

The use of either the quintuple mutant or the methionine point mutants may allow studies on the influence of these negative dominant CPT Is, which are expected to be independent of malonyl-CoA concentration in a range of tissues such as liver, muscle, and the β-cell, in which the metabolism of fatty acids plays important roles in ketone body synthesis, resistance to insulin, and glucose-stimulated insulin secretion, respectively. Some of these topics are the subject of current investigations in our laboratory.

Acknowledgment—We are grateful to Robin Rycroft of the Language Service for valuable assistance in the preparation of the manuscript.

REFERENCES

1. McGarry, J. D., and Brown, N. F. (1997) *Eur. J. Biochem.* **244,** 1–14
2. Zammit, V. A. (1999) *Biochem. J.* **343,** 505–515
3. Anderson, R. C. (1998) *Curr. Pharmaceut. Design* **4,** 1–16
4. Esser, V., Britton, C. H., Weis, B. C., Foster, D. W., and McGarry, J. D. (1993) *J. Biol. Chem.* **268,** 5817–5822
5. Yamazaki, N., Shinohara, Y., Shima, A., and Terada, H. (1995) *FEBS Lett.* **363,** 41–45
6. Esser, V., Brown, N. F., Cowan, A. T., Foster, D. W., and McGarry, J. D. (1996) *J. Biol. Chem.* **271,** 6972–6977
7. Mills, S. E., Foster, D. W., and McGarry, J. D. (1984) *Biochem. J.* **219,** 601–608
8. Bird, M. I., and Saggerson, E. D. (1984) *Biochem. J.* **222,** 639–647
9. Nic a'Bhaird, N., and Ramsay, R. R. (1992) *Biochem. J.* **286,** 637–640
10. Saggerson, E. D., and Carpenter, C. A. (1981) *FEBS Lett.* **132,** 166–168
11. Cook, G. A., Mynatt, R. L., and Kashfi, K. (1994) *J. Biol. Chem.* **269,** 8803–8807
12. Kashfi, K., Mynatt, R. L., and Cook, G. A. (1994) *Biochim. Biophys. Acta* **1212,** 245–252
13. Grantham, B. D., and Zammit, V. A. (1986) *Biochem. J.* **233,** 589–593
14. Jackson, V. N., Zammit, V. A., and Price, N. T. (2000) *J. Biol. Chem.* **275,** 38410–38416
15. Swanson, S. T., Foster, D. W., McGarry, J. D., and Brown, N. F. (1998) *Biochem. J.* **335,** 513–519
16. Shi, J., Zhu, H., Arvidson, D. N., and Woldegiorgis, G. (1999) *J. Biol. Chem.* **274,** 9421–9426
17. Shi, J., Zhu, H., Arvidson, D. N., Cregg, J. M., and Woldegiorgis, G. (1998) *Biochemistry* **37,** 11033–11038
18. Shi, J., Zhu, H., Arvidson, D. N., and Woldegiorgis, G. (2000) *Biochemistry* **39,** 712–717
19. Morillas, M., Gómez-Puertas, P., Roca, R., Serra, D., Asins, G., Valencia, A., and Hegardt, F. G. (2001) *J. Biol. Chem.* **276,** 45001–45008
20. Morillas, M., Gómez-Puertas, P., Rubí, B., Clotet, J., Ariño, J., Valencia, A., Hegardt, F. G., Serra, D., and Asins, G. (2002) *J. Biol. Chem.* **277,** 11473–11480
21. Altschul, S. F., Gish, W., Miller, W., Myers, E. W., and Lipman, D. J. (1990) *J. Mol. Biol.* **215,** 403–410
22. Thompson, J. D., Higgins, D. G., and Gibson, T. J. (1994) *Nucleic Acids Res.* **22,** 4673–4680
23. Casari, G., Sander, C., and Valencia, A. (1995) *Nat. Struct. Biol.* **2,** 171–178
24. Pazos, F., Sanchez-Pulido, L., García-Ranea, J. A., Andrade, M. A., Atrian, S., and Valencia, A. (1997) in *Biocomputing and Emergent Computation* (Lundh, D., Olsson, B., and Narayanan, A., eds) pp. 132–145, World Scientific, Singapore
25. Bauer, B., Mirey, G., Vetter, I. R., Garcia-Ranea, J. A., Valencia, A., Wittinghofer, A., Camonis, J. H., and Cool, R. H. (1999) *J. Biol. Chem.* **274,** 17763–17770
26. Morillas, M., Clotet, J., Rubí, B., Serra, D., Asins, G., Ariño, J., and Hegardt F. G. (2000) *FEBS Lett.* **466,** 183–186
27. McGarry, J. D., Mills, S. E., Long, C. S., and Foster, D. W. (1983) *Biochem. J.* **214,** 21–28
28. Bird, M. I., and Saggerson, E. D. (1985) *Biochem. J.* **230,** 161–167
29. Bremer, J., and Norum, K. (1967) *J. Biol. Chem.* **242,** 1744–1748
30. Cronin, C. N. (1998) *J. Biol. Chem.* **273,** 24465–24469

BIOCHEMISTRY

© Copyright 2006 by the American Chemical Society Volume 45, Number 14 April 11, 2006

Articles

Novel Effect of C75 on Carnitine Palmitoyltransferase I Activity and Palmitate Oxidation†

Assia Bentebibel,‡ David Sebastián,‡ Laura Herrero,‡ Eduardo López-Viñas,§ Dolors Serra,‡ Guillermina Asins,‡ Paulino Gómez-Puertas,§ and Fausto G. Hegardt*,‡

Department of Biochemistry and Molecular Biology, School of Pharmacy, University of Barcelona, E-08028 Barcelona, Spain, and Centro de Biologia Molecular "Severo Ochoa", Universidad Autonoma de Madrid, Consejo Superior de Investigaciones Científicas, Cantoblanco, E-28049 Madrid, Spain

Received October 26, 2005; Revised Manuscript Received January 23, 2006

ABSTRACT: C75 is a potential drug for the treatment of obesity. It was first identified as a competitive, irreversible inhibitor of fatty acid synthase (FAS). It has also been described as a malonyl-CoA analogue that antagonizes the allosteric inhibitory effect of malonyl-CoA on carnitine palmitoyltransferase I (CPT I), the main regulatory enzyme involved in fatty acid oxidation. On the basis of MALDI-TOF analysis, we now provide evidence that C75 can be transformed to its C75-CoA derivative. Unlike the activation produced by C75, the CoA derivative is a potent competitive inhibitor that binds tightly but reversibly to CPT I. IC_{50} values for yeast-overexpressed L- or M-CPT I isoforms, as well as for purified mitochondria from rat liver and muscle, were within the same range as those observed for etomoxiryl-CoA, a potent inhibitor of CPT I. When a pancreatic INS(823/13), muscle L6E9, or kidney HEK293 cell line was incubated directly with C75, fatty acid oxidation was inhibited. This suggests that C75 could be transformed in the cell to its C75-CoA derivative, inhibiting CPT I activity and consequently fatty acid oxidation. In vivo, a single intraperitoneal injection of C75 in mice produced short-term inhibition of CPT I activity in mitochondria from the liver, soleus, and pancreas, indicating that C75 could be transformed to its C75-CoA derivative in these tissues. Finally, in silico molecular docking studies showed that C75-CoA occupies the same pocket in CPT I as palmitoyl-CoA, suggesting an inhibiting mechanism based on mutual exclusion. Overall, our results describe a novel role for C75 in CPT I activity, highlighting the inhibitory effect of its C75-CoA derivative.

C75 is a chemically stable synthetic inhibitor of fatty acid synthase (FAS).[1] Structurally, it is a cell-permeable α-methylene-γ-butyrolactone, designed to be less reactive and potentially safer than cerulenin, a natural product obtained from the fungus *Cephalosporium caerulens*. C75 lacks the reactive epoxide present in cerulenin, which enhances

† This study was supported by Grant SAF2004-06843-C03 from the Ministerio de Educación y Ciencia, Grant C3/08 from the Fondo de Investigación Sanitaria of the Instituto de Salud Carlos III, Red de Centros en Metabolismo y Nutrición (RCMN) from the Ministerio de Educación y Ciencia, Research Prize 2004 from Fundación Puleva, and the Ajut de Suport als Grups de Recerca de Catalunya (2001SGR-00129), Spain. A.B. and L.H. are recipients of fellowships from the Ministerio de Educación y Ciencia, and D. Sebastian is a recipient of a fellowship from the University of Barcelona.

* To whom correspondence should be addressed: Department of Biochemistry and Molecular Biology, School of Pharmacy, University of Barcelona, Diagonal 643, E-08028 Barcelona, Spain. Phone: +34 93 4024523. Fax: +34 93 4024520. E-mail: fgarciaheg@ub.edu and dserra@ub.edu.

‡ University of Barcelona.

§ Consejo Superior de Investigaciones Científicas.

10.1021/bi052186q CCC: $33.50 © 2006 American Chemical Society
Published on Web 03/14/2006

chemical stability. In contrast to cerulenin, which only inactivates the β-ketoacyl-acyl synthase activity of FAS, C75 inhibits two additional FAS activities: enoyl reductase and thioesterase. With respect to the overall FAS reaction, C75 is a competitive, irreversible inhibitor against all three substrates: acetyl-CoA, malonyl-CoA, and NADPH (*1*, *2*).

C75 has been proposed for two therapeutic applications. The first is as an antitumor agent, since it induces cytostatic and cytotoxic effects in cultured tumor cells where the increase in malonyl-CoA levels, due to FAS inhibition, causes cancer cell-specific apoptosis (*3*). The second is as an anti-obesity agent, since it can alter the metabolism of neurons in the hypothalamus, where an increase in the level of malonyl-CoA serves as a secondary messenger of nutrient status, thereby mediating appetite suppression (*4*, *5*). Furthermore, it appears that C75 exerts both short- and long-term effects on food intake by preventing the upregulation of orexigenic neuropeptides and the downregulation of anorexigenic neuropeptides (*6*). In peripheral tissues (*7*), C75 has been postulated not only to increase the level of malonyl-CoA but also to act as a malonyl-CoA analogue that antagonizes the inhibitory effect on carnitine palmitoyltransferase (CPT I), the main regulatory step of mitochondrial β-oxidation (*8*). Both its central and the peripheral actions could reduce weight in lean and fat mice.

Mammalian tissues express three isoforms of CPT I: liver (L-CPT I), muscle (M-CPT I) (*8*), and brain (CPT I-C) (*9*). The liver and muscle isoforms are tightly regulated by their physiological inhibitor malonyl-CoA, which allows CPT I to signal the availability of lipid and carbohydrate fuels to the cell. The malonyl-CoA sensitivity of L-CPT I in the adult rat depends on the physiological state. It is increased by renewed feeding of carbohydrates to fasted rats, by obesity, or following administration of insulin to diabetic rats, whereas it is decreased by starvation and diabetes (*10*, *11*).

In addition to the physiological inhibition by malonyl-CoA, CPT I activity may also be inhibited by several synthetic epoxy-containing fatty acid compounds such as etomoxir, 2-TDGA (palmoxirate-tetradecyl-2-oxiranecarboxylate) and POCA {2-[5-(4-chlorophenyl)pentyl]oxirane-2-carboxylic acid}. The CoA esters of these compounds formed in the cytosol inhibit long-chain fatty acid oxidation via their potent inhibitory effect on CPT I (*12*). Taking into account that the CoA derivatives, rather than their free acid forms, are the inhibitory forms of these compounds, we hypothesize that C75 could constitute an acyl-CoA synthetase substrate, with the resulting C75-CoA derivative acting as a potential inhibitor of CPT I activity. We found that C75-CoA is produced in vitro and inhibits CPT I with competitive inhibition kinetics. CPT I activity was also inhibited in mitochondria from pancreas-, muscle-, and kidney-derived cell lines incubated with C75 directly, as observed with etomoxir, revealing that the CoA derivatives of both compounds may be produced within the cell. These inhibitory effects were followed by a decrease in the level of fatty acid oxidation. Finally, in mice treated with a single intraperitoneal (ip) injection of C75, CPT I activity decreased but subsequently recovered. We conclude that the inhibitory effect of C75-CoA is caused by strong, reversible binding to CPT I inside the palmitoyl-CoA pocket.

[1] Abbreviations: FAS, fatty acid synthase; L-CPT I, carnitine palmitoyltransferase I, liver isoform; M-CPT I, carnitine palmitoyltransferase I, muscle isoform; KRBH buffer, Krebs-Ringer bicarbonate Hepes buffer.

EXPERIMENTAL PROCEDURES

Animals. Six-week-old C57BL/6J male mice were purchased from Harlam Co. Animals were maintained under a 12 h dark/light cycle at 23 °C with free access to food and water. Experiments were performed following a 1 week acclimatization period. Male Sprague-Dawley rats (180−200 g) bred in our laboratory were used to obtain liver, pancreas, and soleus. All experimental protocols were approved by the Animal Ethics Committee at the University of Barcelona.

Materials. L-[*methyl*-^{3}H]Carnitine hydrochloride and [1-^{14}C]-palmitic acid were purchased from Amersham Biosciences. C75 was purchased from Alexis Biochemicals, and etomoxir was provided by H. P. O. Wolf (GMBH, Allensbach, Germany). Yeast culture media products were from Difco. The Bradford solution for protein assays was from Bio-Rad. Dulbecco's modified Eagle's medium (DMEM), RPMI 1640, and antibiotics were from Gibco-Invitrogen Corp. Defatted bovine serum albumin (BSA), palmitate, malonyl-CoA, and other chemicals were purchased from Sigma-Aldrich. Acyl-CoA synthetase from *Pseudomonas* sp. was obtained from Sigma.

Synthesis of C75-CoA and Etomoxiryl-CoA. Etomoxir and C75 were activated to CoA derivatives by long-chain acyl-CoA synthetase in the presence of CoA-SH (*13*). Etomoxir and C75 were dissolved in DMSO to a final concentration of 100 mM. The synthesis was performed with 1 μmol of each drug separately, in a total volume of 1 mL of a buffer containing 0.1% (w/v) Triton X-100, 5 mM CoA-SH, 10 mM ATP, 1 mM DTT, 10 mM $MgCl_2$, 100 mM MOPS-NaOH (pH 7.5), and 0.25 unit of long-chain acyl-CoA synthetase from *Pseudomonas* sp. The reaction was carried out at 35 °C for 2 h. The conversion of etomoxir and C75 to etomoxiryl-CoA and C75-CoA, respectively, was complete, as deduced from the spectrophotometric assay of the remaining free CoA, as described elsewhere (*14*). Stock aliquots, in which the final concentration of each CoA derivative was 1 mM, were stored at −20 °C and diluted in 100 mM MOPS-NaOH (pH 7.5) for activity assays.

Mass Spectrometry. The MALDI-TOF mass spectra of C75 and etomoxir, as well as their CoA derivatives C75-CoA and etomoxiryl-CoA, were obtained on a Voyager DE-RP (Applied Biosystems) mass spectrometer equipped with a nitrogen laser (337 nm, 3 ns pulse). The acceleration voltage was set to 20 kV. Data were acquired in the reflector mode with delay times of 320 ns for both positive and negative polarities. Spectra were calibrated externally using a calibration mixture (Calibration Mixture 1, Applied Biosystems): CHCA, des-Arg^1-bradykinin, angiotensin I, Glu^1-fibrinopeptide B, and neurotensin m/z 300−1700. Samples were prepared by diluting 1 μL of each drug in the activation buffer to 100 μL with H_2O, and mixing 1 μL of this diluted solution with 1 μL of matrix solution [10 mg/mL 2,5-dihydroxybenzoic acid (2,5-DHB, Aldrich) in a 1:1 methanol/water mixture]. One microliter of the sample/matrix mixture was spotted onto the stainless steel sample plate, allowed to evaporate to dryness in air, and introduced into the mass spectrometer. Spectra were acquired in the positive and

negative ion mode. MALDI-TOF spectra were recorded by the Mass Spectrometry Service (SCT, University of Barcelona).

Expression of CPT I in Saccharomyces cerevisiae. S. cerevisiae was chosen as a heterologous expression system because it does not express endogenous CPT I activity. The plasmid pYES2-L-CPT I, which encodes the liver isoform of CPT I, was obtained as previously described (*15*). The plasmid pYES2-M-CPT I was obtained from the plasmid DS112-36 (*16*) containing the coding cDNA of the rat muscle CPT I isoform. The fragment that encompassed nucleotides 27−2432, including the coding region of M-CPT I, was subcloned into the *S. cerevisiae* expression plasmid pYES2 (Invitrogen). A *Hin*dIII site (underlined) was introduced by PCR immediately 5′ of the ATG start codon of M-CPT I to enable cloning into the unique *Hin*dIII site of plasmid pYES2. A consensus sequence (in boldface type), optimized for efficient translation in yeast, was also introduced in the same PCR, using the forward primer CPT I *Hin*dIII.for (5′-TCG ATA AGC TTA TAA AAT GGC GGA AGC ACA CCA GGC AG-3′) and the reverse primer CPT I *Hin*dIII.rev (5′-GGA AGC TTG GGC AGT GAT GT-3′). The resulting 550 bp fragment, obtained after the digestion of PCR products with *Hin*dIII, was ligated on pYES2 plasmid digested with the same restriction enzyme, thereby yielding the plasmid pYES2-M-CPT I-ATG. This plasmid was digested with *Sal*I (in cDNA of M-CPT I) and *Sph*I (in plasmid pYES2) and ligated with the CPT I *Sal*I−*Sph*I fragment (purified band of 2351 bp), producing pYES2-M-CPT Ipre. The TTTTTTA sequence (nucleotides 387−393) present in the M-CPT I cDNA, which resembles a known yeast polyadenylation signal (*17*), was subsequently changed by PCR to increase expression levels in yeast without changing the amino acid sequence, producing pYES2-M-CPT I. The appropriate substitutions and the absence of unwanted mutations were confirmed by sequencing the inserts in both directions with an Applied Biosystems 373 automated DNA sequencer. The expression of the plasmids pYES2-L-CPT I and pYES2-M-CPT I in yeast was performed as previously described (*15*).

Cell Cultures. The clonal β cell line INS(832/13), derived and selected from the parental rat insulinoma INS-1 (*18*), was cultured (passages 48−60) in a humidified atmosphere of 5% CO_2 in complete medium composed of RPMI 1640, containing 11 mM glucose and supplemented with 10% heat-inactivated FBS (Wisent Inc.), 10 mM HEPES, 2 mM glutamine, 1 mM sodium pyruvate, 50 mM 2-mercaptoethanol, 100 units/mL penicillin, and 100 μg/mL streptomycin. The maintenance culture was passaged once a week by gentle trypsinization, and cells were grown to confluence in Falcon dishes.

The L6E9 rat skeletal muscle cells were cultured in a humidified atmosphere containing 5% CO_2 in complete medium composed of DMEM containing 10% FBS (Gibco-Invitrogen Corp.), 100 units/mL penicillin, 100 μg/mL streptomycin, and 25 mM HEPES (pH 7.4) (growth medium). Preconfluent myoblasts (80−90%) were induced to differentiate by lowering the level of FBS to a final concentration of 2% (differentiation medium). All experiments were performed with completely differentiated myotubes (after 4 days in differentiation medium).

Human embryonic kidney (HEK) 293 cells obtained from ECACC (European Collection of Cell Cultures) were cultured in a humidified atmosphere containing 5% CO_2 in complete medium composed of DMEM containing 10% FCS (Biological Industries), 100 units/mL penicillin, and 100 μg/mL streptomycin. Cells were grown to 80% confluence.

Preparation of Mitochondrial Fractions. Mitochondria-enriched fractions from yeast overexpressing L- and M-CPT I were obtained as previously described (*15*). Mitochondria-enriched cell fractions from INS(832/13), L6E9, and HEK293 cells cultured in 15 cm dishes were obtained with a glass homogenizer as previously described (*19*). The pellet, in which the mitochondria remain largely intact, was used directly for CPT I activity assays. Mitochondria-enriched fractions were obtained from rat and mouse muscle as described elsewhere (*20*), with minor modifications. Two soleus muscle samples of each animal were homogenized separately in 250 mM sucrose buffer using an omni mixer and then centrifuged at 1000*g* for 15 min. The pellet was homogenized and centrifuged at 600*g* for 10 min. The resulting supernatant was centrifuged at 15000*g* for 15 min, and the pellet was resuspended in 100 μL of a buffer containing 250 mM sucrose and 150 mM KCl. Mitochondria-enriched fractions from rat and mouse liver were obtained by homogenization in a buffer containing 250 mM sucrose, 1 mM EDTA, and 10 mM Tris-HCl (pH 7.4) (*21*). The liver suspension was centrifuged at 560*g* for 15 min, and the supernatant was further centrifuged at 12000*g* for 20 min. The pellet was resuspended in 2 mL of homogenization buffer, centrifuged for 10 min at 7000*g*, washed, and resuspended in 1 mL of the homogenization buffer. To obtain mitochondria-enriched fractions from mice pancreas, tissue was homogenized in a buffer containing 250 mM sucrose, 20 mM Tris-HCl (pH 7.4), 0.5 mM EDTA, 0.5 mM EGTA, 1 mM DTT, 10 μg/mL leupeptin, 4 μg/mL aprotinin, 2 μg/mL pepstatin, and 100 μM PMSF. The homogenate was subjected to differential centrifugation at 900*g* for 10 min and at 5500*g* for 10 min. The pellet was resuspended with a Dounce homogenizer and centrifuged at 2000*g* for 2 min and at 4000*g* for 8 min. Finally, the pellet was resuspended in 250 μL of 250 mM sucrose (*22*). All the processes were performed at 4 °C, and fractions were assayed immediately for determination of CPT I activity.

Determination of CPT I Activity. CPT I activity was measured in mitochondria-enriched fractions obtained from yeast, cultured cells, or tissues as described above. CPT I activity in 3−4 μg of yeast protein extracts, 10−15 μg of mitochondria-enriched cell fractions, or 20 μg of mitochondria fractions from tissues was determined by the radiometric method as previously described (*15*). Extracts were preincubated at 30 °C for different times in the presence or absence of drugs. Enzyme activity was assayed for 4 min at 30 °C in a total volume of 200 μL. The substrates were 50 μM palmitoyl-CoA and 400 or 1000 μM L-[*methyl*-^{3}H]-carnitine for L- and M-CPT I isoforms, respectively. In yeast extracts, only the overexpressed L-CPT I or M-CPT I activity was present. In tissues and cell culture extracts, both CPT I (malonyl-CoA-sensitive) and CPT II (insensitive to malonyl-CoA) were present. Thus, in these fractions, CPT I activity was determined as the malonyl-CoA/etomoxiryl-CoA-sensitive CPT activity. CPT II activity, which is also present in mammalian mitochondrial extracts, was always subtracted

from the total activity to calculate specific CPT I activity. The presence of CPT activity insensitive to malonyl-CoA (CPT II activity) in mitochondria obtained from cell cultures was less than 5% and thus was not taken into consideration. Drugs or their CoA derivatives were preincubated with the enzyme between 1 and 5 min depending on the assay. Drug concentrations ranging from 0.01 to 50 μM were used to estimate the IC_{50} value. IC_{50} corresponds to the inhibitor concentration that inhibits 50% of the enzyme activity. Malonyl-CoA (50 μM) was used for malonyl-CoA inhibition assays. C75-CoA concentrations were varied from 1 to 5 μM to examine the dependence of CPT I activity on increasing palmitoyl-CoA concentration. In all cases, the molar ratio of palmitoyl-CoA to albumin was kept at 5:1 to avoid the presence of free acyl-CoA and its deleterious detergent effects and to prevent the formation of micelles. Kinetic constants (K_m and V_{max}) were determined by Lineweaver−Burk analysis. Inhibition constants (K_I and k_{inact}) were determined at 20 μM palmitoyl-CoA by nonlinear parameter estimation (*23*, *24*), using SigmaPlot version 8.0. All protein concentrations were determined using the Bio-Rad protein assay with bovine albumin as a standard.

Washing and Dialysis Assays. The binding of CoA derivatives to CPT I was assessed as described previously (*25*), with some modifications. Yeast mitochondria-enriched fractions overexpressing L-CPT I were preincubated for 5 min at 30 °C with each CoA derivative at 50 μM. One aliquot was used directly for the CPT I activity assay (unwashed), and the other aliquot was centrifuged at 13000*g* for 5 min at 4 °C and resuspended (washed) in 5 mM Tris-HCl (pH 7.2), 150 mM KCl, 2 μg/mL leupeptine, 0.5 μM benzamidine, 1 μg/mL pepstatin, and 1 mM PMSF before the assay. The CPT I activity assay was conducted for 4 min at 30 °C as described above.

To verify the reversibility of the interaction of C75-CoA with CPT I, dialysis assays were performed. Mitochondria-enriched fractions (160 μg) obtained from yeast cells expressing L-CPT I were preincubated at 30 °C for 5 min (without the drug) or with a final concentration of 50 μM C75-CoA or 50 μM etomoxiryl-CoA and then dialyzed in buffer containing 10 mM Hepes (pH 7.4), 1 mM EDTA, and 10% glycerol at 4 °C. Aliquots were taken before dialysis (0 h), and 24 and 36 h thereafter, and assayed for CPT I activity.

C75 Treatment of Cell Cultures and Administration to Mice. Cells were incubated with either C75 at 10, 20, 30, or 40 μg/mL or etomoxir at 30 or 40 μg/mL in culture medium. Stock solutions of C75 and etomoxir were prepared at 100 mM in DMSO. Control cells were incubated with the same amount of DMSO. L6E9 myotubes were incubated for 2 h at 37 °C, and INS(832/13) and HEK293 cells were incubated for 1 h at 37 °C. Subsequently, the cells were washed in PBS, and either the CPT I activity, the level of palmitate oxidation, or cell viability was measured.

Mice were given a single ip injection of either C75 or etomoxir, dissolved in RPMI 1640 medium, at 20 mg/kg of body weight or medium alone for control. Animals were killed at different times postinjection, and mitochondria-enriched fractions from liver, soleus, and pancreas were obtained as described above. Fractions were assayed immediately to measure CPT I activity.

Assessment of Fatty Acid Oxidation. Palmitate oxidation to CO_2 was assessed in culture cells grown in 12-well plates. On the day of the assay, cells were washed in KRBH with 0.1% defatted BSA, preincubated at 37 °C for 30 min in KRBH with 1% BSA, and washed in KRBH with 0.1% BSA. Cells were then incubated for 2 h at 37 °C with fresh KRBH containing 2.5 mM glucose in the presence of 0.8 mM carnitine with 0.25 mM palmitate and 1 μCi/mL [1-^{14}C]-palmitic acid bound to 1% (w/v) BSA. Oxidation measurements were performed by a CO_2-capture system assay as previously described (*26*).

Viability Cell Culture Assays. To evaluate the cytotoxic effect of the drugs, an MTT [3-(4,5-dimethylthiazol-2-yl)-2,5-diphenyltetrazolium bromide] assay was performed (*27*). Cells were seeded in 12-well plates and incubated with drugs as described above. Subsequently, 200 μL of 0.25% (w/v) MTT was added to each well, and cells were further incubated for 2 h. The resulting formazan crystals were then solubilized by adding 1 mL of MTT lysis solution [10% (w/v) SDS and 1 mM acetic acid in DMSO], and the absorbance at 570 nm was measured. The results are expressed as the percentage of absorbance related to control cells.

In Silico Molecular Docking. A new three-dimensional model for CPT I was constructed using homology modeling procedures based on structural alignments of CPT I sequence and utilizing the coordinates of the recently described protein structure of the mouse carnitine octanoyltransferase (*28*). The three-dimensional model of the free C75-CoA molecule was prepared using molecular-orbital calculation methods implemented in Mopac (*29*). The in silico docking programs Autogrid and Autodock (*30*, *31*) were used to generate and evaluate low-energy conformational models for the putative ligand position, thus providing a model for the interaction of C75-CoA with the active center of CPT I.

Statistical Analysis. Data are expressed as the mean ± the standard error of at least three independent experiments. The significance of differences was assessed using the unpaired Student's *t* test.

RESULTS

Synthesis and Analysis of C75-CoA. To determine whether C75 is converted to C75-CoA as described for etomoxir, each drug was incubated independently in the presence of CoA and acyl-CoA synthetase, as described in Experimental Procedures. The production of stable CoA derivatives was then analyzed by MALDI-TOF. Figure 1A shows a peak of 1020.4 Da corresponding to the molecular mass of the C75-CoA formed in the reaction. According to this molecular mass, CoA-SH binds to C75 by opening the furan group (Figure 6B), without the loss of a water molecule. A similar analysis was performed for etomoxir (Figure 1B). This figure shows a peak of 1064.0 Da for etomoxiryl-CoA. The chemical structure of the product formed is shown in Figure 6B, in which the CoA-SH binds to etomoxir by opening the epoxid group, without the loss of a water molecule. Other peaks correspond to products derived from CoA, C75, or etomoxir.

Effects of C75 and C75-CoA on Yeast-Expressed L- and M-CPT I Activity. Increasing concentrations of synthesized C75-CoA or etomoxiryl-CoA were independently incubated with yeast-overexpressed mitochondrial L- or M-CPT I. Both

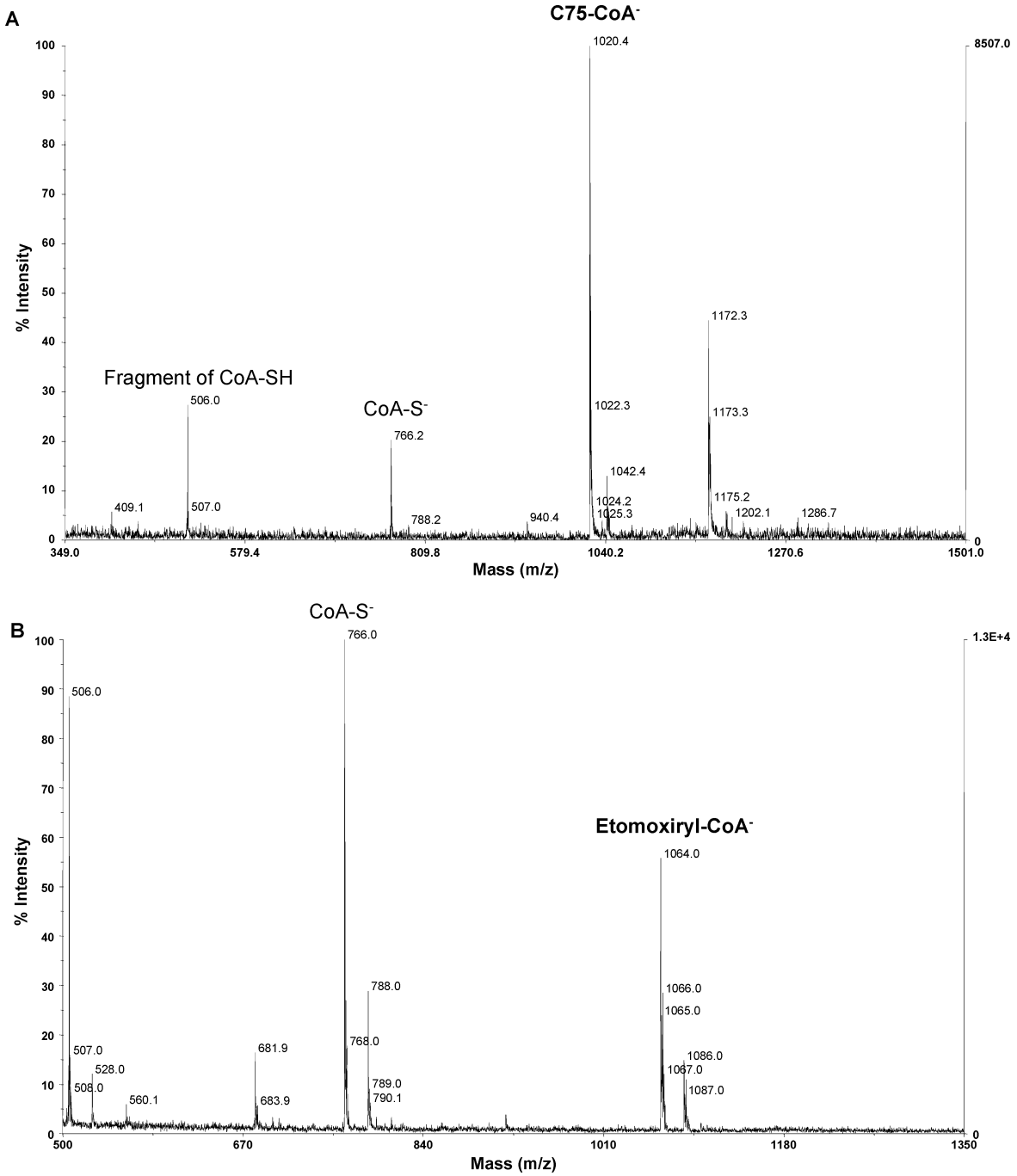

FIGURE 1: MALDI-TOF spectra of C75-CoA and etomoxiryl-CoA. Spectra were directly obtained from the reaction product of C75 and CoA-SH, and etomoxir and CoA-SH using a Voyager-DE-RP from Applied Biosystems with DHB (10 mg/mL in a 1:1 water/methanol mixture). Detection was accomplished with a reflector and in the negative mode. The product C75-CoA (A) is confirmed by the peak at 1020.4 Da and etomoxiryl-CoA (B) by the peak at 1064.0 Da.

CoA derivatives strongly inhibited L- and M-CPT I isoforms with similar kinetics (Figure 2). Almost complete inhibition of CPT I was observed at 50 μM C75-CoA. IC_{50} values for C75-CoA were 0.24 and 0.36 μM for L- and M-CPT I isoforms, respectively (Table 1). IC_{50} values for etomoxiryl-CoA were 4.06 and 3.10 μM for L- and M-CPT I isoforms, respectively (Table 1). Only the CoA derivatives inhibited CPT I activity. When mitochondrial yeast extracts were incubated with 40 or 200 μM C75, a 20−30% increase in CPT I activity was observed. However, etomoxir did not produce CPT I activation.

Analysis of Binding of C75-CoA to CPT I. To assess whether binding of C75-CoA to CPT I is stable, yeast mitochondria-enriched fractions overexpressing L-CPT I were incubated with 50 μM C75-CoA, etomoxiryl-CoA, or malonyl-CoA, or with buffer alone as a control. Following preincubation for 5 min, the effects of washing were tested. Extracts were assayed directly (unwashed samples) or centrifuged and resuspended in buffer (washed samples) (see Experimental Procedures) and assayed for CPT I activity. As shown in Figure 3A, the inhibition by malonyl-CoA was lost when extracts were washed, with CPT I activity recovering by 91% with respect to the washed control. However, both C75-CoA and etomoxiryl-CoA produced persistent inhibition, at levels of 75 and 79%, respectively, with respect to washed control fractions. The experiments

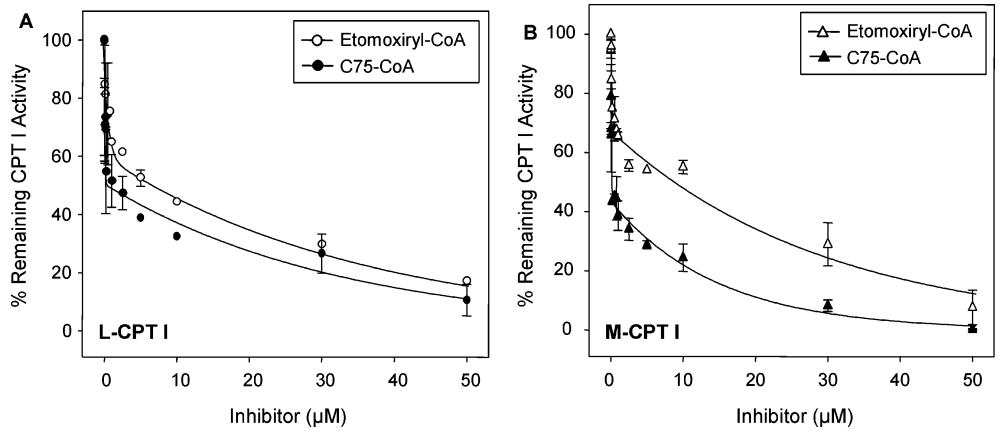

FIGURE 2: Effects of C75-CoA and etomoxiryl-CoA on the activity of liver (L) and muscle (M) isoforms of CPT I overexpressed in yeast *S. cerevisiae*. L-CPT I (A) and M-CPT I (B) were overexpressed in yeast and mitochondrial fractions were preincubated for 5 min with increasing concentrations of etomoxiryl-CoA (○ and △) and C75-CoA (● and ▲). CPT I activity was measured, and data are expressed relative to control values in the absence of drugs (100%) as the mean of three independent experiments.

Table 1: IC_{50} Values of CPT I for C75-CoA and Etomoxiryl-CoA[a]

	IC_{50} (μM)	
	C75-CoA	etomoxiryl-CoA
yeast overexpressing L-CPT I	0.24 ± 0.01	4.06 ± 0.78
yeast overexpressing M-CPT I	0.36 ± 0.18	3.10 ± 0.06
rat liver	0.25 ± 0.13	0.70 ± 0.10
rat muscle	0.015 ± 0.005	0.04 ± 0.01
INS(832/13) cells	0.25 ± 0.16	1.21 ± 0.35
L6E9 myotubes	0.46 ± 0.21	2.87 ± 0.8

[a] Mitochondrial fractions obtained from rat liver, rat muscle, cultured cells, and yeast overexpressing CPT I were assayed for CPT I activity in the presence of C75-CoA and etomoxiryl-CoA. IC_{50} values were calculated as described in Experimental Procedures.

with C75-CoA and etomoxiryl-CoA demonstrate that they were tightly bound to CPT I.

Fifty and one hundred percent of the CPT I activity was recovered after dialysis for 24 and 36 h, respectively, in C75-CoA-treated fractions, though not in those treated with etomoxiryl-CoA (Figure 3B). The C75-CoA−protein complex was undone during dialysis, showing tight but reversible binding. In contrast, there was no CPT I activity recovery when etomoxiryl-CoA was used, which is consistent with data demonstrating that protein and etomoxiryl-CoA formed covalent adducts.

C75-CoA Inhibits CPT I Activity. To examine whether the CPT I enzyme source could modify the response to C75-CoA, we carried out additional experiments with freshly isolated mitochondria from rat liver (L-CPT I) and rat muscle (M-CPT I). Both C75-CoA and etomoxiryl-CoA inhibited CPT I activity with similar kinetics (Figure 4A,B). CPT I from fresh mitochondria proved to be more sensitive than that from yeast extract; at 10 μM CoA derivative, CPT I was almost completely inhibited. IC_{50} values for C75-CoA were 0.25 and 0.015 μM for CPT I from rat liver and rat muscle, respectively (Table 1). IC_{50} values for etomoxiryl-CoA were 0.70 and 0.04 μM for CPT I from rat liver and rat muscle, respectively (Table 1). C75-CoA appears to be a stronger inhibitor for M- than for L-CPT I.

The inhibitory effects of C75-CoA and etomoxiryl-CoA were also tested on purified mitochondria from pancreas [INS(832/13)] and muscle (L6E9) cultured cell lines. In all cases, CPT I activity was strongly inhibited by increasing concentrations of both CoA derivatives (Figure 4C,D). The

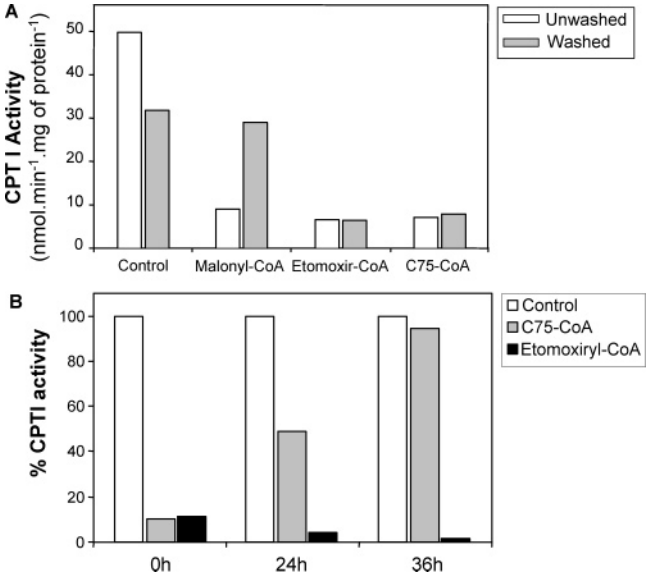

FIGURE 3: Analysis of binding of C75-CoA to L-CPT I activity overexpressed in yeast *S. cerevisiae*. (A) Three micrograms of mitochondria from yeast overexpressing L-CPT I was preincubated for 5 min with 50 μM C75-CoA, etomoxiryl-CoA, and malonyl-CoA and washed with buffer or left unwashed, as described in Experimental Procedures. Specific activity is represented as the mean of three independent experiments. (B) The resulting 160 μg of mitochondria-enriched fractions from yeast cells expressing L-CPT I was preincubated at 30 °C for 5 min without the drug or with a final concentration of 50 μM C75-CoA or 50 μM etomoxiryl-CoA and then dialyzed. Aliquots were taken prior to dialysis (0 h) and 24 and 36 h after dialysis and assayed for CPT I activity.

IC_{50} values for C75-CoA were 0.25 and 0.46 μM for INS-(812/13) and L6E9 cells, respectively. The IC_{50} values for etomoxiryl-CoA were 1.21 and 2.87 μM for INS(823/13) and L6E9 cells, respectively (Table 1). C75-CoA was a more potent CPT I inhibitor than etomoxiryl-CoA in all cases.

To define the type of inhibition of C75-CoA on CPT I activity, we performed experiments with varying C75-CoA and palmitoyl-CoA concentrations. Lineweaver−Burk plots for CPT I activity at different palmitoyl-CoA concentrations for the enzyme were linear (Figure 5). The palmitoyl-CoA concentrations ranged from 1 to 100 μM. The observed K_m values for palmitoyl-CoA were 4.5, 33.6, 61.6, and 126.0 μM at C75-CoA concentrations of 0, 1, 2, and 5 μM, respectively, but no change was observed in the intrinsic

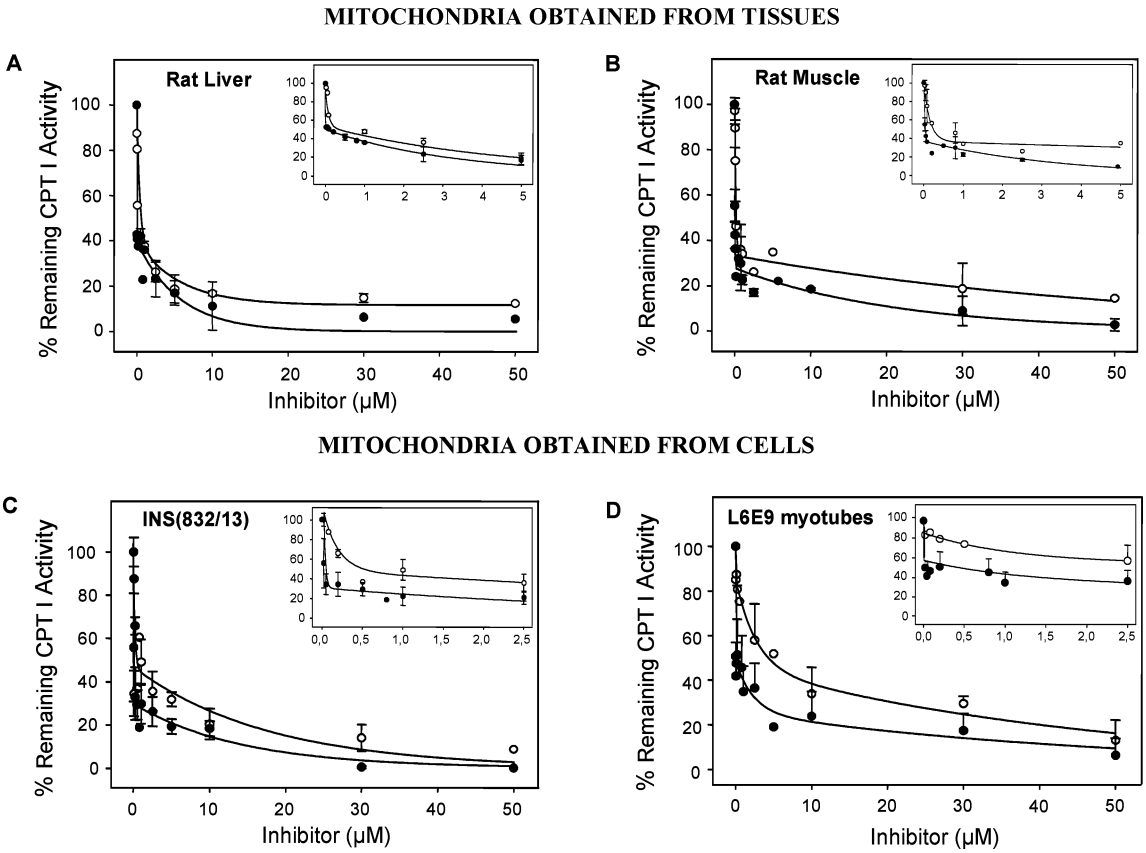

FIGURE 4: Effects of C75-CoA and etomoxiryl-CoA on CPT I activity. Mitochondria isolated from rat liver (A), rat muscle (B), INS(823/13) cells (C), or L6E9 myotubes (D) were preincubated for 1 min with increasing concentrations of C75-CoA (●) or etomoxiryl-CoA (○), and CPT I activity was assayed as described in Experimental Procedures. Data represent the mean of at least three independent experiments and are expressed relative to control values in the absence of the inhibitor (100%). The inset shows an expanded dose−response curve for the two inhibitors.

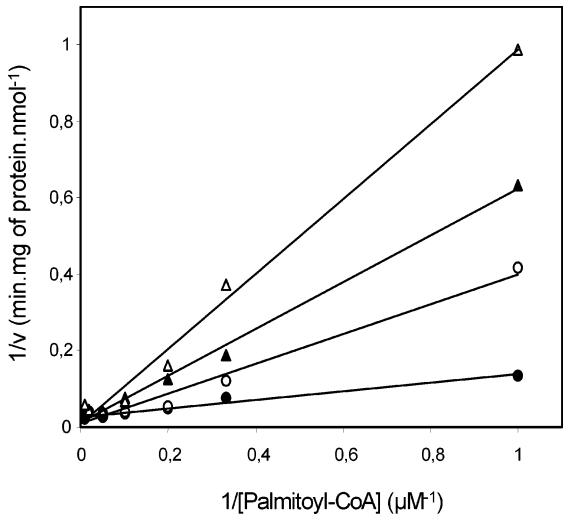

FIGURE 5: Lineweaver−Burk plot for the inhibition of L-CPT I by C75-CoA. Mitochondria-enriched fractions from yeast-overexpressed L-CPT I (3−4 μg) were preincubated with C75-CoA for 5 min and then incubated for 4 min at 30 °C with various palmitoyl-CoA concentrations in the presence of 400 μM carnitine. The concentrations of C75-CoA were (●) 0, (○) 1, (▲) 2, and (△) 5 μM. Each point is the mean of two different experiments.

catalytic activity of the enzyme (3.98 ± 0.83 nmol min^{-1} mg^{-1}). Inhibition constants were determined by nonlinear regression analysis and were 0.23 ± 0.08 μM for the apparent inhibition constant (K_I) and 0.09 ± 0.004 min^{-1} for the inactivation constant (k_{inact}). The results of the inhibition kinetics revealed that C75-CoA is a competitive inhibitor with respect to palmitoyl-CoA.

Molecular Model of Docking of C75-CoA into L-CPT I. The recent crystallization of carnitine octanoyltransferase (COT) (*28*), a member of the carnitine acyltransferase family, allowed us to improve the previous three-dimensional model of CPT I based on the carnitine acetyltransferase crystal (*32*). Using docking analysis, an in silico model was constructed for the interaction between the active center of CPT I and C75-CoA (Figure 5A). Refined in silico docking techniques were used, allowing free rotation of the ligand acyl chain bonds. This model suggests that the inhibitor C75-CoA fits into the enzyme in a manner similar to that of the physiological substrate palmitoyl-CoA. While the CoA segment in both molecules is positioned in almost the same orientation, the aliphatic tail of C75 fits into the hydrophobic cavity of CPT I defined by α-helix 12 and β-strands 1, 13, and 14 of the protein, just where the acyl group of palmitoyl-CoA is most likely positioned during normal enzymatic processes. The head of C75, bound to the sulfur atom of CoA, is located in the proximity of the catalytic residue His473.

Effects of C75 on CPT I Activity and Fatty Acid Oxidation in Cultured Cells. To assess whether CPT I inhibition is followed by a similar decrease in the extent of fatty acid oxidation, the three cultured cell lines [INS(812/13), L6E9, and HEK293] were incubated with C75 or etomoxir. It was not necessary in this case to transform the drugs to their CoA derivatives, since this conversion is assumed to occur inside the cells via endogenous acyl-CoA synthetase. CPT I activity

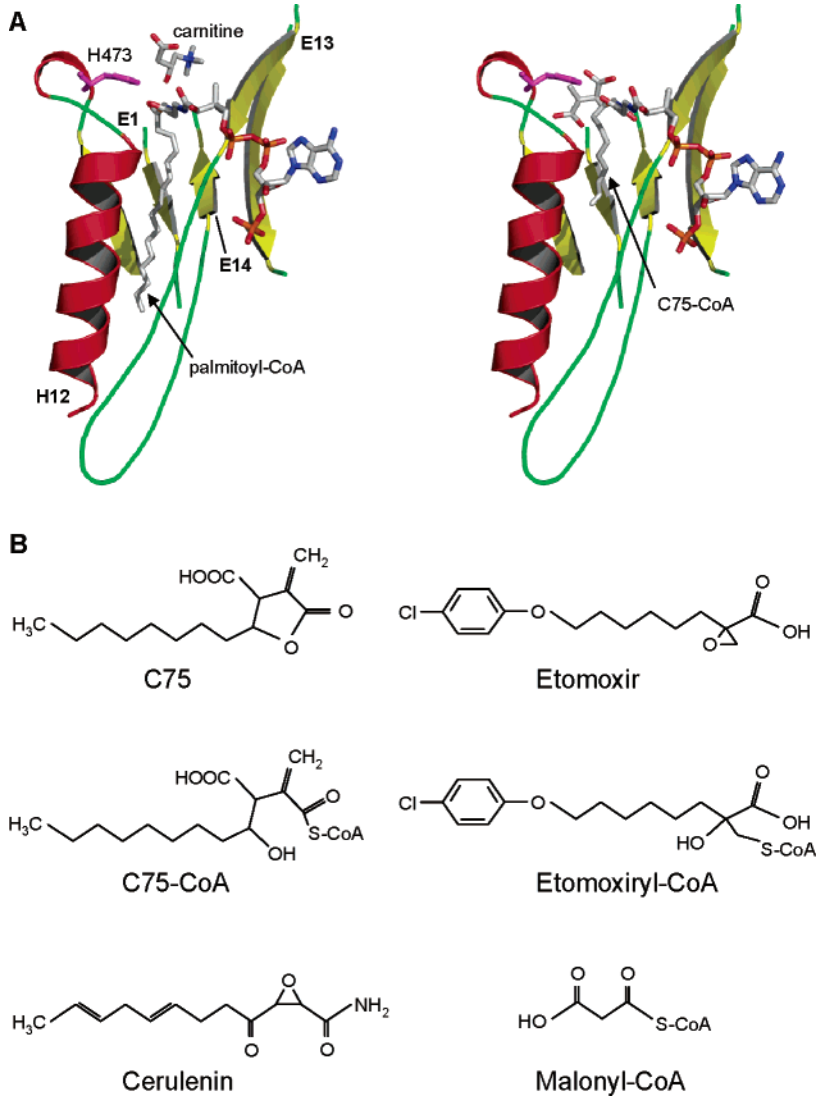

FIGURE 6: Proposed model for the location of C75-CoA in the CPT I active center. (A) Comparison of the location of a molecule of palmitoyl-CoA in the active center of CPT I (left) and the proposed model for the location of C75-CoA in the same enzyme locus (right). The positions of carnitine and catalytic His473 (magenta), as well as secondary structure elements α-helix 12 and β-strands 1, 13, and 14, surrounding the acyl cavity, are indicated. The aliphatic tail of the inhibitor molecule is located in the hydrophobic pocket present in the CPT I active center, a position similar to that proposed for the substrate. The "head" of C75 occupies the central cavity of the enzyme. (B) Structures of known compounds affecting CPT I activity are included at the bottom for comparison.

decreased with increasing C75 concentrations (Figure 7). CPT I activity was reduced by 49, 62, and 62% in pancreatic INS(832/13), muscle L6E9, and kidney HEK293 cells, respectively, at maximal C75 concentrations of 30, 40, and 30 μg/mL, respectively. In parallel, the level of [1-^{14}C]-palmitate oxidation was reduced by 62, 84, and 68% in pancreatic INS(832/13), muscle L6E9, and kidney HEK293 cells, respectively, at maximal C75 concentrations of 30, 40, and 30 μg/mL, respectively. When etomoxir was used, CPT I activity was reduced by 80, 52, and 71% in pancreatic INS-(832/13), muscle L6E9, and kidney HEK293 cells, respectively, while the level of palmitate oxidation was consequently reduced by 71, 78, and 77%, respectively. To rule out the possibility that the inhibition of palmitate oxidation reflected an increase in the level of cell death caused by C75 or etomoxir, we performed viability experiments using the MTT assay. In all cases, cell viability at the drug concentrations that were used was higher than 98% of that of control samples.

Effects of C75 Treatment on Whole Animals. We examined the effect of C75 on CPT I activity in vivo. Mice were injected (ip) with a single dose of either C75 or etomoxir (20 mg/kg of body weight) and killed at different time points thereafter. Tissue samples (liver, soleus, and pancreas) were taken to isolate mitochondria, as described in Experimental Procedures. CPT I activity decreased rapidly in all tissues that were assayed (Figure 8) but subsequently recovered, with tissue-dependent kinetics. The level of inhibition of liver CPT I decreased by 56% at 1 h and by 73% after treatment for 3 h, while at 5 h, CPT I values were similar to those of the control. Muscle CPT I was inhibited by 80% after being treated for 30 min, recovering more rapidly than liver CPT I. In the pancreas, CPT I activity decreased by 36% after C75 treatment for 30 min, compared with the control, recovering thereafter. In no case did the level of CPT I activation exceed the control. Etomoxir also provoked an inhibition of CPT I activity in these tissues (Figure 8). After treatment for 3 h, the levels of CPT I inhibition were 97,

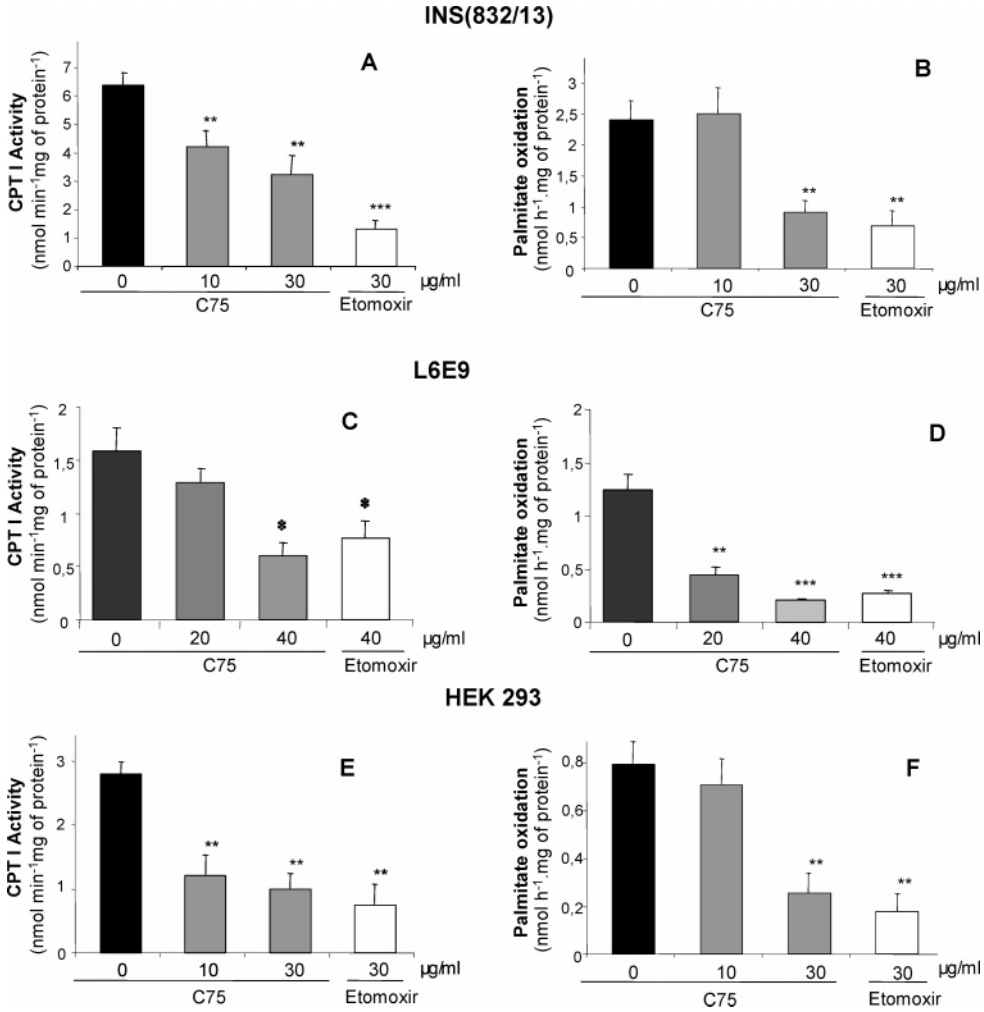

FIGURE 7: CPT I activity and palmitate oxidation in cell cultures. Cells were incubated for 2 h (L6E9) or 1 h [INS(832/13) and HEK293] with complete medium containing either 0, 10, 20, 30, and 40 μg/mL C75 or 30 and 40 μg/mL etomoxir. Mitochondria-enriched cell fractions were obtained, and 10 μg of protein was used for the CPT I activity assay. In palmitate oxidation assays, cells were preincubated for 30 min at 37 °C with KRBH with 1% BSA and then incubated for 2 h at 2.5 mM glucose in the presence of 0.8 mM carnitine, 0.25 mM palmitate, and 1 μCi/mL [1-^{14}C]palmitate. Palmitate oxidation to CO_2 was assessed as described in Experimental Procedures. Data are presented as the mean ± the standard error of three independent experiments. *P < 0.05, **P < 0.01, and ***P < 0.001 compared with the control without inhibitors.

71, and 60% in liver, muscle, and pancreas, respectively, and they were always lower than those observed following C75 treatment. These inhibitory effects of etomoxir on CPT I activity, unlike those observed following C75 treatment, were maintained for up to 5 h, producing 96, 82, and 72% CPT I inhibition in liver, muscle, and pancreas, respectively.

DISCUSSION

In this study, we show that C75 and etomoxir were transformed to their CoA derivatives by the action of an acyl-CoA synthetase. Within the cell, acyl-CoAs are formed as part of the metabolism of a variety of endogenous fatty acids, as well as some xenobiotic carboxylic acids. The synthesis of CoA derivatives is the rate-limiting step for both conjugation and inactivation of most xenobiotics. CoA conjugates increase the chemical reactivity of these compounds and may function as alternative substrates in intermediate metabolism pathways of short-, medium-, and long-chain fatty acids (*33*). Distinct mammalian long-chain and xenobiotic/medium-chain fatty acid:CoA ligases [termed acyl-CoA synthetase in revised nomenclature (*34*)] can activate long-chain, xenobiotic, and medium-chain fatty acids. The substrate specificity and intracellular location of the acyl-CoA synthetases may explain the rate differences in the synthesis of the xenobiotic-CoA derivatives and their possible toxicity. Although C75 is a potential substrate for acyl-CoA synthetase, due to its aliphatic C8 chain and its esterifiable carboxylate groups, no studies have addressed this fact. The MALDI-TOF analysis performed in this study showed that C75-CoA was synthesized when C75 was incubated in vitro in the presence of CoA, long-chain acyl-CoA synthetase, and ATP.

Compounds such as etomoxir, TDGA, and POCA must be converted to their CoA derivative before acting as inhibitors of CPT I activity (*12*). In the same way, when C75 is transformed into its CoA derivative, it also becomes a potent inhibitor of CPT I. Under all the in vitro conditions that were tested, CPT I was clearly inhibited in a dose-dependent manner by C75-CoA. IC_{50} values observed for C75-CoA ranged from the micromolar level to the nanomolar level and were lower than those obtained for etomoxiryl-CoA, showing that C75-CoA is a stronger CPT I inhibitor

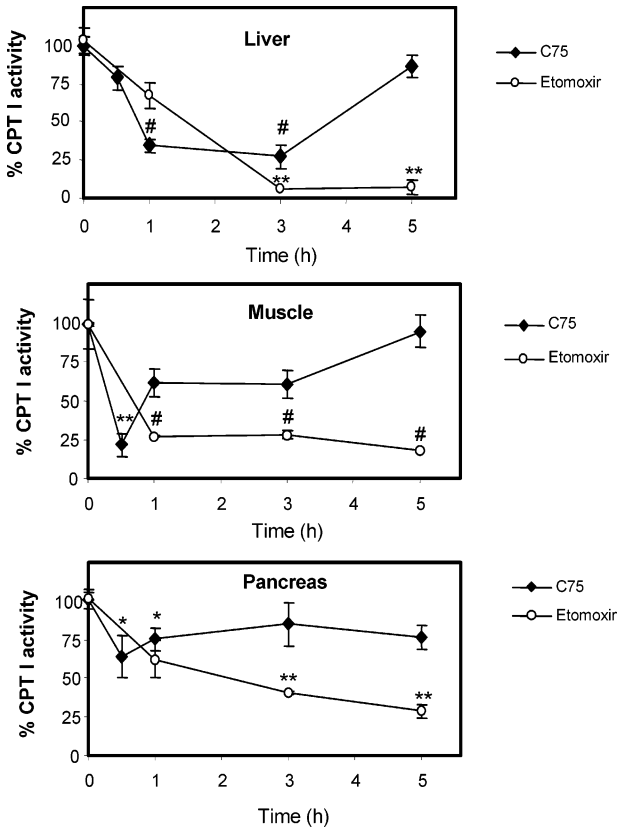

FIGURE 8: C75 effects on the whole animal. C75 or etomoxir was injected in an ip manner in mice, and animals were killed 0, 0.5, 1, 3, and 5 h after injection. Mitochondria-enriched fractions from liver, soleus, and pancreas were obtained, and CPT I activity was assayed. Results represent the mean ± the standard error of data obtained from six mice. $^{*}P < 0.05$, $^{**}P < 0.01$, $^{\#}P < 0.001$ vs control (0 h).

than etomoxiryl-CoA. It is well-known that the M-CPT I isoform is more sensitive than L-CPT I to its physiological inhibitor malonyl-CoA. This effect was also observed for C75-CoA. The IC_{50} value for C75-CoA acting on L-CPT I from liver mitochondrial fractions was 16-fold higher than that observed for the M-CPT I isoform from muscle mitochondria. However, these differences were not observed in overexpressed yeast extracts, which most likely reflects the expression of these proteins in a foreign system. In L6E9 myotubes, the IC_{50} value was similar to that observed in rat liver and INS(832/13) cells, consistent with the fact that L6E9 myotubes express the L-CPT I isoform rather than M-CPT I (*35*). Consistent with the results obtained by Yang et al. (*36*) and Nicot et al. (*37*), we also observed an increase in CPT I activity when incubating C75 alone with yeast extracts. Nevertheless, it is important to stress that the concentration of C75 alone (200 μM) used to produce maximal CPT I activation was at least 100-fold higher than that of C75-CoA (0.25 and 0.015 μM) needed to produce 50% CPT I inhibition. This suggests that C75-CoA, rather than C75 alone, is the agent responsible for these effects in vivo.

The two known CPT I inhibitors, malonyl-CoA and etomoxiryl-CoA, bind to the enzyme in different ways. Malonyl-CoA binding is reversible and not tight, consistent with its physiological role as a regulator of CPT I activity and β-oxidation, adapting its binding to each metabolic situation. Etomoxiryl-CoA is a synthetic drug designed to inhibit CPT I strongly and permanently (*38*). C75-CoA exhibited certain different CPT I binding characteristics with respect to these two inhibitors. On one hand, C75-CoA bound more tightly than malonyl-CoA, as it was not released by washing. On the other hand, it also bound noncovalently, in contrast to etomoxiryl-CoA, as C75-CoA was removed by dialysis. However, the presence of carboxylic groups and the hydrocarbon chain, both in C75 and in etomoxir (Figure 5B), suggests a common mode of interaction for these two inhibitors with the active center of CPT I. Our three-dimensional model illustrating the interaction of C75-CoA with the active center of CPT I indicated a common location for the substrate palmitoyl-CoA and the inhibitor. The main differences between the two molecules, apart from the length of the hydrocarbon chain introduced into the hydrophobic cavity, are the size and chemical characteristics of the C75 "head", which is absent in the case of the natural substrate. These three-dimensional data and those from the kinetic experiments suggest a competitive mechanism between the substrate and C75-CoA. Three-dimensional data intriguingly fail to explain the action of C75 alone as a CPT I activator. Although Yang et al. (*36*) deduced from competitive binding experiments that C75 alone binds to different malonyl-CoA sites, the exact site at which it interacts with CPT I has yet to be determined. The lack of a CPT I crystal and the lack of a computer-generated partial three-dimensional model containing the N-terminal domain of the enzyme essential to the regulation of CPT I activity are the main handicaps to performing new docking studies which would explain C75 binding and CPT I activation.

The results obtained in cultured pancreatic, muscle, and kidney cells suggest that C75 is transformed to its CoA derivative by endogenous acyl-CoA synthetase and intracellular ATP, since the decrease in the level of palmitate oxidation correlated with the inhibition of CPT I activity. In all cases, etomoxir was used as a control of transformation, inhibition, and oxidation. To rule out the possibility that the decrease in the level of palmitate oxidation was produced by C75 cytotoxicity, viability studies were performed. Under our conditions, the viability of the three cellular models proved to be higher than 98%. Therefore, the cytotoxicity experiments provided evidence that the decrease in CPT I activity was not generated by cellular death. Instead, C75-CoA appears to be the true inhibitory molecule of CPT I activity. Depending on lipid composition and metabolism, each cell line may become more sensitive to the cytotoxic effects of C75. For instance, pancreatic INS(832/13) β-cells and kidney HEK293 cells were incubated for shorter time periods and at lower C75 concentrations than L6E9 myotubes. Other studies performed in SKBR3 breast carcinoma cells, which have a higher lipid content, exhibited increased cytotoxicity resistance. This cell line required C75 preincubation for 6 h to achieve the same cytotoxic effects (*39*).

Discrepancies with the findings of others, who observed CPT I activation in primary hepatocytes, in adipocytes, and in MCF-7 cells following C75 treatment, could be attributable to methodological differences (*7*, *36*). Therefore, while Thupari et al. (*7*) studied permeabilized cells, we isolated purified mitochondria from tissues and from cultured cells. We believe that digitonin permeabilization, in tandem with C75 treatment, may affect the interactions between mitochondria and the cytoskeleton (*40*), thereby either altering CPT I activity or disturbing the assay. In this context, it has

been suggested that changes in the lipid composition of CPT I's membrane microenvironment may be important for alterations in CPT I activity (*41*, *42*).

Our in vitro experiments were also corroborated by in vivo experiments. A single intraperitoneal C75 injection produced a short-term inhibition of CPT I in mouse liver, muscle (soleus), and pancreas. In all tissues that were analyzed, CPT I activity returned to control levels after treatment for 5 h. The extent of CPT I inhibition observed in various tissues may reflect differences in the pharmacokinetics of each tissue or, alternatively, the rate of endogenous C75-CoA transformation. In contrast, the inhibition by etomoxir was maximal at 5 h. This can be explained by the fact that etomoxir covalently binds to CPT I, but C75-CoA appears to be a strong and a reversible inhibitor.

Cerulenin, the natural FAS inhibitor which formed the basis of C75's design, has been shown to inhibit CPT I and fatty acid oxidation. Our results on the effects of C75 on CPT I activity and fatty acid oxidation are similar to those reported by other groups working with cerulenin. In pancreatic islets, the level of palmitate oxidation was reduced following cerulenin incubation (*43*), consistent with our results in pancreatic cultured cells incubated with C75. In mice, cerulenin inhibits liver and muscle CPT I activity after ip injection, subsequently recovering and becoming slightly activated after a few hours (*44*). These authors concluded that the late stimulating effects of cerulenin on CPT I activity occurred via the sympathetic nervous system. Indeed, C75 may behave like cerulenin in mice, producing a biphasic effect on CPT I, i.e., an initial inhibition followed by recovery. The short-term CPT I inhibition witnessed in our experiments following ip C75 injection in mice is consistent with results obtained by Clegg et al. (*45*), who observed a reduction in the peripheral energy expenditure of rats 12 h after an ip dose of C75. Furthermore, it has recently been demonstrated that intra-cerebroventricular C75 administration increased the level of fatty acid oxidation in muscle, which was mediated by the sympathetic nervous system (*46*). Thus, the recovery of CPT I activity reported in this study might be explained if we weigh the possibility that the central C75 effect overcomes the short-term C75 peripheral action.

Finally, the fact that C75 could be transformed into its C75-CoA derivative in vivo may have implications not only for CPT I activity but also for FAS and other enzymes in different cellular pathways. This observation may explain certain contradictory findings recently published by Rohrbach et al. (*47*). These authors observed that the maximal C75 concentration in plasma was 2.6 μM after ip administration of C75 at 30 mg/kg (a concentration that suppresses appetite within 4 h), which was substantially lower than that needed to inhibit FAS in vitro ($IC_{50} \sim 200$ μM). They postulated that these results could only be explained if C75's effect on appetite suppression was independent of its inhibition of FAS in the hypothalamus. An alternative explanation would be that a metabolic product more potent than C75 (i.e., C75-CoA) might act on FAS.

In conclusion, the results presented here provide compelling evidence that C75-CoA is a potent and direct inhibitor of the two isoforms L- and M-CPT I in vitro and in vivo. Moreover, our findings suggest that both in cellular models and in lean mice C75 is expected to be transformed into its CoA derivative, thereby directly inhibiting CPT I activity.

ACKNOWLEDGMENT

We thank Dr. Yamazaki for supplying plasmid DS112-36 containing the cDNA from rat M-CPT I. The rat insulinoma INS (832/13) was kindly given by Dr. M. Prentki (University of Montreal, Montreal, PQ). The L6E9 rat skeletal muscle cell line was kindly provided by Dr. A. Zorzano (University of Barcelona). We are also grateful to Robin Rycroft of the Language Service for valuable assistance in the preparation of the manuscript.

REFERENCES

1. Price, A. C., Choi, K.-H., Heath, R. J., Li, Z., White, S. W., and Rock, C. O. (2001) Inhibition of β-ketoacyl-acyl carrier protein synthases by thiolactomycin and cerulenin. Structure and mechanism, *J. Biol. Chem. 276*, 6551−6559.
2. Rendina, A. R., and Cheng, D. (2005) Characterization of the inactivation of rat fatty acid synthase by C75: Inhibition of partial reactions and protection by substrates, *Biochem. J. 388*, 895−903.
3. Li, J.-N., Gorospe, M., Chrest, F. J., Kumaravel, T. S., Evans, M. K., Han, W. F., and Pizer, E. S. (2001) Pharmacological inhibition of fatty acid synthase activity produces both cytostatic and cytotoxic effects modulated by p53, *Cancer Res. 61*, 1493−1499.
4. Loftus, T. M., Jaworsky, D. E., Frehywot, G. L., Townsend, C. A., Ronnett, G. V., Lane, M. D., and Kuhajda, F. P. (2000) Reduced food intake and body weight in mice treated with fatty acid synthase inhibitors, *Science 288*, 2379−2381.
5. Hu, Z., Cha, S. H., Chohnan, S., and Lane, M. D. (2003) Hypothalamic malonyl-CoA as a mediator of feeding behaviour, *Proc. Natl. Acad. Sci. U.S.A. 100*, 12624−12629.
6. Kim, E.-K., Miller, I., Landree, L. E., Borisy-Rudin, F. F., Brown, P., Tihan, T., Townsend, C. A., Witters, L. A., Moran, T. H., Kuhajda, F. P., and Ronnett, G. V. (2002) Expression of FAS within hypothalamic neurons: A model for decreased food intake after C75 treatment, *Am. J. Physiol. 283*, E867−E879.
7. Thupari, J. N., Landree, L. E., Ronnett, G. V., and Kuhajda, F. P. (2002) C75 increases peripheral energy utilization and fatty acid oxidation in diet-induced obesity, *Proc. Natl. Acad. Sci. U.S.A. 99*, 9498−9502.
8. McGarry, J. D., and Brown, N. F. (1997) The mitochondrial carnitine palmitoyltransferase system. From concept to molecular analysis, *Eur. J. Biochem. 244*, 1−14.
9. Price, N., van der Leij, F., Jackson, V., Corstorphine, C., Thomson, R., Sorensen, A., and Zammit, V. A. (2002) A novel brain-expressed protein related to carnitine palmitoyltransferase I, *Genomics 80*, 433−442.
10. Grantham, B. D., and Zammit, V. A. (1986) Restoration of the properties of carnitine palmitoyltransferase I in liver mitochondria during re-feeding of starved rats, *Biochem. J. 239*, 485−488.
11. Grantham, B. D., and Zammit, V. A. (1988) Role of carnitine palmitoyltransferase I in the regulation of hepatic ketogenesis during the onset and reversal of chronic diabetes, *Biochem. J. 249*, 409−414.
12. Selby, P. L., and Sherratt, H. S. A. (1989) Substitutted 2-oxiranecarboxylic acids: A new group of candidate hypoglycaemic drugs, *Trends Pharmacol. Sci. 10*, 495−500.
13. Taylor, D. C., Weber, N., Hogge, L. R., and Underhill, E. W. (1990) A simple enzymatic method for the preparation of radiolabeled erucoyl-CoA and other long-chain fatty acyl-CoAs and their characterization by mass spectrometry, *Anal. Biochem. 184*, 311−316.
14. Fritz, I. B., and Schultz, S. K. (1965) Carnitine acetyltransferase. Inhibition by carnitine analogues and by sulfhydryl reagents, *J. Biol. Chem. 240*, 2188−2192.
15. Morillas, M., Gómez-Puertas, P., Roca, R., Serra, D., Asins, G., Valencia, A., and Hegardt, F. G. (2001) Structural model of the catalytic core of carnitine palmitoyltransferase I and carnitine octanoyltransferase (COT): Mutation of CPT I histidine 473 and alanine 381 and COT alanine 238 impairs the catalytic activity, *J. Biol. Chem. 276*, 45001−45008.
16. Yamazaki, N., Shinohara, Y., Shima, A., and Terada, H. (1995) High expression of a novel carnitine palmitoyltransferase I like protein in rat brown adipose tissue and heart: Isolation and characterization of its cDNA clone, *FEBS Lett. 363*, 41−45.

17. Jackson, V. N., Cameron, J. M., Fraser, F., Zammit, V. A., and Price, N. T. (2000) Use of six chimeric proteins to investigate the role of intramolecular interactions in determining the kinetics of carnitine palmitoyltransferase I isoforms, *J. Biol. Chem. 275*, 19560−19566.
18. Asfari, M., Janjic, D., Meda, P., Li, G., Halban, P. A., and Wollheim, C. B. (1992) Establishment of 2-mercaptoethanol-dependent differentiated insulin-secreting cell lines, *Endocrinology 130*, 167−178.
19. Rubí, B., Antinozzi, P. A., Herrero, L., Ishihara, H., Asins, G., Serra, D., Wollheim, C. B., Maechler, P., and Hegardt, F. G. (2002) Adenovirus-mediated overexpression of liver carnitine palmitoyltransferase I in INS1E cells: Effects on cell metabolism and insulin secretion, *Biochem. J. 364*, 219−226.
20. Saggerson, E. D., and Carpenter, C. A (1981) Carnitine palmitoyltransferase and carnitine octanoyltransferase activities in liver, kidney cortex, adipocyte, lactating mammary gland, skeletal muscle and heart, *FEBS Lett. 129*, 229−232.
21. Saggerson, E. D. (1982) Carnitine palmitoyltransferase activities in rat liver and heart measured with palmitoyl-CoA and octanoyl-CoA, *Biochem. J. 202*, 397−405.
22. Li, G., Kowluru, A., and Metz, S. A. (1996) Characterization of prenylcysteine methyltransferase in insulin-secreting cells, *Biochem. J. 316*, 345−351.
23. Kitz, R., and Wilson, I. B (1962) Esters of methanesulfonic acid as irreversible inhibitors of acetylcholinesterase, *J. Biol. Chem. 237*, 3245−3249.
24. Maurer, T., and Fung, H. L. (2000) Comparison of methods for analyzing kinetic data from mechanism-based enzyme inactivation: Application to nitric oxide synthase, *AAPS Pharm. Sci. 2* (1), E8.
25. Tutwiler, G. F., and Ryzlak, M. T. (1980) Inhibition of mitochondrial carnitine palmitoyl transferase by 2-tetradecylglycidic acid (McN-3802), *Life Sci. 26*, 393−397.
26. Collins, C. L., Bode, B. P., Souba, W. W., and Abcouwer, S. F. (1998) Multiwell $^{14}CO_2$-capture assay for evaluation of substrate oxidation rates of cells in culture, *BioTechniques 24*, 803−808.
27. Mosmann, T. (1983) Rapid colorimetric assay for cellular growth and survival: Application to proliferation and cytotoxicity assays, *J. Immunol. Methods 65*, 55−63.
28. Jogl, G., Hsiao, Y. S., and Tong, L. (2005) Crystal structure of mouse carnitine octanoyltransferase and molecular determinants of substrate selectivity, *J. Biol. Chem. 280*, 738−744.
29. Stewart, J. J. (1990) MOPAC: A semiempirical molecular orbital program, *J. Comput.-Aided Mol. Des. 4*, 1−45.
30. Goodsell, D. S., Morris, G. M., and Olson, A. J. (1996) Automated docking of flexible ligands: Applications of AutoDock, *J. Mol. Recognit. 9*, 1−5.
31. Morris, G. M., Goodsell, D. S., Halliday, R. S., Huey, R., Hart, E., Belew, R. K., and Olson, A. J. (1998) Automated Docking Using a Lamarckian Genetic Algorithm and Empirical Binding Free Energy Function, *J. Comput. Chem. 19*, 1639−1662.
32. Morillas, M., López-Viñas, E., Valencia, A., Serra, D., Gómez-Puertas, P., Hegardt, F. G., and Asins, G. (2004) Structural model of carnitine palmitoyltransferase I based on the carnitine acetyltransferase crystal, *Biochem. J. 379*, 777−784.
33. Knights, K. M. (1998) Role of hepatic fatty acid:coenzyme A ligases in the metabolism of xenobiotic carboxylic acids, *Clin. Exp. Pharmacol. Physiol. 10*, 776−782.
34. Mashek, D. D. G., Bornfeldt, K. E., Coleman, R. A., Berger, J., Bernlohr, D. A., Black, P., DiRusso, C. C., Farber, S. A., Guo, W., Hashimoto, N., Khodiyar, V., Kuypers, F. A., Maltais, L. J., Nebert, D. W., Renieri, A., Schaffer, J. E., Stahl, A., Watkins, P. A., Vasiliou, V., and Yamamoto, T. T. (2004) Revised nomenclature for the mammalian long-chain acyl-CoA synthetase gene family, *J. Lipid Res. 45*, 1958−1961.
35. Perdomo, G., Commerford, S. R., Richard, A. M., Adams, S. H., Corkey, B. E., O'Doherty, R. M., and Brown, N. F. (2004) Increased β-oxidation in muscle cells enhances insulin-stimulated glucose metabolism and protects against fatty acid-induced insulin resistance despite intramyocellular lipid accumulation, *J. Biol. Chem. 279*, 27177−27186.
36. Yang, N., Kays, J. S., Skillman, T. R., Burris, L., Seng, T. W., and Hammond, C. (2005) C75 [4-methylene-2-octyl-5-oxo-tetrahydro-furan-3-carboxylic acid] activates carnitine palmitoyltransferase-1 in isolated mitochondria and intact cells without displacement of bound malonyl-CoA, *J. Pharmacol. Exp. Ther. 312*, 127−133.
37. Nicot, C., Napal, L., Relat, J., Gonzalez, S., Llebaria, A., Woldegiorgis, G., Marrero, P. F., and Haro, D. (2004) C75 activates malonyl-CoA sensitive and insensitive components of the CPT system, *Biochem. Biophys. Res. Commun. 325*, 660−666.
38. Weis, B. C., Cowan, A. T., Brown, N., Foster, D. W., and McGarry, J. D. (1994) Use of a selective inhibitor of liver carnitine palmitoyltransferase I (CPT I) allows quantification of its contribution to total CPT I activity in rat heart. Evidence that the dominant cardiac CPT I isoform is identical to the skeletal muscle enzyme, *J. Biol. Chem. 269*, 26443−26448.
39. Pizer, E. S., Thupari, J., Han, W. F., Pinn, M. L., Chrest, F. J., Frehywot, G. L., Townsend, C. A., and Kuhajda, F. P. (2000) Malonyl-coenzyme-A is a potential mediator of cytotoxicity induced by fatty-acid synthase inhibition in human breast cancer cells and xenografts, *Cancer Res. 60*, 213−218.
40. Guzmán, M., Velasco, G., and Geelen, M. J. (2000) Do cytoskeletal components control fatty acid translocation into liver mitochondria? *Trends Endocrinol. Metab. 11*, 49−53.
41. Zammit, V. A., Corstorphine, C. G., Kolodziej, M. P., and Fraser, F. (1998) Lipid molecular order in liver mitochondrial outer membranes, and sensitivity of carnitine palmitoyltransferase I to malonyl-CoA, *Lipids 33*, 371−376.
42. Zammit, V. A. (1999) Carnitine acyltransferases: Functional significance of subcellular distribution and membrane topology, *Prog. Lipid Res. 38*, 199−224.
43. Yajima, H., Komatsu, M., Yamada, S., Straub, S. G., Kaneko, T., Sato, Y., Yamauchi, K., Hashizume, K., Sharp, G. W., and Aizawa, T. (2000) Cerulenin, an inhibitor of protein acylation, selectively attenuates nutrient stimulation of insulin release: A study in rat pancreatic islets, *Diabetes 49*, 712−717.
44. Jin, Y.-J., Li, S.-Z., Zhao, Z.-S., An, J. J., Kim, R. Y., Kim, Y. M., Baik, J.-H., and Lim, S.-K. (2004) Carnitine palmitoyltransferase-1 (CPT-1) activity stimulation by cerulenin via sympathetic nervous system activation overrides cerulenin's peripheral effect, *Endocrinology 145*, 3197−3204.
45. Clegg, D. J., Wortman, M. D., Benoit, S. C., McOsker, C. C., and Seeley, R. J. (2002) Comparison of central and peripheral administration of C75 on food intake, body weight, and conditioned taste aversion, *Diabetes 51*, 196−201.
46. Cha, S. H., Hu, Z., Chohnan, S., and Lane, M. D. (2005) Inhibition of hypothalamic fatty acid synthase triggers rapid activation of fatty acid oxidation in skeletal muscle, *Proc. Natl. Acad. Sci. U.S.A. 102*, 14557−14562.
47. Rohrbach, K. W., Han, S., Gan, J., O'Tanyi, E. J., Zhang, H., Chi, C. L., Taub, R., Largent, B. L., and Cheng, D. (2005) Disconnection between the early onset anorectic effects by C75 and hypothalamic fatty acid synthase inhibition in rodents, *Eur. J. Pharmacol. 21*, 31−41.

BI052186Q

Supplemental Material can be found at:
http://www.jbc.org/cgi/content/full/M700885200/DC1

THE JOURNAL OF BIOLOGICAL CHEMISTRY VOL. 282, NO. 25, pp. 18212–18224, June 22, 2007
© 2007 by The American Society for Biochemistry and Molecular Biology, Inc. Printed in the U.S.A.

Definition by Functional and Structural Analysis of Two Malonyl-CoA Sites in Carnitine Palmitoyltransferase 1A*[S]

Received for publication, January 30, 2007, and in revised form, April 17, 2007 Published, JBC Papers in Press, April 23, 2007, DOI 10.1074/jbc.M700885200

Eduardo López-Viñas[‡‖1], Assia Bentebibel[§‖1], Chandrashekaran Gurunathan[§‖], Montserrat Morillas[§‖2], Dolores de Arriaga[¶], Dolors Serra[§‖], Guillermina Asins[§‖], Fausto G. Hegardt[§‖3], and Paulino Gómez-Puertas[‡‖]

From the [‡]Centro de Biología Molecular "Severo Ochoa" (Consejo Superior de Investigaciones Científicas-Universidad Autónoma de Madrid), Cantoblanco, E-28049 Madrid, Spain, [§]Departamento de Bioquímica y Biología Molecular, Facultad de Farmacia, Universidad de Barcelona, E-08028 Barcelona, Spain, [¶]Departamento de Biología Molecular, Universidad de León, E-24071 León, Spain, and [‖]CIBER Institute of Fisiopatología de la Obesidad y Nutrición (CB06/03), Instituto de Salud Carlos III, 28049 Madrid, Spain

Carnitine palmitoyltransferase 1 (CPT1) catalyzes the conversion of palmitoyl-CoA to palmitoylcarnitine in the presence of L-carnitine, thus facilitating the entry of fatty acids to mitochondria, in a process that is physiologically inhibited by malonyl-CoA. To examine the mechanism of CPT1 liver isoform (CPT1A) inhibition by malonyl-CoA, we constructed an *in silico* model of both its NH_2- and COOH-terminal domains. Two malonyl-CoA binding sites were found. One of these, the "CoA site" or "A site," is involved in the interactions between NH_2- and COOH-terminal domains and shares the acyl-CoA hemitunnel. The other, the "opposite-to-CoA site" or "O site," is on the opposite side of the enzyme, in the catalytic channel. The two sites share the carnitine-binding locus. To prevent the interaction between NH_2- and COOH-terminal regions, we produced CPT1A E26K and K561E mutants. A double mutant E26K/K561E (swap), which was expected to conserve the interaction, was also produced. Inhibition assays showed a 12-fold decrease in the sensitivity (IC_{50}) toward malonyl-CoA for CPT1A E26K and K561E single mutants, whereas swap mutant reverts to wild-type IC_{50} value. We conclude that structural interaction between both domains is critical for enzyme sensitivity to malonyl-CoA inhibition at the "A site." The location of the "O site" for malonyl-CoA binding was supported by inhibition assays of expressed R243T mutant. The model is also sustained by kinetic experiments that indicated linear mixed type malonyl-CoA inhibition for carnitine. Malonyl-CoA alters the affinity of carnitine, and there appears to be an exponential inverse relation between carnitine K_m and malonyl-CoA IC_{50}.

Carnitine palmitoyltransferase 1 (CPT1)[4] catalyzes the conversion of long-chain fatty acyl-CoAs to acylcarnitines in the presence of L-carnitine. This is the first step in the transport of long-chain fatty acids from the cytoplasm to the mitochondrial matrix, where they undergo β-oxidation. CPT1 is tightly regulated by its physiological inhibitor malonyl-CoA. This regulation allows CPT1 to signal the availability of lipid and carbohydrate fuels to the cell (1). Mammalian tissues express three isoforms: CPT1A (liver), CPT1B (muscle and heart), and CPT1C (brain), which are the products of different genes (2–4). CPT1A and -B have 62% amino acid identity, but they are differentially regulated by malonyl-CoA. CPT1A is inhibited to a much lesser extent than CPT1B, which may explain why fatty acid oxidation is more finely regulated in the heart than in the liver. CPT1 is a potential target for the treatment of metabolic disorders involving diabetes and coronary heart disease (5). The interaction between malonyl-CoA and CPT1C may be involved in the "malonyl-CoA signal" in hypothalamic neurons regulating food intake and peripheral energy expenditure (6).

It has been postulated that there are two malonyl-CoA binding sites in the molecule of CPT1A (7, 8). Kinetic studies indicate that there is a high affinity binding site and a low affinity binding site (9–13). The probable binding sites of malonyl-CoA in CPT1A were deduced to be at the COOH terminus, after the preparation of several CPT1A and CPT1B chimeras (14). Our group has reported that the conserved Met^{593}, which is located in the COOH-terminal domain, plays a critical permissive role in the interaction between the enzyme and malonyl-CoA. The mutation of this amino acid to serine abolished the malonyl-CoA sensitivity of CPT1A (15). However, the NH_2 terminus of CPT1A (residues 1–47) was also shown to influence the enzyme/inhibitor interaction. Mutation of either Glu^3 or His^5 reduced malonyl-CoA sensitivity (12, 16). In addition, the removal of the segment comprised between amino acids 3 and 18 in both CPT1A and CPT1B decreased sensitivity to malonyl-CoA, which emphasizes the importance of the NH_2 terminus before the first transmembrane region as a modulator of malonyl-CoA inhibition (17). Further, it has been demon-

* This study was supported by Dirección General de Investigación Científica y Técnica, Spain, Grants BMC2001-3048 and SAF2004-06843; Ajut de Suport als Grups de Recerca de Catalunya Grant 2005SGR-00733 (to F. G. H.); and a grant from Fundación Ramón Areces (to the Centro de Biología Molecular "Severo Ochoa"). The costs of publication of this article were defrayed in part by the payment of page charges. This article must therefore be hereby marked "*advertisement*" in accordance with 18 U.S.C. Section 1734 solely to indicate this fact.

[S] The on-line version of this article (available at http://www.jbc.org) contains supplemental Table S1.

[1] Both authors contributed equally to this work.

[2] Present address: Dept. de Ciencias Experimentales y de la Salud, Universidad Pompeu Fabra, Parc de Recerca Biomèdica de Barcelona, E-08003 Barcelona, Spain.

[3] To whom correspondence should be addressed: Dept. of Biochemistry and Molecular Biology, University of Barcelona, School of Pharmacy, Diagonal 643, E-08028 Barcelona, Spain. E-mail: fgarciaheg@ub.edu.

[4] The abbreviations used are: CPT1, carnitine palmitoyltransferase 1; CPT1A, carnitine palmitoyltransferase 1 liver isoform; CPT1B, carnitine palmitoyltransferase 1 muscle isoform; CPT2, carnitine palmitoyltransferase 2.

strated by a physico-chemical method that CPT1A adopts different conformational states that are more or less sensitive to malonyl-CoA inhibition. These conformational states also involve different degrees of proximity between specific residues within the NH_2- and COOH-terminal domains in conditions characterized by changes in malonyl-CoA sensitivity (18). Moreover, it has recently been observed that changes (whether insertions or deletions) in the length of the loop proximal to the transmembrane 2 region of CPT1A can increase its sensitivity to malonyl-CoA (19).

Several authors report data relating the inverse association between the effects of malonyl-CoA and carnitine on CPT1 activity. These can be summarized as follows: 1) in liver, the inhibitory effect of malonyl-CoA on CPT1 activity is weaker after starvation and ketosis, when the carnitine content of the cell increases (20, 21); 2) tissues in which CPT1 is most sensitive to malonyl-CoA (muscle and heart) require the highest concentration of carnitine to drive the reaction (22); 3) there is a reciprocal relationship between the affinity of carnitine and malonyl-CoA concentration, since malonyl-CoA increases the K_m of the enzyme for carnitine, and hence the inhibitory effect of malonyl-CoA varies with carnitine concentration (11, 23); 4) mutations designed to decrease malonyl-CoA sensitivity increase catalytic efficiency of CPT1 for carnitine, which appears to be roughly proportional to the extent of the alteration in malonyl-CoA sensitivity (15). This indicates that such mutants can position carnitine better at the catalytic site, thus displacing malonyl-CoA and reducing the inhibition of CPT1.

Since CPT1 has not been crystallized, many attempts have been made to identify the domains in CPT1 that may bind malonyl-CoA. However, the location of such binding sites has not yet been reported. In the present paper, we describe two putative binding sites for malonyl-CoA in rat CPT1A. They were inferred from the analysis of computational docking models developed for this interaction. The presence of malonyl-CoA on the protein-ligand interaction sites interferes with the positioning of carnitine. One of the sites, the "CoA site" or "A site," is involved in the interactions between its NH_2- and COOH-terminal domains, and the other, "opposite-to-CoA site" or "O site," only intervenes in the COOH-terminal domain. Mutations of specific amino acids from both NH_2 and COOH termini support their involvement in CPT1 malonyl-CoA sensitivity.

This model is also supported by kinetic experiments that indicated linear mixed type malonyl-CoA inhibition for carnitine, suggesting that the positioning of malonyl-CoA near to the carnitine binding locus produces competitive-noncompetitive inhibition. Furthermore, a linear inverse correlation between the logarithm of the IC_{50} for malonyl-CoA and the logarithm of K_m for carnitine was observed. Overall, these data indicate a close relationship between the effects of malonyl-CoA on CPT1 and its affinity for carnitine. This conclusion is supported not only by experimental data but also by the two putative binding sites for malonyl-CoA in the three-dimensional structural model of CPT1A deduced from docking calculations.

EXPERIMENTAL PROCEDURES

Construction of Site-directed Mutants—Plasmids, pYESLCPTI^{E26K}, pYESLCPTI^{K561E}, pYESLCPTI^{R45D}, pYESLCPTI^{D698R}, and pYESLCPTI^{R243T} were constructed using the QuikChange PCR-based mutagenesis procedure (Stratagene) with the plasmid pYESLCPTI^{wt}, obtained as previously described (15), as template. Plasmids containing double mutations pYESLCPTI$^{E26K/K561E}$, pYESLCPTI$^{R45D/D698R}$, and pYESLCPTI$^{R243T/A478G}$ were constructed using the same procedure with the plasmids pYESLCPTI^{E26K}, pYESLCPTI^{R45D}, and pYESLCPTI^{R243T} as templates, respectively. The primers used for PCR are described in supplemental Table 1. The appropriate substitutions and the absence of unwanted mutations were confirmed by sequencing the inserts in both directions with an Applied Biosystems 373 automated DNA sequencer.

Expression of CPT1A in Saccharomyces cerevisiae—The expression of the constructs containing wild type and mutants CPT1A in yeast cells and the preparation of the cell extracts were performed as described elsewhere (15). *S. cerevisiae* was chosen as an expression system for wild type and mutant CPT1A, because it does not have endogenous CPT1A activity.

Determination of Carnitine Acyltransferase Activity—Carnitine palmitoyltransferase activity was determined by the radiometric method as described elsewhere (15) with minor modifications. The substrates were L-[methyl-^{3}H]carnitine and palmitoyl-CoA. Enzyme activity was assayed for 4 min at 30 °C in a total volume of 200 μl.

Substrate saturation data were fitted to rectangular hyperbolae by nonlinear regression using the program EnzFitter (Biosoft). K_m was estimated by analyzing the data from three experiments. For determination of the apparent K_m for carnitine, palmitoyl-CoA concentration was fixed at 135 μM, and for determination of the K_m for palmitoyl-CoA, carnitine concentration was fixed at 400 μM.

When malonyl-CoA inhibition was assayed, increasing concentrations of malonyl-CoA comprised between 0.05 and 100 μM were included. The IC_{50}, defined as the malonyl-CoA concentration that produces 50% inhibition of enzyme activity, was determined at 50 μM palmitoyl-CoA and 400 μM carnitine. IC_{50} was calculated by Excel software using linear regression analysis.

Values reported here are the means and S.D. of 3–5 determinations. Curve fitting was carried out using Sigma plot software version 8.0. All protein concentrations were determined using the Bio-Rad protein assay with bovine albumin as a standard.

Immunological Techniques—Western blot analysis of wild type CPT1A and the assayed mutants using polyclonal antibodies was performed as described (24). The antibody for rat CPT1A was kindly given by Dr. C. Prip-Buus (Institut Cochin, Université René Descartes, Paris, France) and was directed against peptide 317–430, in the cytosolic catalytic C-terminal domain. For the CPT1A wild type and mutants, proteins of predicted sizes were synthesized with similar levels of expression.

Search of Homologous Proteins of Rat CPT1A Amino-terminal Domain—In order to find structural homologues for the amino-terminal domain sequence of rat CPT1A, the FFAS03 server (25, 26) facilities were used on the World Wide Web at ffas.ljcrf.edu/ffas-cgi/cgi/ffas.pl. The PSI-BLAST (27)-based profile-profile comparisons were performed against the SCOP data base (28, 29) as a source of protein classification. From the output set of possible structural homologues among the SCOP data base representatives, the best candidate structure in terms of the FFAS03 server's empirical evaluation of matching significance was selected for further three-dimensional model building.

Three-dimensional Protein Modeling of the CPT1A Amino- and Carboxyl-terminal Domains—The structural model for the rat CPT1A amino-terminal domain was assembled using homology modeling procedures, supported on the profile-based sequence alignment from the FFAS03 server output, and using the Protein Data Bank (30) coordinates of the selected structural homologue (1TF3; *Xenopus laevis* transcription factor IIIa (31)) as three-dimensional template. The structural model for rat CPT1A carboxyl-terminal domain was constructed using homology modeling procedures based on multiple structure-based amino acid sequence alignments of the carnitine acyltransferase family and the crystallographic coordinates of carnitine octanoyltransferase bound to acylcarnitine (Protein Data Bank entry 1XL8, chain A) (32) and carnitine palmitoyltransferase 2 (Protein Data Bank entry 2H4T) (33). Structural three-dimensional models were built using the SWISS-MODEL server (34–36) facilities on the World Wide Web at www.expasy.ch/swissmod/SWISS-MODEL.html, and their structural quality was checked using the WHAT-CHECK routines (37) from the WHAT IF program (38) from the same server. Finally, in order to optimize geometries, release local constraints, and correct possible inappropriate contacts, the modeled structures were energy-minimized with the implementation of the GROMOS 43B1 force field in the program DeepView (39), using 500 steps of steepest descent minimization followed by 500 steps of conjugate-gradient minimization.

CPT1A Amino- and Carboxyl-terminal Domain Structural Interaction—The structural model for the molecular interaction between rat CPT1A amino- and carboxyl-terminal domains was built using the computational methods for protein-protein rigid docking implemented in the program Hex (40). In order to reduce the complexity of the 6D positional search between both protein structures, the initial relative positioning of the amino-terminal domain was restrained to the CoA binding pocket side of the carboxyl terminal as proposed by Faye *et al.* (18). For all of the docking models generated, molecular mechanics energy minimization over the force field implemented in Hex was finally performed. From the overall models, the best complex in terms of highest steric and electrostatic correlation between the pair of protein structures was selected.

Malonyl-CoA Molecular Docking—In order to obtain a structural model of the interaction between CPT1A and its principal physiological inhibitor malonyl-CoA, molecular docking procedures between both structures were performed using the methods implemented in the program suite Autodock 3.0 (41–43) as described previously (44).

RESULTS

Structural Model for the CPT1A NH_2-terminal Domain and Its Interaction with the COOH-terminal Domain—Both NH_2- and COOH-terminal domains of CPT1A are implicated in modulating the enzyme sensitivity to malonyl-CoA. To study the nature of the suggested interactions between the two regions and to determine how such interactions can influence the role of malonyl-CoA, we constructed *in silico* structural models of both domains and their structural contacts. We constructed a three-dimensional model of the residues in the NH_2-terminal domain, comprising amino acids 1–61 of human CPT1A. Classic homology-based modeling techniques failed to provide a feasible template for the NH_2-terminal domain, due to the lack of a close relative of known structure that could be detected using a simple BLAST search in the Protein Data Bank. To overcome this difficulty, an iterative procedure was implemented through the use of the FFAS03 server based on PSI-BLAST profile-profile searching against the classified protein structure data base SCOP as described under "Experimental Procedures." Iterative techniques like PSI-BLAST allow a more extensive search through sequence databases for remote homologues, usually maintaining structural constraints in terms of secondary and three-dimensional organization in the absence of high sequence identity. The first hit obtained on the FFAS03 server was the SCOP region *d1tf3a3*, corresponding to the three-dimensional structure of the a3 domain of the three-dimensional structure of *X. laevis* transcription factor IIIA (Protein Data Bank code 1TF3 (31)), with a score of −6.860 and a sequence identity of 50% over an alignment length of 44 residues; this result was within the limits of the technique. A structure-based multiple sequence alignment of several CPT1A and CPT1B NH_2-terminal sequences and the sequence of the Protein Data Bank structure 1TF3 is shown in Fig. 1*A*.

Using the crystallographic coordinates of 1TF3 as template and the information obtained from the structural alignment between 1TF3 and the NH_2-terminal sequences of CPT1, a three-dimensional model was constructed for human CPT1A residues 10–50 (Fig. 1*B*). The model shows four β strands (E1, residues 12–14; E2, residues 20–22; E3, residues 27–30; E4, residues 34–37) and an α helix (H1, residues 38–47). The first two strands and the helix were completely aligned with the template, but beta strands E3 and E4 were modeled with less structural confidence. A model for the COOH-terminal domain of human CPT1A was constructed over the crystallographic structure of mouse carnitine octanoyltransferase (32) and CPT2 (33) using standard homology modeling-based techniques, as described elsewhere (45).

Having obtained three-dimensional models both for NH_2- and COOH-terminal domains of CPT1A, we then used the resulting structures to build a model for the putative interaction between them, using the *in silico* method Hex for protein-protein rigid docking, as described under "Experimental Procedures." Initial positioning of both protein domains was selected on the basis of the relative location on the NH_2-terminal domain in the nucleotide fragment of the

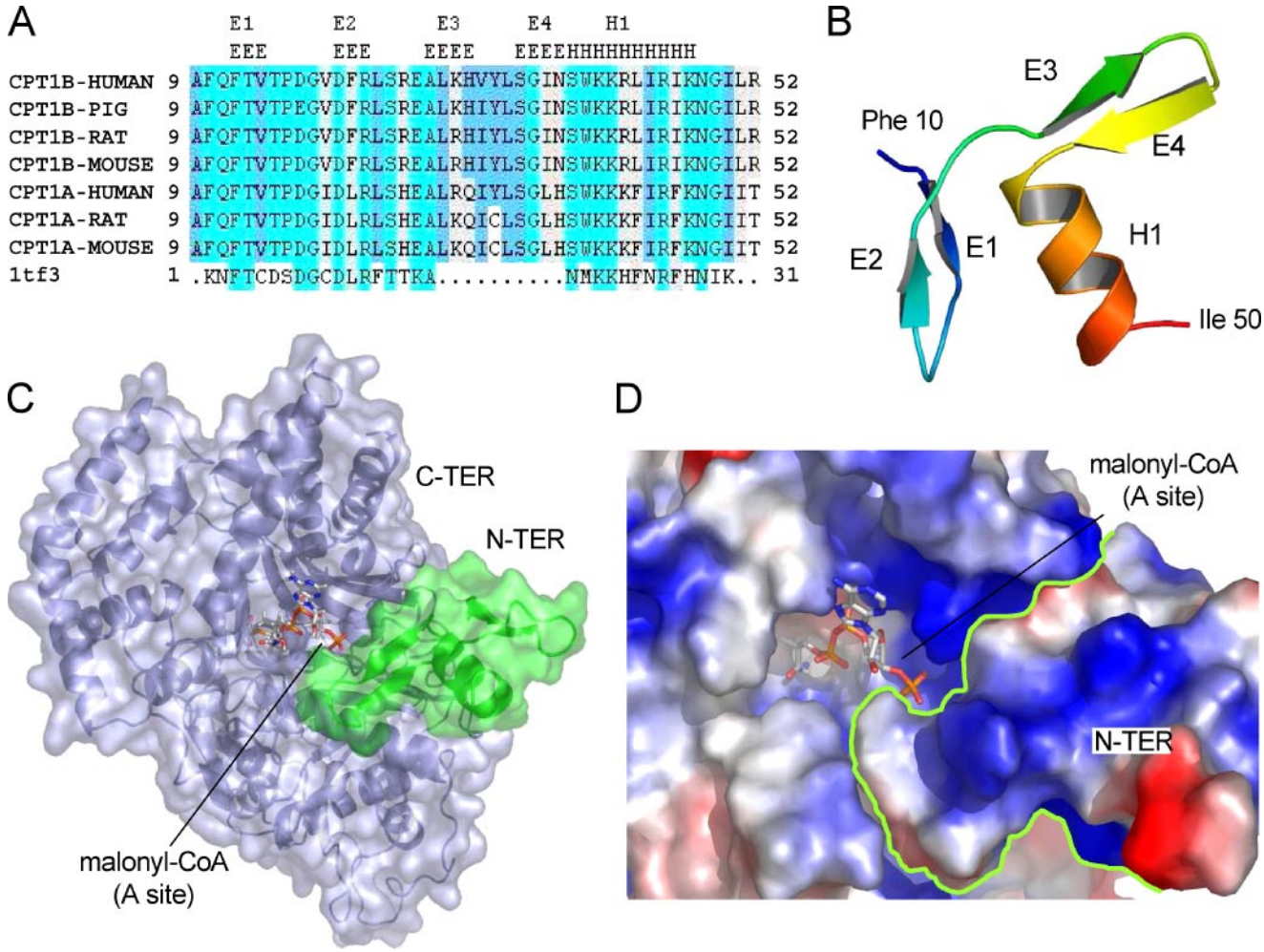

FIGURE 1. **Structural model for NH_2- and COOH-terminal domains of CPT1A.** *A*, structural alignment *colored* according to conservation of NH_2-terminal domains of CPT1A and CPT1B sequences obtained from several organisms. The sequence of Protein Data Bank structure 1TF3 (*X. laevis* transcription factor IIIA) is included for comparison. Secondary structure elements of the NH_2-terminal domain model are also indicated. *B*, structural model of human CPT1A residues 10–50. The position of predicted structural elements is indicated. *C*, using *in silico* docking procedures for prediction of protein-protein and protein-ligand interaction, a putative complex between NH_2- (*green*) and COOH-terminal (*blue*) domains of human CPT1A was used to predict a site for malonyl-CoA binding at the substrate cavity of the molecule. *D*, detail of the interaction site showing the electrostatic characteristics of the surrounding area. The boundary between NH_2- and COOH-terminal domains has been *highlighted*. Protein representations were performed using PyMOL (DeLano Scientific, San Carlos CA).

TABLE 1

Residues involved in the interactions between NH_2- and COOH-terminal domains of human CPT1A

Listed are residues in the modeled NH_2-terminal domain of human CPT1A located at less than 4 Å from the surface of the COOH-terminal domain and their interacting counterparts.

NH_2-terminal	COOH-terminal	Interactions
Phe^{10}	Glu^{729}, Asn^{730}	Amide of Phe^{10} interacts with the partially charged carboxylic oxygen in Glu^{729} and with the Asn^{730} carboxamide side chain.
Gln^{11}	Glu^{729}, Asn^{730}	The triad of residues Phe^{10}-Gln^{11}-Phe^{12} is conserved in CPT1A and CPT1AB NH_2-terminal domain multiple sequence alignment.
Phe^{12}	Gly^{728}, Glu^{729}	The triad of residues Gly^{728}-Glu^{729}-Asn^{730} is conserved in CPT1A, CPT1B, and CPT1C sequences.
Ser^{24}	Gly^{728}, Glu^{729}	Pair Gly^{728}-Glu^{729}, as well as Ser^{24}, is conserved in all CPT1 sequences.
His^{25}	Lys^{556}, Gly^{557}, Gly^{728}	Lys^{556} is in contact with the modeled position of malonyl-CoA.
Glu^{26}	Lys^{561}	The side-chain carboxyl group of Glu^{26} is in contact with the amino group of Lys^{561}.
Leu^{28}	Lys^{556}, Lys^{560}	Lys^{556} and Lys^{560} show a contact between their respective hexanoyl side-chain groups and the N-terminal hydrophobic residue Leu^{28}.
Ile^{31}	Ser^{299}, Gly^{298}	Ile^{31} is in contact with the proposed site for malonyl-CoA.
Gln^{30}	Gln^{693}	Gln^{693} is located on the external side of the elongated loop, positioned between β strands E13 and E14 and present only in CPT1, which wraps the internal palmitoyl cavity (45).
Tyr^{32}	Pro^{293}, Arg^{295}, Leu^{296}	Tyr^{32} is in contact with Ile^{31}, which is proposed to interact with malonyl-CoA.

acyl-CoA binding face (18). We selected the model with the highest score in terms of steric and electrostatic correlation, and we applied energy minimization steps to correct unrealistic contacts. The final model for the NH_2-terminal domain on the surface of COOH-terminal CPT1A structure is shown in Fig. 1, *C* and *D*. Table 1 summarizes the residues involved in the interactions between NH_2- and COOH-terminal domains.

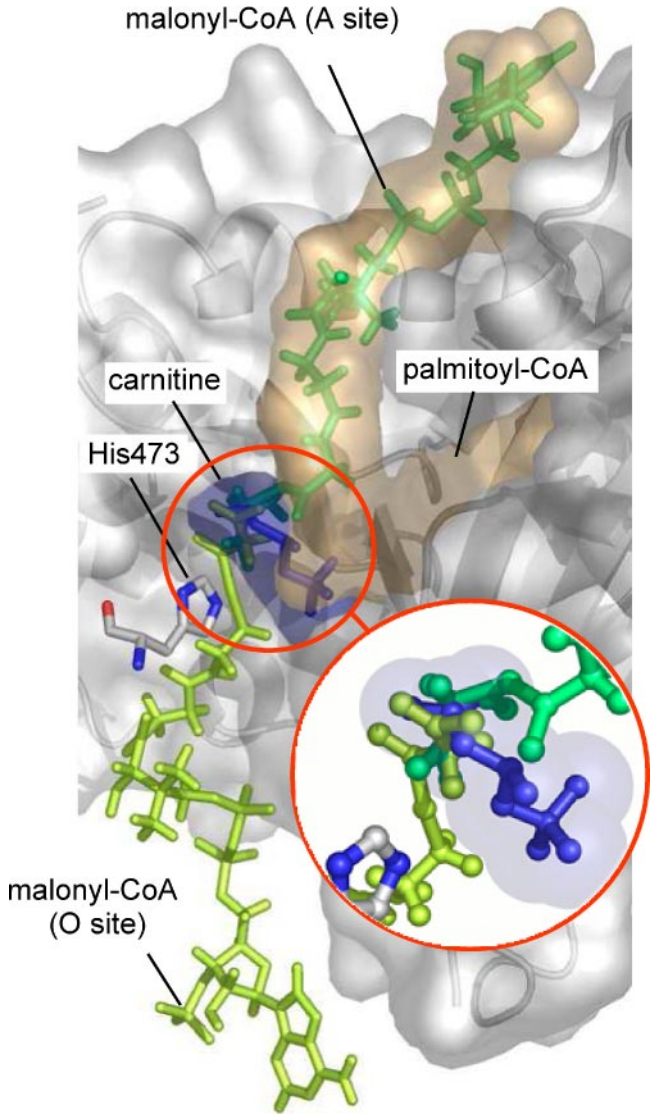

FIGURE 2. **Two sites for malonyl-CoA binding to CPT1A.** Longitudinal section of CPT1A structure illustrating the two putative binding loci for malonyl-CoA: A site (*dark green*) and O site (*light green*). The loci of substrates palmitoyl-CoA (*shaded yellow*) and carnitine (*shaded blue*) are shown. A molecule of carnitine (*blue*) in the active site of the enzyme is shown to illustrate the interference of the malonyl-CoA molecule (in both orientations). The position of catalytic residue His^{473} is also indicated. The *inset* shows in detail the predicted clashes between carnitine and malonyl moieties of malonyl-CoA molecules.

In Silico Docking of the Malonyl-CoA Molecule in CPT1A Structure—The final docking model for interacting NH_2- and COOH-terminal domains in human CPT1A was used as a structural frame to perform a search for a putative location of both substrates carnitine and palmitoyl-CoA and the physiological inhibitor malonyl-CoA in the active center of the enzyme. A three-dimensional model of the free malonyl-CoA molecule was prepared using molecular-orbital calculation methods implemented in Mopac (46), and then low energy conformational *in silico* models for putative inhibitor positions were generated and evaluated applying the algorithms Autogrid and Autodock (see "Experimental Procedures"). Two runs of Autodock3 using the LGA algorithm rendered 200 conformations that were clustered with a root mean square deviation cut-off of 1 Å for all atoms of each docked solution, discarding unrealistic solutions. Docking methodology rendered a binding site for malonyl-CoA close to the interaction of NH_2- and COOH-terminal domains, and residues from both domains were implicated (Figs. 1 and 2). A putative second site for the inhibitor molecule, located on the opposite side of the molecule, was also predicted (Fig. 2). In both models, the best docked conformation belonging to the lowest energy docked model of the most populated cluster was selected as a reference structure for further analysis. The two predicted binding sites for malonyl-CoA were named as follows: the one close to the predicted site on the NH_2-terminal domain and the acyl-CoA entrance was called the "A site" (for CoA site), and the other, on the opposite side of the molecule in the catalytic channel, was called the "O site" (for opposite-to-CoA site) (Fig. 2). Table 2 lists the residues predicted to be related to the malonyl-CoA binding to the enzyme.

Mutational Analysis of CPT1A NH_2- and COOH-terminal Residues Predicted to be Involved in Malonyl-CoA Binding to the A Site—To provide experimental support for the model of the interaction between NH_2- and COOH-terminal domains and for the modeled location of malonyl-CoA contacting residues in both protein segments, some of the CPT1 residues at the interface were mutated, and their enzymatic activities were measured at different malonyl-CoA concentrations. A pair of interacting residues, Glu^{26}-Lys^{561}, was selected due to the clear electrostatic nature of their interaction (Table 1). Residue

TABLE 2

Residues contacting inhibitor malonyl-CoA located in NH_2- or COOH-terminal domains of human CPT1A

Shown are amino acids located in the vicinity (less than 4 Å) of the putative A site and O site for malonyl-CoA classified according to their position in the NH_2-terminal domain or in the A site and O site docking CoA grooves or the carnitine pocket of the C terminus of human CPT1A. Residues located in the enzyme catalytic site that contact both positions of malonyl-CoA in the proposed models are shown in boldface type.

Malonyl-CoA-contacting residues at human CPT1A A site			Malonyl-CoA-contacting residues at human CPT1A O site		
Carnitine pocket	A site docking CoA groove	N-terminal domain	Carnitine pocket	O site docking groove	
Tyr^{241}	Lys^{556}	Arg^{29}	**Tyr^{241}**	Ile^{240}	Leu^{539}
His^{473}	Lys^{560}	Ile^{31}	**His^{473}**	Arg^{243}	Leu^{540}
Asp^{477}	Ser^{565}		**Asp^{477}**	Gly^{244}	Ser^{685}
Ala^{478}	Asp^{567}		**Ala^{478}**	Arg^{245}	Phe^{712}
Tyr^{589}	Glu^{590}		**Tyr^{589}**	Gly^{246}	Gly^{713}
Ala^{591}	His^{640}		**Ala^{591}**	Leu^{248}	Pro^{714}
Ser^{592}	Met^{643}		**Thr^{602}**	Asn^{251}	Val^{715}
Met^{593}	Gln^{688}		Arg^{655}	Ser^{252}	Lys^{739}
Thr^{602}	Pro^{690}		**Ser^{687}**		
Thr^{686}	Gln^{691}				
Ser^{687}	Gln^{692}				
Thr^{689}					

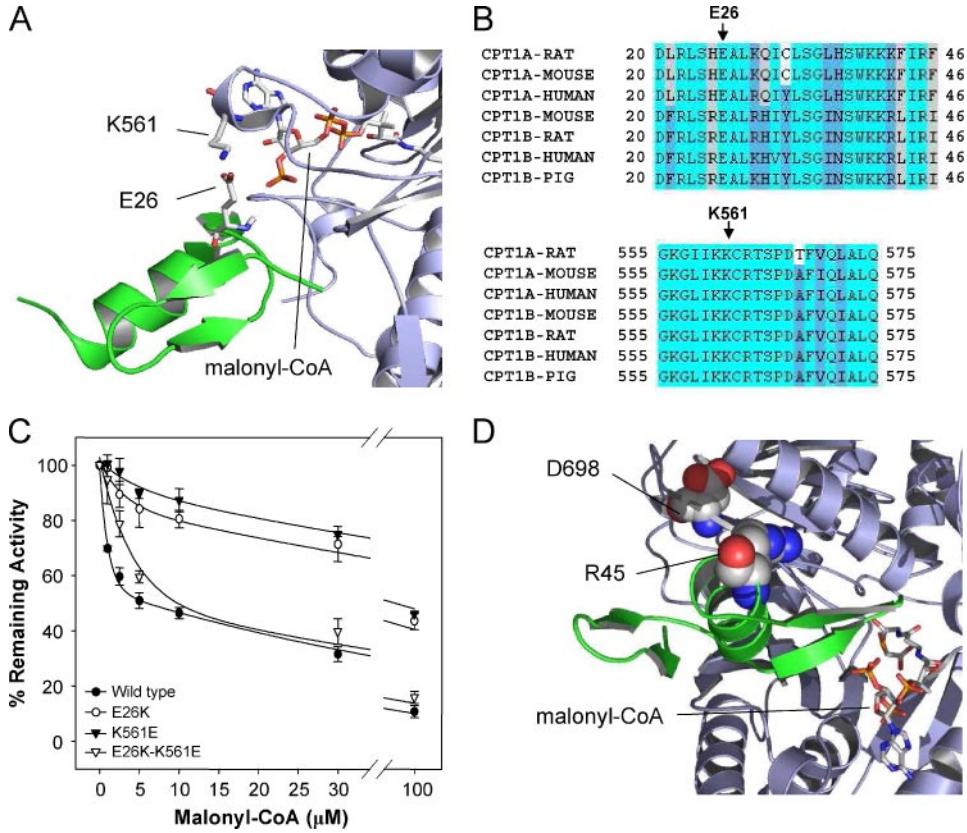

FIGURE 3. **Specific contacts between COOH- and NH_2-terminal domains are necessary for malonyl-CoA inhibition at the A site.** *A*, detail of the interaction between residues Glu^{26} and Lys^{561}, located at the NH_2- and COOH-terminal domains of the protein, respectively. *B*, multiple sequence alignment of residues located in the vicinity of Glu^{26} and Lys^{561}, showing complete conservation of both residues in CPT1A and CPT1B sequences. *C*, effect of malonyl-CoA on the activity of CPT1A wild type (*black circles*), mutant E26K (*open circles*), mutant K561E (*black triangles*), and double mutant E26K/K561E (*open triangles*). CPT1A activity was measured, and data are expressed relative to control values in the absence of inhibitor (100%) as the mean of three independent experiments. *D*, detail of the residues Arg^{45} and Asp^{698} at the NH_2- and COOH-terminal domains of the protein. The malonyl-CoA molecule is also shown.

Lys^{561} of the COOH-terminal domain was seen to be in close proximity to Glu^{26} of the NH_2-terminal domain (Fig. 3*A*). Both residues are completely conserved across the NH_2- and COOH-terminal structure-based sequence alignment (Fig. 3*B*). In the modeled three-dimensional structure of the COOH-terminal domain, Lys^{561} is located in a loop between α helices H14 and H15. In addition, Lys^{561} would be fully exposed to solvent and does not appear to form salt bridges with any other COOH-terminal residue within the conserved catalytic core of CPT1A.

On the basis of the structural model, we predicted that mutation of Glu^{26} to Lys and of Lys^{561} to Glu would drastically alter the mutual recognition of interacting NH_2- and COOH-terminal domain surfaces and strongly reduce malonyl-CoA sensitivity. To confirm these predictions, E26K and K561E single mutants and a double mutant (swap) E26K/K561E were generated and tested for CPT1A activity and malonyl-CoA inhibition. Results are shown in Fig. 3*C*. Single mutant E26K decreased malonyl-CoA sensitivity, producing an increase in the IC_{50} from 7.3 ± 0.5 μM (wild type) to 92.4 ± 9 μM. Analogous results were observed for the CPT1A K561E mutant, whose IC_{50} increased to 88.1 ± 6 μM. Double mutant E26K/K561E, which is the result of a swap, rescued the modified malonyl-CoA sensitivity of each single mutant (IC_{50} was 9.8 ± 0.3 μM). The specific activities of mutants E26K, K561E, and E26K/K561E were 21.6 ± 2.1, 22.8 ± 2.5, and 38.9 ± 4.4, respectively, and were similar to CPT1A wild type (25.0 ± 1.9 nmol·min^{-1}·mg of $protein^{-1}$). In addition, Western blot analysis showed that protein expression of single and double mutants was similar to the wild type (data not shown).

A second pair of residues, Arg^{45} and Asp^{698}, were subjected to double mutation on the basis of their complementary charge, although they were more than 15 Å apart in the proposed model of NH_2- and COOH-terminal domain interaction (Fig. 3*D*). This mutation strategy was applied as a negative control to ensure that the relative position of the NH_2- and COOH-terminal domains, as well as the contact surface between them, had been correctly defined in the model. Mutants R45D and D698R and the double mutant (swap) R45D/D698R were expressed in *S. cerevisiae*, and the mitochondrial extracts were assayed for CPT1 activity and malonyl-CoA inhibition. As expected, none of the three mutants displayed different activity or sensitivity from the wild type (data not shown), suggesting that neither amino acid participated in NH_2- to COOH-terminal domain binding or malonyl-CoA location.

Mutation of Arg^{243}, Located in the Second Predicted O Site for Malonyl-CoA, Diminished the Sensitivity of the Enzyme for the Inhibitor—At the O site, up to 24 amino acid residues are within 4 Å of malonyl-CoA (Table 2). One of them, Arg^{243}, was mutated to Thr^{243}, the residue at the same position in CPT2, which is insensitive to malonyl-CoA. We reasoned that by altering the charge, we could prevent the positioning of malonyl-CoA. In the model, the positively charged Arg^{243} lies close to the OH group in the pantothenic acid moiety of malonyl-CoA (Fig. 4*A*). Replacing it by the polar, albeit noncharged, threonine would be expected to modify the electrostatic characteristics of the surrounding area, thus preventing correct location of malonyl-CoA.

CPT1A mutant R243T was expressed in *S. cerevisiae* and tested for activity and malonyl-CoA inhibition. Results of the kinetic analysis are shown in Fig. 4. Apparent K_m values for carnitine and palmitoyl-CoA (56.3 ± 2.9 and 7.0 ± 2.2 μM) of CPT1A R243T were similar to those of CPT1A wild type (59.7 ± 2.5 and 3.6 ± 0.4 μM). V_{max} values for carnitine and palmitoyl-CoA were 64.9 ± 7.1 and 34.1 ± 9.4 μM and 70.6 ± 10.3 and 36.3 ± 6.9 μM, respectively, for CPT1A wild type and

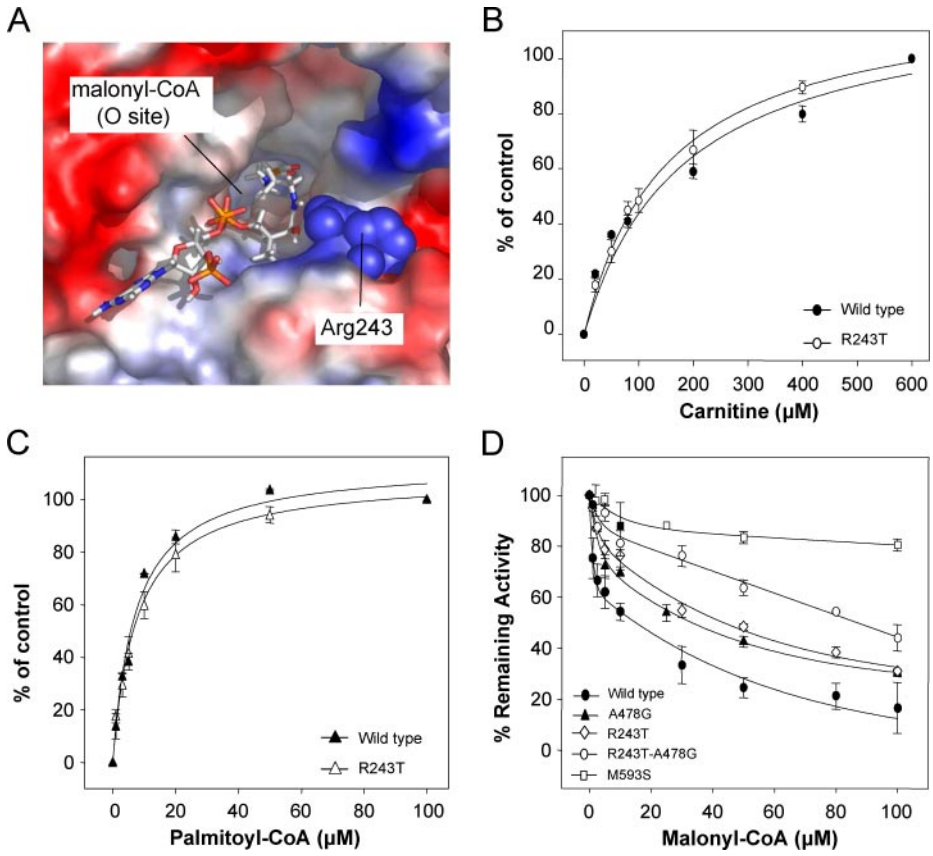

FIGURE 4. **CPT1A R243T mutant at the malonyl-CoA O site.** *A*, proposed location of malonyl-CoA molecule in the carnitine entrance O site of CPT1A surface. The position of residue Arg^{243} is indicated, in close proximity with the inhibitor. *B* and *C*, kinetic analysis of the expressed wild type and mutant R243T of rat CPT1A. Isolated mitochondria from the yeast overexpressing wild type (●, ▲) and CPT1A R243T mutant (○, △) were assayed for CPT1 activity in the presence of increased carnitine and palmitoyl-CoA concentrations. The mean data from three to four curves obtained from separate yeast expressions are shown. *D*, effect of malonyl-CoA on the activity of yeast overexpressed wild type CPT1A (*black circles*), point mutants R243T (*open rhombus*), A478G (*black triangles*), and M593S (*open squares*) and double mutant R243T/A478G (*open circles*). Mitochondrially enriched fractions were incubated with increasing malonyl-CoA concentrations, and the enzyme activity was measured. Data are expressed relative to control values in the absence of inhibitor (100%) as the mean of three independent measurements. CPT1A M593S and CPT1A A478G mutants were previously reported (15).

mutant (Fig. 4, *B* and *C*). The IC_{50} malonyl-CoA value for CPT1A R243T was 38.4 ± 1.9 μM, showing lower malonyl-CoA sensitivity than the wild type (IC_{50} = 7.3 ± 0.5 μM).

According to Table 2, Ala^{478} would be involved in both A site and O site for malonyl-CoA. Furthermore, previous studies had reported that the mutant CPT1A A478G showed reduced malonyl-CoA sensitivity (IC_{50} = 39.5 ± 4.1 μM) (15). To test whether a double mutation of residues Arg^{243} and Ala^{478} located far apart, one in the carnitine pocket and the other in the O site groove, could further decrease CPT1 malonyl-CoA sensitivity, we generated a double mutant. CPT1A R243T/A478G was expressed in *S. cerevisiae*, and the mitochondria-enriched fractions were tested for CPT1 activity and sensitivity to malonyl-CoA. CPT1A R243T/A478G showed a 20-fold increase in IC_{50} (IC_{50} > 150 μM) with respect to the wild type protein (IC_{50} = 7.3 ± 0.5 μM), which is higher than those of the individual mutants but lower than that of the malonyl-CoA-insensitive CPT1A M593S (IC_{50} > 300 μM) (15). Western blot analysis showed that protein expression levels from CPT1 mutants were similar to the wild type (data not shown).

Malonyl-CoA and Carnitine Molecules Competed for the Same Location in the Active Center of CPT1A—The positions of the residues in CPT1 predicted by the model (Fig. 2) indicate that carnitine and malonyl-CoA would compete for binding at both the A site and O site. To examine this hypothesis, we performed several studies based on results taken from the literature and on the measurement of inhibitory kinetics. We collected data on the IC_{50} for the inhibition of CPT1 by malonyl-CoA and the K_m for carnitine from publications by several laboratories. When we plotted log IC_{50} (y) against log K_m for carnitine (x), the result was a straight line. We classified the data from the literature as follows: 1) data from various tissues, such as rat liver, human fetal liver, rat heart, guinea pig liver, human skeletal muscle, rat skeletal muscle, dog skeletal muscle, and dog heart; 2) data from CPT1 cDNAs expressed in *Pichia pastoris* and data from CPT1 wild type and mutant cDNAs expressed in *S. cerevisiae* from our laboratory classified in two groups (one includes all mutants whose sensitivity to malonyl-CoA was virtually unchanged, and the other includes all mutants whose sensitivity to the inhibitor was nearly abolished). Logarithmic plots and the corresponding equations are represented in Fig. 5, *A* and *B*. In all cases, the linear equations have similar slopes, irrespective of the fact that 1) the CPT1 data were obtained from expression in two species of yeast, *P. pastoris* and *S. cerevisiae* (Fig. 5*B*); 2) the data were obtained from the cDNAs of the two isoforms CPT1A and CPT1B, (Fig. 5*B*); and 3) the data were obtained from diverse animal tissues (heart, skeletal muscle, and liver) and from various organisms (rat, human, and dog) (Fig. 5*A*). The average value for all slopes is as follows.

$$\frac{\Delta \log IC_{50}\ \text{malonyl-CoA}}{\Delta \log K_m\ \text{carnitine}} = -1.49 \pm 0.13 \qquad \text{(Eq. 1)}$$

We interpret this result as showing that malonyl-CoA and carnitine bind close to each other in the enzyme, and they repulse each other from the site of catalysis.

To further examine how carnitine interferes with malonyl-CoA inhibition, CPT1A wild type expressed in *S. cerevisiae* was assayed for activity and malonyl-CoA inhibition at carnitine concentrations of 100, 400, 800, and 1,600 μM (Fig. 5*C*). The

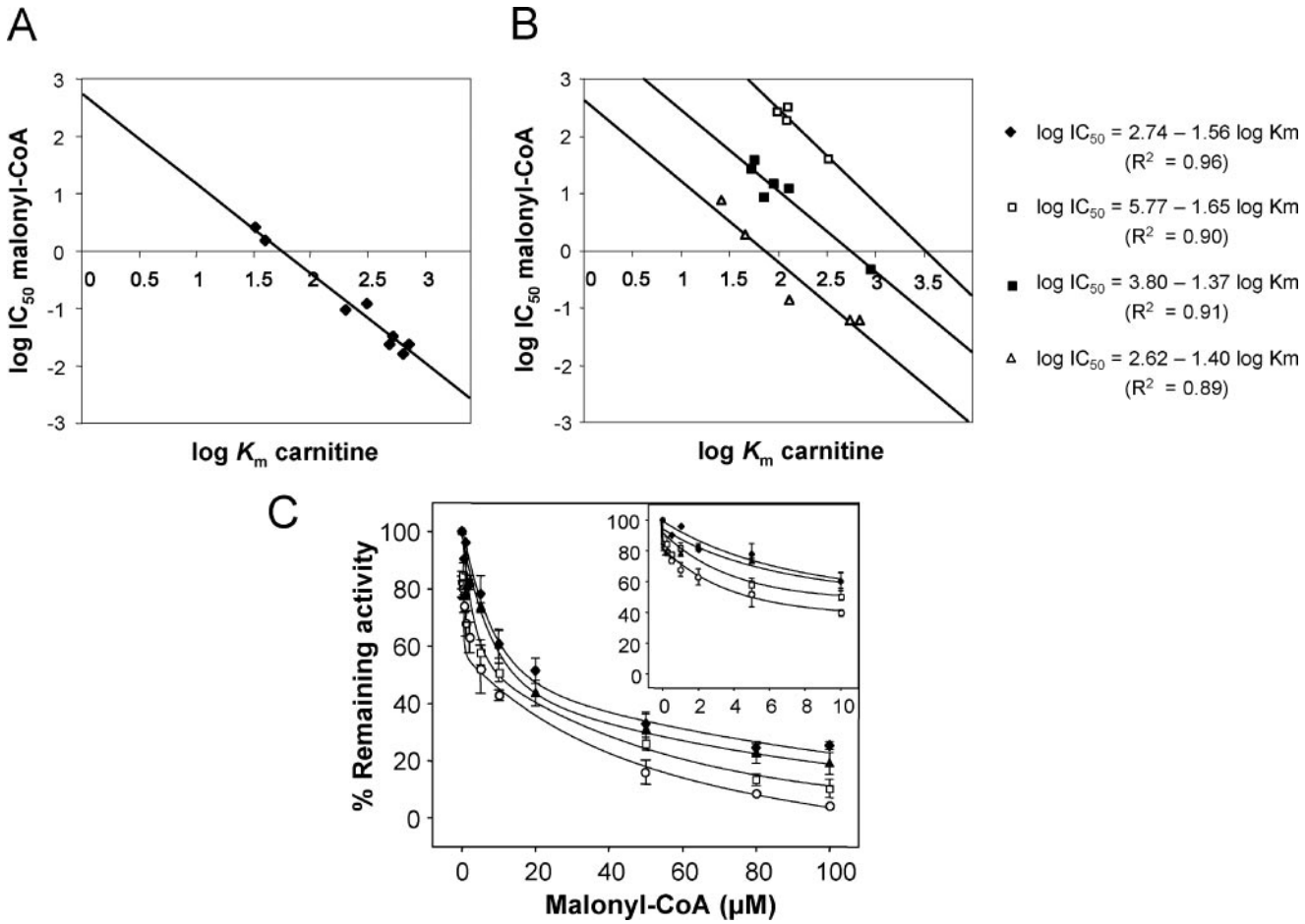

FIGURE 5. **Kinetic analysis of wild type CPT1A inhibition by malonyl-CoA at different carnitine concentrations and linear relationship between log IC_{50} from malonyl-CoA inhibition and log K_m for carnitine.** *A*, the data have been taken from literature (*black diamonds*) from rat liver, human fetal liver, rat heart, guinea pig liver, human skeletal muscle, rat skeletal muscle, dog skeletal muscle, and dog heart (22). *B*, the data are taken from rat and pig CPT1A wild type and human CPT1B wild type expressed in *P. pastoris* (*open triangles*) (12, 13, 54–56) and from rat CPT1 expressed in *S. cerevisiae*, either wild type and mutants (CPT1A wild type, CPT1B wild type, CPT1A T314S, CPT1A N464D, CPT1A C608A, and CPT1A R243T) that present unchanged sensitivity to malonyl-CoA (*black squares*) or CPT1 mutants (CPT1A H277A, CPT1A A478G, CPT1A M593S, and CPT1A T314S/N464D/A478G/M593S/C608A) that nearly abolish the sensitivity to the inhibitor (*open squares*) (15, 24). *C*, isolated mitochondria from yeast strain overexpressing wild type CPT1A were inhibited at increasing malonyl-CoA concentrations in the presence of various carnitine concentrations of 100 μM (*open circles*), 400 μM (*open squares*), 800 μM (*black triangles*), and 1,600 μM (*black diamonds*). Data are expressed relative to control values in the absence of inhibitor (100%) as the mean of three independent measurements. *Inset*, expanded dose-response curve for the inhibitor.

TABLE 3

CPT1A activity and malonyl-CoA inhibition at increased carnitine concentrations

Yeast mitochondrial extracts overexpressing CPT1A were assayed for CPT1A activity and malonyl-CoA inhibition in the presence of 50 μM palmitoyl-CoA and increasing concentrations of carnitine (as described under "Experimental Procedures"). CPT1A activity and IC_{50} values increased depending on increased carnitine concentrations.

Carnitine	CPT1A wild type activity	IC_{50} malonyl-CoA
μM	*nmol·min^{-1}·mg^{-1}*	μM
100	39.1 ± 4.1	4.1 ± 0.7
400	65.8 ± 6.4	7.3 ± 0.5
800	70.7 ± 3.1	13.5 ± 1.6
1,600	74.3 ± 1.8	18.7 ± 0.5

curves show similar profiles, but inhibition was partially relieved at higher carnitine concentrations. IC_{50} values of inhibition by malonyl-CoA were progressively higher as carnitine concentration increased. The values were 4.3, 7.3, 13.5, and 18.7 μM at carnitine concentrations of 100, 400, 800, and 1,600 μM, respectively. These values correlate with the specific activity of the protein at each carnitine concentration (Table 3).

Another set of kinetic experiments was performed to identify the type of inhibition exerted by malonyl-CoA on CPT1A catalysis of carnitine. We performed experiments by varying malonyl-CoA and carnitine concentrations while maintaining palmitoyl-CoA and enzyme concentrations constant. The enzyme showed standard saturation kinetics for carnitine (Fig. 6*A*). Lineweaver-Burk plots for CPT1A activity were linear, and the K_m values observed for carnitine were 75.6, 80.9, and 102.9 μM at malonyl-CoA concentrations of 0, 10, and 50 μM, respectively (Table 4). Changes were observed in the intrinsic catalytic activity of the enzyme and in the catalytic efficiency (defined as V_{max}/K_m ratio). Increasing malonyl-CoA concentrations produced a decrease in V_{max}/K_m ratio (0.86, 0.49, and 0.22 for 0, 10, and 50 μM malonyl-CoA, respectively), which indicates that CPT1A decreased its preference for carnitine when malonyl-CoA increased. This reduction is due to both the decrease in the V_{max} and the increase in the K_m value for carnitine, the former being the stronger factor. Lineweaver-Burk plots for CPT1A at differ-

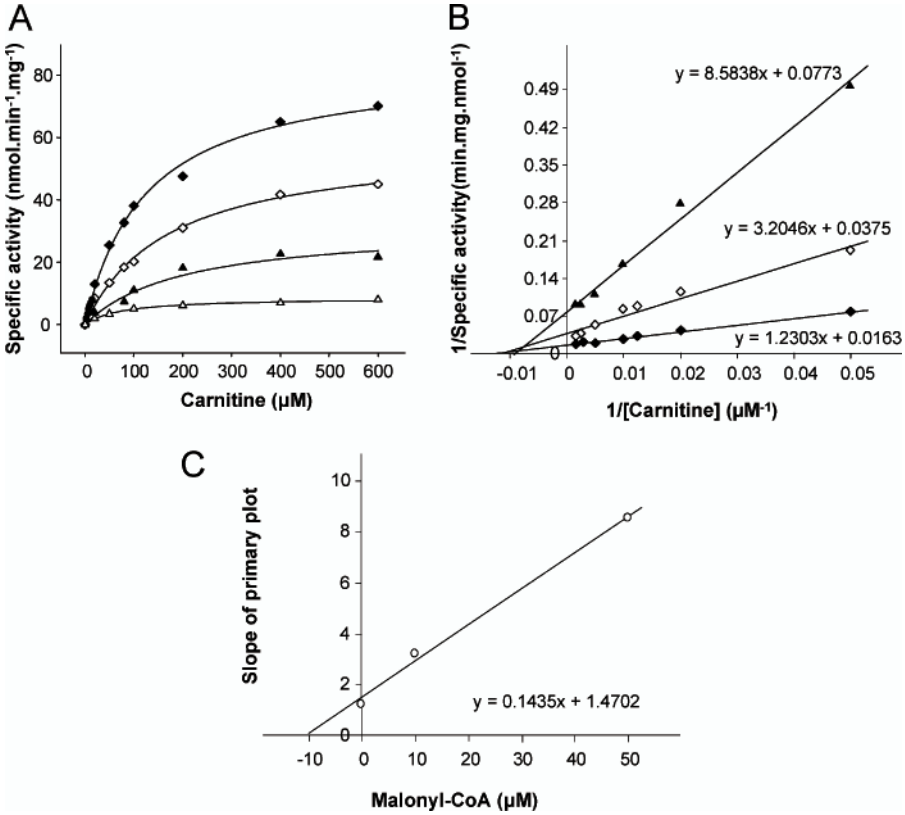

FIGURE 6. **Kinetic analysis of wild type CPT1A for carnitine as a substrate at different malonyl-CoA concentrations.** *A*, yeast extracts of 10 μg of protein were used for rat CPT1A activity. Shown is a Michaelis-Menten representation of activity *versus* increasing carnitine concentrations at four different malonyl-CoA levels: 0 μM (*black diamonds*), 10 μM (*open diamonds*), 50 μM (*black triangles*), and 100 μM (*open triangles*). *B*, Lineweaver-Burk plot of the kinetics shown in *A*. *C*, secondary plot of kinetic data from *B*. Data are the means of two separate experiments.

ent malonyl-CoA concentrations gave a set of straight lines intersecting to the *left* of the $1/v$ axis but *above* the 1/[carnitine] axis (Fig. 6*B*). Secondary plots of the slopes *versus* [I] and the $1/v$ axis intercept *versus* [I] are linear (Fig. 6). Dixon plots of the inhibition data are also linear (data not shown). These kinetic results are compatible with linear mixed type inhibition and may be considered a mixture of partial competitive inhibition and pure noncompetitive inhibition, in which the ESI complex is catalytically inefficient. In this type of inhibition, there are two processes by which the inhibitor may bind to the enzyme and to the enzyme-substrate complex.

$$\begin{array}{ccc} & \overset{K_m}{} & \\ E + S & \rightleftharpoons & ES \\ + & & + \\ I & & I \\ K_i \Updownarrow & & \Updownarrow \alpha K_i \\ EI + S & \rightleftharpoons & ESI \\ & \underset{\alpha K_m}{} & \end{array}$$

SCHEME 1

In this context, two inhibition constants appear: K_i and $K_I = \alpha K_i$. Hence, $K_i = [E][I]/[EI]$ and $\alpha K_i = [ES][I]/[ESI]$. K_i is the dissociation constant of the enzyme-malonyl-CoA complex and an indicator of the affinity of the enzyme for malonyl-CoA, and K_I refers to the enzyme-substrate-inhibitor complex. The Lineweaver-Burk equation for linear mixed inhibition can be written as follows.

$$\frac{1}{V} = \frac{1}{V_{max(app)}} + \frac{K_{m(app)}}{V_{max(app)}} \times \frac{1}{[S]} \quad \text{(Eq. 2)}$$

where

$$V_{max(app)} = \frac{V_{max}}{\left(1 + \frac{I}{\alpha K_i}\right)} \quad \text{(Eq. 3)}$$

and

$$K_{m(app)} = K_m \times \frac{\left(1 + \frac{I}{K_i}\right)}{\left(1 + \frac{I}{\alpha K_i}\right)} \quad \text{(Eq. 4)}$$

The value of αK_i (K_I) was obtained from the intercept on the [I] axis when we plotted $1/V_{maxapp}$ against [I]. The value of K_i was obtained when we plotted the slopes of primary plots against [I] as the intercept on the [I] axis. The values obtained for $K_I = \alpha K_i$ and K_i were 13.2 ± 1.4 and 10.6 ± 0.8 μM, respectively, thus indicating that the value of α is greater than 1 (in this case, $\alpha = 1.24$), which is consistent with the intersection point position showed in Lineweaver-Burk plots.

However, our kinetic results are also compatible with inhibition produced by the binding of the inhibitor at two separate sites on the enzyme. Data from the present study and from other authors indicate that there are two malonyl-CoA binding sites. Therefore, the kinetic data should be discussed in terms of kinetic models based on two binding sites for malonyl-CoA. The first model would involve the following scheme that is a mixture of pure competitive and pure noncompetitive inhibition (Scheme 2).

$$\begin{array}{rcl} \text{Competitive} & \leftarrow & EI \\ & & \gamma K_i \Updownarrow \\ & & I \\ & & + \qquad \overset{K_m}{} \\ & & E + S \rightleftharpoons ES \\ & & + \qquad\quad + \\ & & I \qquad\quad I \\ & & K_i \Updownarrow \qquad \Updownarrow \alpha K_i \\ \text{Noncompetitive} & \leftarrow & EI + S \rightleftharpoons ESI \\ & & \qquad\quad \underset{\alpha K_m}{} \end{array}$$

SCHEME 2

TABLE 4

Kinetic parameters of CPT1A expressed in *S. cerevisiae*

Mitochondrial enriched fractions from yeast overexpressed CPT1A were assayed at different malonyl-CoA concentrations with palmitoyl-CoA and carnitine, as described under "Experimental Procedures." Results are the mean ± S.D. of at least three independent experiments. ND, not determined.

Malonyl-CoA	CPT1A wild type activity	Carnitine		Catalytic efficiency (V_{max}/K_m)
		Observed K_m	Observed V_{max}	
μM	$nmol \cdot min^{-1} \cdot mg^{-1}$	μM	$nmol \cdot min^{-1} \cdot mg^{-1}$	
0	65.8 ± 6.4	75.6 ± 0.6	65.4 ± 4.4	0.86
10	42.2 ± 14.3	80.9 ± 4.4	40.1 ± 13.5	0.49
50	22.9 ± 11.5	102.9 ± 8.0	22.9 ± 10.0	0.22
100	7.3 ± 0.2	ND	ND	ND

Calculations from the data obtained gave the following results: $\alpha K_i = 13.2$ and $\gamma K_i/1 + \gamma = 10.6$. If $\alpha = 1$, therefore, $K_i = 13.2$ and $\gamma = 4.1$. The second model would correspond to the following scheme (*i.e.* a mixture of pure competitive and pure uncompetitive inhibition) (Scheme 3).

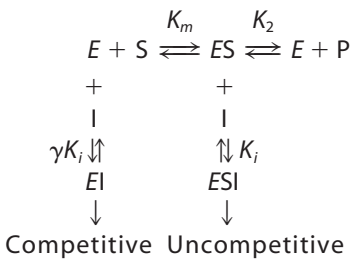

SCHEME 3

Calculations from the data obtained gave the following results: $\gamma = 0.80$, when $K_i = 13.2$.

At this point, we cannot predict which of the two models would better fit CPT1A; both models support the kinetic data obtained for V_{max} and K_m at the malonyl-CoA and carnitine concentrations assayed.

DISCUSSION

Despite several efforts to characterize CPT1, its mode of action is not yet completely understood, probably due to the difficulty of obtaining an appropriate crystal, since it is an integral membrane protein. The aim of this study was to develop a structural model of the NH_2-terminal domain and to examine its interactions with the C-terminal domain in order to predict the location of malonyl-CoA in CPT1 enzyme and its ability to interact with the substrates carnitine and palmitoyl-CoA. We present, for the first time, a partial bioinformatic model of the NH_2-terminal domain, which lacks only the first 9 amino acids. Unfortunately, the very first residues in the NH_2-terminal domain cannot be modeled due to the lack of a feasible template. Thus, we cannot explain the role of several residues located in this segment, like Glu^3 or His^5, previously implicated in sensitivity to malonyl-CoA. Nevertheless, the spatial position of the first modeled residues at the NH_2-terminal end suggests that the first 9 residues could be allocated close to, or in contact with, the surface of the COOH-terminal modeled structure. In an earlier attempt to predict part of the NH_2-terminal domain structure, it was proposed that the residues within region 19–31 had an α-helical structure (16). However, this predicted α-helical structure does not match the α-helix (residues 38–48) of our NH_2-terminal model. Whereas the predicted α-helical structure was based only on amino acid sequence, our model is based on both amino acid sequence and structural homology. Our NH_2-terminal model includes not only an α-helix but also four β-strands. The segment comprising β strands 3 and 4 has a lower confidence index than the surrounding amino acids, since in this region the modeling procedures have rebuilt a missing inner loop region not present in the structural template 1TF3. Although we cannot affirm that this conformation and its secondary structure assignment reflect the true domain structure, the model seems self-consistent according to the continuity of the α-carbon backbone trace and the favorable interactions within the force field energy of the NH_2-terminal model.

Interestingly, the topology of the *in silico* modeled NH_2-terminal domain of CPT1A resembles the characteristic subdomain (residues 175–210, containing two flanking β-strands plus two α-helices) present in the CPT2 structure (33, 47), which mimics the interactions of the NH_2-domain with the COOH-terminal domain. Furthermore, the *in silico* docking model of NH_2- and COOH-terminal domains suggests specific interactions between them. The main set of contacting residues can be mapped onto the surface of the CPT1A COOH-terminal domain and, to a lesser extent, the NH_2-terminal domain. A pair of residues, (Glu^{26}-Lys^{561}), located in the NH_2- and COOH-terminal domain, respectively, were selected for mutation, because their side chains could form a saline bridge between their functional groups. The decrease in the malonyl-CoA sensitivity of these point mutants could be a result of the disturbed electrostatic interactions between their charged side chains. Moreover, the recovery of malonyl-CoA sensitivity of the double mutant (swap) suggests that the relative position of NH_2- and COOH-terminal domains bound to each other is more important in terms of overall functionality than the individual nature of the residues involved in the interaction, an evolutionary phenomenon known as correlated mutations (48). In contrast to the loss of sensitivity to malonyl-CoA, point mutants did not show any change in CPT1 activity, which suggests that this contact between NH_2- and COOH-terminal domains is not important for activity. This is consistent with previous studies, in which deletions between residues 19 and 30 did not change CPT1A activity (17). Other important interactions are highlighted by the model. It predicts the positioning of Leu^{28} (NH_2-terminal domain) mostly sheathed by the hexanoyl fragments of Lys^{556} and Lys^{560} side chains (COOH-terminal domain). Leu^{28} is fully conserved in CPT1A and CPT1B members, and it could be involved in positioning the positive net charge of the two lysine residues on the binding surface of the

COOH-terminal domain. Leu^{28} is in close proximity to the ribose in the CoA moiety of palmitoyl-CoA. Regarding the nucleotide moiety of the palmitoyl-CoA, residues Lys^{556} and Lys^{560} would be fully exposed to the solvent and in contact with the phosphate group attached to the nucleoside ribose in the CoA moiety. Both lysine residues flank α helix H14 and are fully conserved in all members of the carnitine acyltransferase family, which suggests a conserved electrostatic-mediated interaction between charged lysine residues and phosphate functional groups in CoA-based ligands. The mutant K560A showed less activity than the wild type (49), probably due to a decrease in the CPT 1 binding stability of the CoA substrates.

The model also predicts a contact between malonyl-CoA and the NH_2-terminal domain via Arg^{29}, which could establish a polar interaction with the hydroxyl group of the ribose in the CoA fragment of the inhibitor. The alkaline character of this amino acid is conserved in CPT1A and CPT1B. The palmitoyl-CoA substrate and the inhibitor would occupy the same position in the "A site." Several authors (7–13) have reported that malonyl-CoA binds to CPT1 at two separate sites, with low and high affinity. The low affinity binding site is the locus at which palmitoyl-CoA and malonyl-CoA compete (50). The A site proposed in the present study would be compatible with this low affinity site. Natural endobiotics like free CoA, acetyl-CoA, and propionyl-CoA inhibit CPT1 by binding at the acyl-CoA (51). The A site would correspond to those molecules that need coenzyme A to bind. CoA would position their acidic moieties at their final location. This site would be distinct from the other malonyl-CoA binding site described by enzymatic methods.

On the basis of our *in silico* docking experiments, an additional locus, the "O site," for malonyl-CoA positioning was proposed, which is located on the opposite side of the molecule. This site might correspond to the proposed second malonyl-CoA binding site exclusive to the inhibitor (50). In this locus, the interaction of malonyl-CoA with the enzyme would mostly depend on the dicarbonyl group (CO-CH_2-CO or CO-CO structures) rather than on interactions of the CoA itself with its surrounding amino acids. Kashfi and Cook (51) have shown that molecules with a dicarbonylic structure (among them, 4-hydroxyphenylglyoxylate and Ro 25-0187) inhibit CPT1 activity to varying degrees by binding to a specific malonyl-CoA binding site, which is quite different from the acyl-CoA binding site. When we performed *in silico* docking studies of Ro 25-0187 on our CPT1A model, we observed a significant preference, in terms of energy stabilization, for the O site over the A site (data not shown). Other compounds with both a dicarbonylic structure and a CoA moiety, such as succinyl-CoA and methylmalonyl-CoA (52) interact with a second specific malonyl-CoA-inhibitory binding site. The coenzyme A moiety of these molecules may increase the potency of these weak inhibitors. However, high potency inhibitors like Ro 25-0187 did not need to be in the form of coenzyme A ester, suggesting that the dicarbonylic structure is responsible for their inhibitory effect.

The docking model also shows that the side chain of residue Arg^{243} is exposed to the solvent in the O site, far from the central catalytic hollow occupied by carnitine. Arg^{243} is completely conserved in all CPT1 members. This residue would establish polar contacts with the CoA moiety of malonyl-CoA, putatively through the hydroxyl group of the pantothenic fragment of the inhibitor. Mutation of Arg^{243} to Thr did not affect CPT1 activity but slightly diminished enzyme sensitivity to malonyl-CoA, thus supporting this O site position. The double mutant CPT1A R243T/A478G was less sensitive to malonyl-CoA than the single mutants. This is caused by the sum of the specific interactions of each residue with the inhibitor, since they are far from each other in the tunnel. The differential surrounding amino acidic composition of the A site and O site indicates that malonyl-CoA could establish a different network of polar and nonpolar interactions with differential stability upon binding. However, a single hydrophobic residue Met^{593}, conserved in all carnitine-acyltransferases susceptible to inhibition by malonyl-CoA, is essential to malonyl-CoA sensitivity (15), although the mechanistic details of its role in the enzyme active center remains still elusive.

From the kinetic data presented (Fig. 6), we conclude that only one of the two inhibition sites is competitive with respect to the substrate carnitine and that the two inhibitory sites are mutually exclusive, showing different affinity for malonyl-CoA. There are two possible explanations for the kinetic data (Schemes 2 and 3); in both cases, the binding of malonyl-CoA to one inhibitory site excludes the binding of carnitine. In Scheme 2, the binding of malonyl-CoA at the second site is independent of the binding of carnitine, whereas in Scheme 3, this binding would be possible only if carnitine was already bound (53). We are not yet in a position to decide which model is the more accurate.

In the present article, we have taken the data from various authors who studied the relationships between IC_{50} for malonyl-CoA and K_m of carnitine under different conditions and attempted to find a formula that might link them. It is noteworthy that, despite the wide variety of sources of data, the relationship between log IC_{50} for malonyl-CoA inhibition and log K_m for carnitine is linear, and the slope is essentially the same (values range between -1.37 and -1.65, with a mean value of -1.49). Kinetic data indicate that malonyl-CoA interferes with the carnitine binding and thus that their respective binding sites are close. Moreover, kinetic experiments performed in this study confirm this hypothesis. It was observed that in yeast-expressed wild type CPT1A, an increase in carnitine concentration produced an increase in IC_{50} values for malonyl-CoA (Fig. 5*C* and Table 3). Equally, when kinetics experiments were performed by varying carnitine concentrations at several fixed malonyl-CoA levels, Michaelis-Menten hyperbolic kinetics were obtained in which the apparent K_m for carnitine increased at progressively higher malonyl-CoA concentrations.

Kinetic results also agree with the *in silico* model for two possible binding sites for malonyl-CoA that would be situated along the catalytic tunnel, from the carnitine hollow where the catalytic His^{473} lies, toward the opposite distal surfaces of CPT1. The docked malonyl-CoA model in the A site shows polar contacts at the carnitine-binding site with the conserved residues Tyr^{241}, His^{473}, Asp^{477}, Ala^{478}, Tyr^{589}, Thr^{602}, Ser^{685}, and Ser^{687} (as shown in Table 2). The catalytic His^{473} (24) would make contact with the carboxyl group of malonyl-CoA, suggesting a possible electrostatic interaction between them. Other polar contacts between malonyl-CoA carboxylic oxygen

atoms and CPT1A include Tyr^{241}, Tyr^{589}, and Thr^{602} hydroxyl groups. Most, but not all, of the residues in the carnitine hollow are shared by the A site and the O site (Table 2).

From the data presented in this study, can we deduce the stoichiometry between malonyl-CoA and CPT1? Data from Fig. 2 indicate that the two malonyl-CoA molecules compete for the same space within the catalytic site. This would support a functional (malonyl-CoA/CPT1A) 1:1 stoichiometry. On the other hand, a 2:1 stoichiometry in our kinetic study would entail that a putative EI_2 complex would give a pattern of straight lines that would not intersect at the same point in a double reciprocal values plot (this is not the case) and also that the secondary representation (slopes *versus* [I]) would produce a parabola. These graphics have not been obtained in our study, from which a 1:1 stoichiometry of malonyl-CoA/CPT1A was suggested.

To our knowledge, no quantitative stoichiometry has been presented elsewhere in the literature. Several biochemical studies, however, have shown that malonyl-CoA binds in two sites: one high affinity and the other low affinity. Scatchard plots of [^{14}C]malonyl-CoA binding in the liver CPT1 isoform clearly show that there are two, kinetically distinguishable malonyl-CoA binding sites (10, 50, 57). However, in 1990, Kolodziej and Zammit (58) re-evaluated the interaction of malonyl-CoA with the rat liver mitochondrial CPT1 system by using purified outer membranes. From the Scatchard plots, they concluded that malonyl-CoA binding was largely accounted for by a single, high affinity component in CPT1, in contrast to the dual site previously found with intact mitochondria. They suggested that the low affinity binding observed with intact rat liver mitochondria may be totally unrelated to the CPT1 system and may be associated with other proteins present in the mitochondrial intermembrane space or inner membrane as well as other structures that contaminate crude mitochondrial preparations (peroxisomes and microsomes). This would suggest a malonyl-CoA/CPT1A stoichiometry of 1:1. Moreover, Cook *et al.* (7), through a Yonetani-Theorell analysis of liver CPT1 inhibition with two CPT1 inhibitors (malonyl-CoA and free CoA), showed that every one binds to a different site, from which it could be inferred that the schoichiometry of CPTI/malonyl-CoA/free CoA could be 1:1:1. This view would support our three-dimensional model, since free CoA could freely bind on the A site without steric hindrance to the simultaneous malonyl-CoA binding in the O site. Our three-dimensional model, in addition, allows the binding of a malonyl-CoA on the O site simultaneous with the palmitoyl-CoA binding on the A site. This view would also be supported by the data by Kolodziej and Zammit (58), which showed that the occurrence of palmitoyl-CoA in the assay had no effect on the maximal binding capacity of [^{14}C]malonyl-CoA on rat liver mitochondria. In this case, the stoichiometry would be as follows: 1:1:1 (CPT1A/malonyl-CoA/palmitoyl-CoA).

In a different study, Zammit and Corstorphine (57) also suggested that the microenvironment of the molecular species responsible for low affinity binding of malonyl-CoA undergoes temperature-related transitions that may derive from changes in membrane fluidity that occur around 25 °C, and evidently only binding at the high affinity site was required to elicit inhibition of CPT1. In other words, temperature might modify the membrane fluidity, and as a consequence, the tertiary structure of CPT could be modified in such a way as to accept, under special circumstances, the second malonyl-CoA molecule in the (second) low affinity site.

In conclusion, we have located malonyl-CoA binding sites by *in silico* procedures, and they have been confirmed by site-directed mutagenesis of those amino acid residues interacting with the inhibitor. Moreover, individual mutations of critical amino acids (Glu^{26} and Lys^{561}) reduced malonyl-CoA sensitivity, showing the precise interactions between NH_2- and COOH-terminal domains. However, when the interaction was preserved in a double mutant, in which the individual positions were swapped (whether NH_2- or COOH-terminal), malonyl-CoA sensitivity was rescued. This study also shows that the relationship between malonyl-CoA and carnitine is mutually exclusive, as deduced from the docking position of both carnitine and malonyl-CoA in the three-dimensional model of CPT1. The inhibitory kinetic studies are also compatible with this view.

Acknowledgments—We are grateful to Robin Rycroft of the Language Service for valuable assistance in the preparation of the manuscript and to Biomol-Informatics SL for bioinformatics consulting.

REFERENCES

1. McGarry, J. D., and Brown, N. F. (1997) *Eur. J. Biochem.* **244,** 1–14
2. Esser, V., Britton, C. H., Weis, B. C., Foster, D. W., and McGarry, J. D. (1993) *J. Biol. Chem.* **268,** 5817–5822
3. Yamazaki, N., Shinohara, Y., Shima, A., and Terada, H. (1995) *FEBS Lett.* **363,** 41–45
4. Price, N., van der Leij, F., Jackson, V., Corstorphine, C., Thomson, R., Sorensen, A., and Zammit, V. (2002) *Genomics* **80,** 433–442
5. Anderson, R. C. (1998) *Curr. Pharm. Des.* **4,** 1–16
6. Cha, S. H., Rodgers, J. T., Puigserver, P., Chohnan, S., and Lane, M. D. (2006) *Proc. Natl. Acad. Sci. U. S. A.* **103,** 15410–15415
7. Cook, G. A., Mynatt, R. L., and Kashfi, K. (1994) *J. Biol. Chem.* **269,** 8803–8807
8. Zammit, V. A., Corstorphine, C. G., and Gray, S. R. (1984) *Biochem. J.* **222,** 335–342
9. Zammit, V. A. (1984) *Biochem. J.* **218,** 379–386
10. Bird, M. I., and Saggerson, E. D. (1984) *Biochem. J.* **222,** 639–647
11. Bird, M. I., and Saggerson, E. D. (1985) *Biochem. J.* **230,** 161–167
12. Shi, J., Zhu, H., Arvidson, D. N., and Woldegiorgis, G. (1999) *J. Biol. Chem.* **274,** 9421–9426
13. Shi, J., Zhu, H., Arvidson, D. N., and Woldegiorgis, G. (2000) *Biochemistry* **39,** 712–717
14. Jackson, V. N., Cameron, J. M., Fraser, F., Zammit, V. A., and Price, N. T. (2000) *J. Biol. Chem.* **275,** 19560–19566
15. Morillas, M., Gomez-Puertas, P., Bentebibel, A., Selles, E., Casals, N., Valencia, A., Hegardt, F. G., Asins, G., and Serra, D. (2003) *J. Biol. Chem.* **278,** 9058–9063
16. Jackson, V. N., Price, N. T., and Zammit, V. A. (2001) *Biochemistry* **40,** 14629–14634
17. Jackson, V. N., Zammit, V. A., and Price, N. T. (2000) *J. Biol. Chem.* **275,** 38410–38416
18. Faye, A., Borthwick, K., Esnous, C., Price, N. T., Gobin, S., Jackson, V. N., Zammit, V. A., Girard, J., and Prip-Buus, C. (2005) *Biochem. J.* **387,** 67–76
19. Borthwick, K., Jackson, V. N., Price, N. T., and Zammit, V. A. (2006) *J. Biol. Chem.* **281,** 32946–32952
20. McGarry, J. D., Robles-Valdes, C., and Foster, D. W. (1975) *Proc. Natl. Acad. Sci. U. S. A.* **72,** 4385–4388
21. Saggerson, E. D., and Carpenter, C. A. (1981) *FEBS Lett.* **129,** 225–228

22. McGarry, J. D., Mills, S. E., Long, C. S., and Foster, D. W. (1983) *Biochem. J.* **214,** 21–28
23. Mills, S. E., Foster, D. W., and McGarry, J. D. (1984) *Biochem. J.* **219,** 601–608
24. Morillas, M., Gomez-Puertas, P., Roca, R., Serra, D., Asins, G., Valencia, A., and Hegardt, F. G. (2001) *J. Biol. Chem.* **276,** 45001–45008
25. Jaroszewski, L., Rychlewski, L., and Godzik, A. (2000) *Protein Sci.* **9,** 1487–1496
26. Jaroszewski, L., Rychlewski, L., Li, Z., Li, W., and Godzik, A. (2005) *Nucleic Acids Res.* **33,** W284–W288
27. Altschul, S. F., Madden, T. L., Schaffer, A. A., Zhang, J., Zhang, Z., Miller, W., and Lipman, D. J. (1997) *Nucleic Acids Res.* **25,** 3389–3402
28. Andreeva, A., Howorth, D., Brenner, S. E., Hubbard, T. J., Chothia, C., and Murzin, A. G. (2004) *Nucleic Acids Res.* **32,** D226–D229
29. Murzin, A. G., Brenner, S. E., Hubbard, T., and Chothia, C. (1995) *J. Mol. Biol.* **247,** 536–540
30. Berman, H. M., Westbrook, J., Feng, Z., Gilliland, G., Bhat, T. N., Weissig, H., Shindyalov, I. N., and Bourne, P. E. (2000) *Nucleic Acids Res.* **28,** 235–242
31. Foster, M. P., Wuttke, D. S., Radhakrishnan, I., Case, D. A., Gottesfeld, J. M., and Wright, P. E. (1997) *Nat. Struct. Biol.* **4,** 605–608
32. Jogl, G., Hsiao, Y. S., and Tong, L. (2005) *J. Biol. Chem.* **280,** 738–744
33. Hsiao, Y. S., Jogl, G., Esser, V., and Tong, L. (2006) *Biochem. Biophys. Res. Commun.* **346,** 974–980
34. Guex, N., Diemand, A., and Peitsch, M. C. (1999) *Trends Biochem. Sci.* **24,** 364–367
35. Peitsch, M. C. (1996) *Biochem. Soc. Trans.* **24,** 274–279
36. Schwede, T., Kopp, J., Guex, N., and Peitsch, M. C. (2003) *Nucleic Acids Res.* **31,** 3381–3385
37. Hooft, R. W., Vriend, G., Sander, C., and Abola, E. E. (1996) *Nature* **381,** 272
38. Vriend, G. (1990) *J. Mol. Graph.* **8,** 52–56
39. Guex, N., and Peitsch, M. C. (1997) *Electrophoresis* **18,** 2714–2723
40. Ritchie, D. W., and Kemp, G. J. (2000) *Proteins* **39,** 178–194
41. Goodsell, D. S., and Olson, A. J. (1990) *Proteins* **8,** 195–202
42. Morris, G. M., Goodsell, D. S., Halliday, R. S., Huey, R., Hart, E., Belew, R. K., and Olson, A. J. (1998) *J. Comput. Chem.* **19,** 1639–1662
43. Morris, G. M., Goodsell, D. S., Huey, R., and Olson, A. J. (1996) *J. Comput. Aided Mol. Des.* **10,** 293–304
44. Cordente, A. G., Lopez-Vinas, E., Vazquez, M. I., Swiegers, J. H., Pretorius, I. S., Gomez-Puertas, P., Hegardt, F. G., Asins, G., and Serra, D. (2004) *J. Biol. Chem.* **279,** 33899–33908
45. Bentebibel, A., Sebastian, D., Herrero, L., Lopez-Vinas, E., Serra, D., Asins, G., Gomez-Puertas, P., and Hegardt, F. G. (2006) *Biochemistry* **45,** 4339–4350
46. Stewart, J. J. (1990) *J. Comput. Aided Mol. Des.* **4,** 1–105
47. Rufer, A. C., Thoma, R., Benz, J., Stihle, M., Gsell, B., De Roo, E., Banner, D. W., Mueller, F., Chomienne, O., and Hennig, M. (2006) *Structure* **14,** 713–723
48. Tress, M., de Juan, D., Grana, O., Gomez, M. J., Gomez-Puertas, P., Gonzalez, J. M., Lopez, G., and Valencia, A. (2005) *Proteins* **60,** 275–280
49. Morillas, M., Lopez, V. E., Valencia, A., Serra, D., Gomez-Puertas, P., Hegardt, F. G., and Asins, G. (2004) *Biochem. J.* **379,** 777–784
50. Grantham, B. D., and Zammit, V. A. (1986) *Biochem. J.* **233,** 589–593
51. Kashfi, K., and Cook, G. A. (1999) *Adv. Exp. Med. Biol.* **466,** 27–42
52. Kashfi, K., Mynatt, R. L., and Cook, G. A. (1994) *Biochim. Biophys. Acta* **1212,** 245–252
53. Segel, I. H. (1993) *Enzyme Kinetics: Behavior and Analysis of Rapid Equilibrium and Steady State Enzyme Systems*, pp. 170–192, John Wiley & Sons, Inc., New York
54. Esser, V., Brown, N. F., Cowan, A. T., Foster, D. W., and McGarry, J. D. (1996) *J. Biol. Chem.* **271,** 6972–6977
55. Nicot, C., Hegardt, F. G., Woldegiorgis, G., Haro, D., and Marrero, P. F. (2001) *Biochemistry* **40,** 2260–2266
56. Zhu, H., Shi, J., de Vries, Y., Arvidson, D. N., Cregg, J. M., and Woldegiorgis, G. (1997) *Arch. Biochem. Biophys.* **347,** 53–61
57. Zammit, V. A., and Corstorphine, C. G. (1985) *Biochem. J.* **231,** 343–347
58. Kolodziej, M. P., and Zammit, V. A. (1990) *Biochem. J.* **267,** 85–90

Am J Physiol Heart Circ Physiol 295: H256–H265, 2008.
First published May 16, 2008; doi:10.1152/ajpheart.91489.2007.

Reduced heart size and increased myocardial fuel substrate oxidation in ACC2 mutant mice

M. Faadiel Essop,[1,2] Heidi S. Camp,[3] Cheol Soo Choi,[4] Saumya Sharma,[5] Ryan M. Fryer,[6] Glenn A. Reinhart,[6] Patrick H. Guthrie,[5] Assia Bentebibel,[7,8] Zeiwei Gu,[7] Gerald I. Shulman,[4] Heinrich Taegtmeyer,[5] Salih J. Wakil,[7] and Lutfi Abu-Elheiga[7]

[1]*Department of Physiological Sciences, Stellenbosch University, Stellenbosch;* [2]*Hatter Heart Research Institute, University of Cape Town Faculty of Health Sciences, Cape Town, South Africa;* [3]*Metabolic Disease Research, Global Pharmaceutical Research and Development, Abbott Laboratories, Abbott Park;* [4]*Departments of Internal Medicine, Yale University School of Medicine, New Haven, Connecticut;* [5]*Department of Internal Medicine, Division of Cardiology, University of Texas-Houston Medical School, Houston;* [6]*Department of Integrative Pharmacology, Abbott Laboratories, Abbott Park, Illinois;* [7]*Verna and Mars McLean Department of Biochemistry and Molecular Biology, Baylor College of Medicine, Houston, Texas; and* [8]*Department of Biochemistry and Molecular Biology, School of Pharmacy, University of Barcelona, Barcelona, Spain*

Submitted 18 December 2007; accepted in final form 28 April 2008

Essop MF, Camp HS, Choi CS, Sharma S, Fryer RM, Reinhart GA, Guthrie PH, Bentebibel A, Gu Z, Shulman GI, Taegtmeyer H, Wakil SJ, Abu-Elheiga L. Reduced heart size and increased myocardial fuel substrate oxidation in ACC2 mutant mice. *Am J Physiol Heart Circ Physiol* 295: H256–H265, 2008. First published May 16, 2008; doi:10.1152/ajpheart.91489.2007.—The cardiac-enriched isoform of acetyl-CoA carboxylase (ACC2) is a key regulator of mitochondrial fatty acid (FA) uptake via carnitine palmitoyltransferase 1 (CPT1). To test the hypothesis that oxidative metabolism is upregulated in hearts from animals lacking ACC2 (employing a transgenic *Acc2*-mutant mouse), we assessed cardiac function in vivo and determined rates of myocardial substrate oxidation ex vivo. When examined by echocardiography, there was no difference in systolic function, but left ventricular mass of the *Acc2*-mutant (MUT) mouse was significantly reduced (~25%) compared with wild-types (WT). Reduced activation of the mammalian target of rapamycin (mTOR) and its downstream target p70S6K was found in MUT hearts. Exogenous oxidation rates of oleate were increased ~22%, and, unexpectedly, exogenous glucose oxidation rates were also increased in MUT hearts. Using a hyperinsulinemic-euglycemic clamp, we found that glucose uptake in MUT hearts was increased by ~83%. Myocardial triglyceride levels were significantly reduced in MUT vs. WT while glycogen content was the same. In parallel, transcript levels of PPARα and its target genes, pyruvate dehydrogenase kinase-4 (PDK-4), malonyl-CoA decarboxylase (MCD), and mCPT1, were downregulated in MUT mice. In summary, we report that *1*) *Acc2*-mutant hearts exhibit a marked preference for the oxidation of both glucose and FAs coupled with greater utilization of endogenous fuel substrates (triglycerides), *2*) attenuated mTOR signaling may result in reduced heart sizes observed in *Acc2*-mutant mice, and *3*) *Acc2*-mutant hearts displayed normal functional parameters despite a significant decrease in size.

acetyl-CoA carboxylase; fatty acid β-oxidation; glucose oxidation; PPARα

CARNITINE PALMITOYLTRANSFERASE 1 (CPT1), which catalyzes the rate-limiting step of mitochondrial fatty acid (FA) uptake, is subject to stringent regulatory mechanisms (24). Malonyl-CoA is a potent allosteric inhibitor of CPT1 and acts as a rheostat for overall mitochondrial FA β-oxidation (FAO) (26). Malonyl-CoA levels are controlled by rates of synthesis [via acetyl-CoA carboxylase (ACC)] and rates of degradation [via malonyl-CoA decarboxylase (MCD)]. Of the two ACC isoforms, ACC1 (≈265 kDa) is predominantly expressed in lipogenic tissues such as the liver and adipocytes (1, 23, 36), while ACC2 (≈280 kDa) is enriched in tissues with enhanced oxidative capacity for example, heart and skeletal muscle (2, 8, 37). The distinct ACC isoform expression profiles suggest that malonyl-CoA generated by ACC1 and ACC2 may differentially regulate FA synthesis and FAO. In support, we presented evidence for separate ACC subcellular locations, with ACC1 localized to the cytosol and ACC2 associated with mitochondria (3). Moreover, *Acc2*-mutant mice (lacking functional ACC2) displayed increased FAO rates in skeletal muscle and reduced body weight and fat content (4). On the contrary, a null mutation of ACC1 in mice resulted in embryonic lethality (6).

Recently, we found that *Acc2*-mutant mice, unlike wild-type controls, did not develop diabetes when fed an obesity-inducing diet (5). Moreover, Debard et al. (13) reported increased ACC2 gene expression levels in skeletal muscle of type 2 diabetic patients. Together, these data suggest that high levels of ACC2 may contribute to the development of the diabetic phenotype and that diminished ACC2 expression in this particular context may hold therapeutic value. In light of these observations, we investigated the effects of in vivo ACC2 lack on the regulation of myocardial fuel substrate oxidation. In this study, we performed Langendorff heart perfusions comparing the previously described *Acc2*-mutant transgenic mouse strain (4) with age-matched controls and matched substrate oxidation data with expression levels of cardiac metabolic genes and functional data generated by echocardiography. Here, we found that both myocardial oleate and glucose oxidation rates were higher in *Acc2*-mutant mice, associated with sustained cardiac contractile function, but reduced heart size. Reduced activation of the mammalian target of rapamycin (mTOR) and its downstream target p70S6K was found in MUT hearts and may account for its decreased size. In parallel, expression of peroxisome pro-

Address for reprint requests and other correspondence: L. Abu-Elheiga, Dept. of Biochemistry and Molecular Biology, Baylor College of Medicine, One Baylor Plaza, MS BCM-125, Houston, TX 77030 (e-mail: lutfia@bcm.tmc.edu).

The costs of publication of this article were defrayed in part by the payment of page charges. The article must therefore be hereby marked "*advertisement*" in accordance with 18 U.S.C. Section 1734 solely to indicate this fact.

 0363-6135/08 $8.00 Copyright © 2008 the American Physiological Society

liferator-activated receptor-α (PPARα) and its target genes was attenuated in *Acc2*-mutant mice compared with controls. We propose that this may help sustain normal function of the *Acc2*-mutant mouse heart.

METHODS

Animals. Generation of the *Acc2*-mutant transgenic mouse strain has been previously described (3). Male mutant and wild-type strains were housed under controlled conditions (12:12-h light-dark cycle; 25°C) in the Animal Care Center at Baylor College of Medicine and had ad libitum access to standard laboratory chow (Purina Mills, Richmond, IN) and water. All experiments were performed using the 129/Sv background strain except for the glucose uptake and echocardiographic studies where the C57/129/Sv background strain (mixed background) was employed. Animal experiments were approved by the Animal Care and Use Commitee at Baylor College of Medicine and conducted in accordance with the Baylor College of Medicine's Animal Care and Use Guidelines. All animals were treated in accordance with the *Guide for the Care and Use of Laboratory Animals* published by the US National Institutes of Health (NIH Publication No. 85-23, revised 1996).

Measurement of myocardial malonyl-CoA levels. Heart tissue was harvested, snap-frozen in liquid nitrogen, and then homogenized in a 1:10 volume (wt/vol) of ice-cold 5% sulfosalicylic acid containing 50 μM dithioerythritol. Homogenates were centrifuged at 15,000 *g* for 60 min at 2°C and the supernatants were filtered through a 0.22-μm filter (Ultrafree-MC, Millipore, Bedford, MA). Samples were stored at −80°C before liquid chromatography mass spectrometry analysis. HPLC was run in binary mode [*A*: 5 mM dimethylbutylamine and 6 mM HOAc; *B*: 0.1% formic acid in CH3CN (EMD Chemicals, Gibbstown, NJ)] at 200 ml/min with the third pump to deliver postcolumn mixing solvent CH3CN. The data were acquired on an Applied Biosystem Pulsar I quadrapole-TOF mass spectrometer (Foster City, CA) using positive ion TOFMS mode.

Measurement of myocardial triglyceride levels. Heart triglyceride levels were measured as described by Chandler et al. (11). Hearts ($n = 5$) were excised, washed with PBS, and stored at −80°C before being processed. Individual hearts were homogenized using a Kinematica Polytron mechanical tissue blender for 30 s (medium speed), followed by extraction with 2 vol of chloroform:methanol (1:1). The organic fraction was evaporated using nitrogen, and the pellet was dissolved in 1% Triton X-100 (diluted in ethanol). Samples were diluted 1:5 and triglyceride levels were measured using the Infinity Triglyceride Kit (Thermo Electron, Rugby, UK) that was adapted for colorimetric analysis in 96-well plate format.

Measurement of myocardial glycogen levels. Wild-type and *Acc2*-mutant mice ($n = 5$) were killed by decapitation, and hearts were rapidly isolated and immediately frozen in liquid nitrogen. Myocardial glycogen levels were determined using the method of Hassid and Abraham (19). Frozen hearts were placed in test tubes and dissolved in 30% KOH (wt/vol) whereafter tubes were immersed in boiling water and glycogen precipitated with ethanol. Glycogen was converted to monosaccharides by boiling the pellet in 1 ml of 3.79 M H_2SO_4 for 3 h followed by the addition of 0.1 ml 0.33 M MOPS. The solution was thereafter neutralized to pH 7 using 10 M KOH. The final volume was recorded and glucose concentration was measured using a glucose-determining kit (Sigma, St. Louis, MO). Glycogen content was expressed as milligrams of glucose per gram (wet wt).

Determination of ex vivo cardiac fuel substrate metabolism. Five-month-old male *Acc2*-mutant and matched wild-type mice were anesthetized with chloral hydrate (0.3 mg/g body wt ip). Hearts were excised and thereafter perfused for 30 min in the Langendorff mode at an afterload of 80 cmH_2O with Krebs-Henseleit (K-H) buffer containing 5 mM D-glucose (plus 27 μCi/l [U-^{14}C]glucose), 0.4 mM sodium oleate (plus 40 μCi/l [9,10-^{3}H]oleate) bound to 1% BSA (Cohn fraction V, FA free; Serologicals, Norcross, GA), and insulin (40 μU/ml; Lilly). Throughout the experiment, the K-H buffer was equilibrated with 95% O_2-5% CO_2. Coronary flow was measured every 5 min. At the end of the perfusions, hearts were freeze-clamped and stored in liquid nitrogen (for dry weight determination). Rates of oleate and glucose oxidation were determined as described previously (17). Myocardial oxygen consumption $M\dot{V}O_2$ was calculated by measuring the arterio-venous O_2 content difference, $O_{2(a-v)}^{-}$, which was multiplied by the coronary flow.

RNA isolation and quantitative RT-PCR. At 5 mo of age, hearts from male *Acc2*-mutant and matched wild-type mice were isolated and freeze-clamped in liquid nitrogen for subsequent RNA extraction and gene expression analysis. RNA isolation and quantitative RT-PCR of samples were performed as previously described (14) for *1*) FA metabolic genes–PPARα, a pivotal transcriptional activator of several FA utilization genes; muscle-type carnitine palmitoyltransferase 1 (mCPT1), the rate-limiting mitochondrial FA transfer enzyme; medium-chain acyl-CoA dehydrogenase (MCAD), a representative FAO enzyme; PPAR-γ coactivator 1α (PGC-1α), a transcriptional coactivator controlling mitochondrial biogenesis and cellular energy metabolic pathways; and *2*) glucose metabolic genes–cardiac-enriched glucose transporter isoforms GLUT1 and GLUT4; pyruvate dehydrogenase kinase-4 (PDK-4), an indirect inhibitor of glucose oxidation. The nucleotide sequences for primers and probes have been previously published (14, 41). Data were normalized to the number of cyclophilin transcripts, which was not significantly different between the treatment groups (data not shown).

Preparation of mitochondrial fractions. Mitochondria-enriched fractions were obtained from wild-type and mutant mouse hearts as previously described (31), with minor modifications. Hearts (3–4 animals) were homogenized in 250 mM sucrose buffer using an omni mixer and subsequently centrifuged at 1,000 *g* for 15 min. The pellet was homogenized and centrifuged at 600 *g* for 10 min. The resulting supernatant was centrifuged at 15,000 *g* for 15 min, and the pellet was resuspended in 100 μl of a buffer containing 250 mM sucrose and 150 mM KCl. All manipulations were performed at 4°C. Mitochondrial protein concentrations were determined using the Bio-Rad protein assay with bovine albumin as a standard.

To determine steady-state peptide levels of mitochondrial mCPT1, 30 μg of mitochondrial protein were subjected to polyacrylamide gel electrophoresis (4–12% NuPAGE MES gels). Mitochondrial mCPT1 peptide levels were detected using an antibody kindly provided by Dr. V. A. Zammit (Warwick Medical School, Coventry, UK). For equal loading controls, the same blot was stripped, washed, and probed with avidin peroxidase that detects mitochondrial biotinylated proteins such as propionyl-CoA carboxylase (PCC), which was equally expressed in hearts of wild-type and *Acc2*-mutant mice.

Total protein isolation and immunoblotting. Hearts from wild-type and mutant *Acc2* mice were excised, snap-frozen, and ground in liquid nitrogen. This powder was added to a homogenization buffer consisting of 3 ml of RIPA buffer [50 mM Tris, pH 7.5; 150 mM NaCl; 1% NP-40; 0.5% deoxy cholic acid; 0.1% SDS; 1 mM $NaVO_3$; 10 mM NaF; 0.2 mM EDTA; protease inhibitor cocktail (1 mM PMSF and 3 μg/ml of leupeptine, pepstatin, aprotinin, and anti-trypsin)]. The suspension was homogenized using a Polytron for 30 s followed by 3 × 10-s sonication bursts. The lysate was thereafter centrifuged at 27,000 *g* for 1 h. Protein concentrations were determined and 30 μg of each sample were separated on 4–12% NuPAGE MES gels.

MCD antibodies were kindly provided by Dr. M. Prentki (University of Montreal, Canada). Steady-state peptide levels of ACC, pyruvate carboxylase (PC), and PCC were detected by avidin peroxidase using either ECL detection (Amersham) or the 3,3′,5,5′-tetramethylbenzidine (TMB) liquid substrate system for membranes (Sigma). Peptide levels of mTOR, pmTOR Ser^{2481}, Akt, and pAKT Ser^{473} were determined by Western blot analysis using antibodies from Cell Signaling (Danvers, MA) and visualized by ECL.

Mouse echocardiography. Transthoracic echocardiography was performed using an Acuson Sequoia (Siemens) ultrasonograph with a

15-MHz transducer as detailed previously (18). For acquisition of two-dimensional guided M-mode images at the tips of papillary muscles and Doppler studies, mice were sedated by intraperitoneal administration of 100 mg/kg ketamine and maintained on a heated platform in a left lateral decubitus position. The chest was shaved and prewarmed coupling gel was applied. Transmitral and aortic velocities were measured using Doppler pulse wave imaging. All images were saved to an on-board optical disk.

End diastolic and systolic left ventricular (LV) diameter as well as anterior and posterior wall (AW and PW, respectively) thickness were measured on line from M-mode images using the leading edge-to-leading edge convention. All parameters were measured over at least three consecutive cardiac cycles and averaged. LV fractional shortening was calculated as [(LV diameter$_{diastole}$ − LV diameter$_{systole}$)/LV diameter$_{diastole}$] × 100 and LV mass was calculated by using the formula {1.05 × [(PW$_{diastole}$ + AW$_{diastole}$ + LV diameter$_{diastole}$)^3 − (LV diameter$_{diastole}$)^3]}. Relative wall thickness was calculated as 2*PW$_{diastole}$/LV diameter$_{diastole}$. Heart rate was determined from at least three consecutive intervals from the pulse wave Doppler tracings of the LV outflow tract. Isovolumic relaxation time was measured as the time from the closing of the aortic value to the opening of the mitral value from pulse wave Doppler tracings of the LV outflow tract and mitral inflow region. To measure E and A waves, heart rates were slowed down using additional doses (1/4 to 1/2) of ketamine. However, all other measurements (except E and A waves) were performed at the higher heart rate. For tissue Doppler measures, the smallest possible sample volume was placed at the septal mitral annulus to capture the early diastolic (Ea) and late diastolic (Aa) velocities (34, 38). The same person obtained all images and measures and was blinded to genotype.

In vivo measurement of insulin-stimulated heart glucose uptake. After an overnight fast, a hyperinsulinemic-euglycemic clamp was conducted for 120 min with a primed/continuous infusion of human insulin (126 pmol/kg prime, 18 pmol·kg^{-1}·min^{-1} infusion; Novo Nordisk, Princeton, NJ) to raise plasma insulin within the physiological range. Plasma glucose was clamped basal concentrations (~6.7 mM). 2-Deoxy-D-[1-^{14}C]glucose (^{14}C-2-DG; Perkin Elmer, Boston, MA) was injected as a bolus at the 75th minute of the clamp to estimate the rate of insulin-stimulated tissue glucose uptake as previously described (32). Blood samples (10 μl) for the measurement of plasma ^{14}C activities were taken during the last 45 min of the clamp. At the end of the clamp, mice were anesthetized with pentobarbital sodium injection and tissues were taken for biochemical measurements within 3 min. For the determination of heart glucose uptake, heart samples were homogenized, and the supernatants were subjected to an ion-exchange column to separate tissue ^{14}C-2-DG-6-phosphate (2-DG-6-P) from 2-DG. Heart glucose uptake was calculated from the area under the curve of the plasma ^{14}C-2-DG profile and muscle ^{14}C-2-DG-6-P content, as previously described (40).

Statistical analysis. The time course data for the heart perfusion studies are presented as means ± SE. Statistical analysis on perfusion data was performed using ANOVA repeated-measures one-way ANOVA. The unpaired Student's *t*-test was used to determine differences between two groups. A value of $P < 0.05$ was considered significant.

RESULTS

In vivo cardiac functional analysis. Echocardiographic studies were performed and data are summarized in Table 1. There was a ~25% decrease in LV mass and LV mass/body wt, consistent with a smaller heart as assessed by dry weight measurement during the metabolic studies. In *Acc2*-mutant mice, LV diastolic and LV systolic dimensions decreased by 17 and 27%, respectively, compared with wild-types ($P < 0.001$). The decrease in both LV dimensions did not cause a significant change in fractional shortening (45 ± 5 and 38 ± 12 in *Acc2*-mutant mouse and matched controls, respectively; Table 1). Although there was a slight increase in the heart rate of *Acc2*-mutant mice, this did not reach statistical significance (530 ± 82 and 578 ± 61 beats/min for wild-type and *Acc2*-mutant mice, respectively). When additional ketamine was administered to measure E and A waves, the heart rate decreased to 316 ± 51 and 325 ± 32 beats/min for wild-type and mutant mice, respectively. All other parameters such as PWd, Awd RWth, E/A, Ea/Aa, and IVRT were similar (Table 1).

Table 1. *Echocardiographic parameters in WT and Acc2-mutant mice*

	WT	*Acc2*-Mutant
Body wt	32.4±3.4	32.5±3.3
LV mass, g	0.15±0.02	0.11±0.02*
LV mass/BW, mg/g	4.75±0.54	3.40±0.36*
Heart rate, beats/min	530±82	578±61
PWd, mm	0.9±0.09	0.9±0.1
Awd, mm	0.9±0.07	0.9±0.1
LVDd, mm	4.2±0.3	3.5±0.2*
LVDs, mm	2.6±0.6	1.9±0.2*
RWth	0.45±0.06	0.51±0.2
Fractional shortening, %	38±12	45±5
E/A	1.67±0.5	1.32±0.21
Ea/Aa	1.58±0.27	1.49±0.21
IVRT, ms	17±2	16±1

All values are means ± SD. PWd, posterior wall in diastole; Awd, anterior (interventricular septum) in diastole; LVDd, left ventricular diameter in diastole; LVDs, left ventricular diameter in systole; RWth, relative wall thickness (2*PWd/LVDd); % Fractional shortening, (LVDd−LVDs)/LVDd; LV mass/BW, left ventricular mass in mg/body wt in g; E/A, ratio of early transmittal filling velocity (E) to late transmittal filling velocity; Ea/Aa, ratio of early diastolic maximal tissue velocity (ea) to late maximal tissue velocity; IVRT, isovolumic relaxation time in s [$n = 10$, *$P < 0.001$ vs. wild-type (WT)]. Animals aged 31 wk ($n = 10$ per group) were subjected to 2-D M-mode echocardiography at University of Madison-Wisconsin.

Heart weight. We also determined the heart dry weight of mice at the end of perfusion studies. Interestingly, heart weight (29 ± 2 vs. 48 ± 4 mg; $n = 8$, $P = 0.001$) and the heart/body wt ratio were significantly reduced in mutant vs. wild-type mice (0.94 ± 0.01 vs. 1.27 ± 0.11; $n = 8$, $P < 0.05$; Fig. 1). These results are consistent with our echocardiography studies, confirming reduced heart size in *Acc2*-mutant mice.

Determination of myocardial malonyl-CoA and MCD levels. Malonyl-CoA levels in *Acc2*-mutant hearts were markedly reduced (~70%) compared with wild-types ($P = 0.0001$; Fig. 2*A*). These levels are consistent with previous measurements in *Acc2*-mutant hearts using the biochemical method of McGarry et al. (25). The significant reduction in malonyl-CoA levels in hearts of *Acc2*-mutant mice further confirms that the ACC2 isoform is the major contributor to the myocardial malonyl-CoA pool. These results are in agreement with earlier studies showing the predominance of ACC2 mRNA/protein levels in heart tissues compared with ACC1 (1, 2, 37). Since MCD is also a major regulator of malonyl-CoA levels in muscle and heart tissues, we also measured MCD expression levels. Here, MCD transcript levels were reduced by ~50% in *Acc2*-mutant hearts compared with wild-types (data not shown). In agreement, we found that MCD protein levels were also decreased ($P = 0.001$ vs. wild-types; Fig. 2, *B* and *C*). As shown in Fig. 2*D*, ACC1 is still expressed to a significant degree in *Acc2*-mutant hearts, suggesting that residual malonyl-CoA is due to

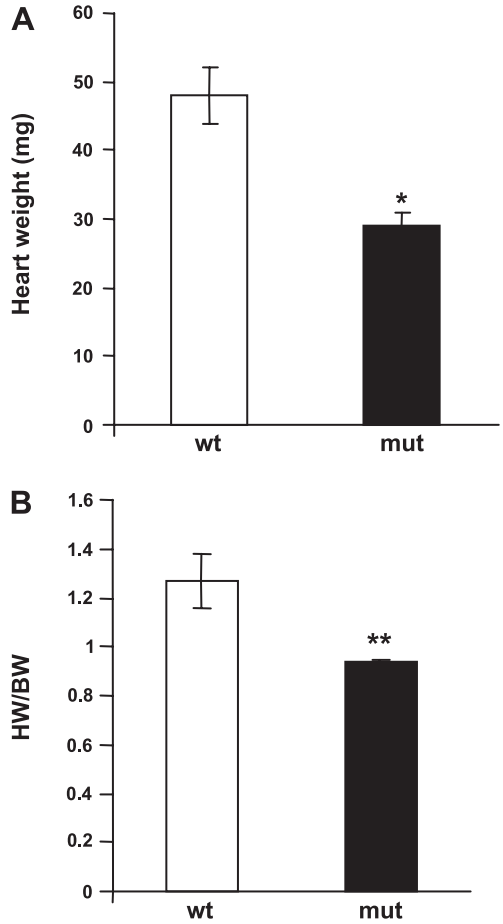

Fig. 1. Heart weight measurements. Hearts were collected at the end of perfusion studies, dried in an oven at 65°C, and weighed. *A*: heart weights (HW; in mg). *B*: heart-to-body wt (BW) ratios for wild-type vs. mutant mice. Values are depicted as means ± SE. *$P < 0.001$ and **$P < 0.05$ vs. wild-type.

both remaining ACC1 and MCD downregulation in mutant hearts. There were no significant changes in the level of two mitochondrial enzymes, i.e., PCC and PC (Fig. 2*D*).

Determination of myocardial glycogen and triglyceride content. Endogenous triglycerides and glycogen are important myocardial energy sources. Here, we found that glycogen levels were similar in hearts of wild-type and *Acc2*-mutant mice (0.27 ± 0.04 and 0.29 ± 0.05 mg/g wet wt, respectively; Fig. 3*A*). However, myocardial triglyceride levels were markedly reduced in mutant hearts vs. wild-types (2.25 ± 0.35 and 1.16 ± 0.41 mg/g wet wt, respectively; $P = 0.007$; Fig. 3*B*). These results therefore suggest that *Acc2*-mutant mice do not spare glucose as glycogen.

Ex vivo cardiac fuel substrate oxidation rates. Myocardial oxygen uptake ($M\dot{V}O_2$) was not statistically different in *Acc2*-mutant compared wild-types (30 ± 4.9 and 22 ± 5.6 $\mu mol \cdot min^{-1} \cdot g^{-1}$ dry wt, respectively; Fig. 4*A*). In agreement with lower malonyl-CoA levels, myocardial oleate oxidation was higher in mutant vs. wild-type mice (Fig. 4, *B* and *C*). Unexpectedly, myocardial glucose oxidation was also significantly higher in *Acc2*-mutant mice compared with the wild-type (0.08 ± 0.012 and 0.03 ± 0.01 $\mu mol \cdot min^{-1} \cdot g^{-1}$ dry wt, respectively; Fig. 5). Coronary flow was not significantly different in *Acc2*-mutant vs. wild-types (43.23 ± 5.59 and 36.10 ± 11.61 $ml \cdot min^{-1} \cdot g^{-1}$ dry wt, respectively).

Myocardial glucose uptake in vivo. We used hyperinsulinemic-euglycemic clamp conditions to determine glucose uptake in hearts. Consistent with the increase in glucose oxidation in isolated hearts of *Acc2*-mutant mice, the glucose uptake was ~83% higher in *Acc2*-mutant hearts compared with the wild-types (Fig. 6).

Expression of genes regulating FA and glucose metabolism. To gain further insight into mechanisms underlying myocardial fuel substrate utilization in the *Acc2*-mutant mouse strain, we measured transcript levels of the nuclear receptor PPARα, a transcription factor that regulates numerous genes involved in the uptake and oxidation of FAs. We found that PPARα transcript levels were significantly decreased in mutant vs. wild-type mice (Table 2). Transcript levels of two other PPARα-regulated genes, i.e., mCPT1 and MCAD, also displayed downward trends. PGC-1α transcript levels did not significantly differ between mutant and wild-type strains.

The rate-limiting step for exogenous glucose utilization is its transport into cardiomyocytes via specific carrier-mediated transporters, i.e., GLUT1 and GLUT4. Transcript levels of both transporters did not differ significantly between *Acc2*-mutant and wild-type mice (Table 2). However, transcript levels of PDK-4, an indirect inhibitor of glucose and lactate oxidation, were markedly downregulated in mutant vs. wild-type mice ($n = 4$, $P < 0.05$; Table 2).

Western blot analysis of mitochondrial protein extracts showed that mCPT1 expression was significantly reduced in the *Acc2*-mutant mouse heart compared with wild-types (Fig. 7). The densitometric analysis shows ~2× higher mCPT1 peptide levels in wild-type vs. mutant hearts (Fig. 7). These results are consistent with lower PPARα mRNA in hearts of *Acc2*-mutant mice shown in Table 2.

To gain insight into mechanisms that may regulate the reduced heart size of *Acc2*-mutant mice, we determined peptide levels of members of the mTOR pathway, which is implicated in the control of protein translation. We found that mTOR levels were similar in both wild-type and mutant hearts (Fig. 8*A*). However, phosphorylation of mTOR on Ser^{2481} was significantly reduced in mutant hearts ($P = 0.01$ vs. wild-types), suggesting decreased autophosphorylation and mTOR activity. Reduced mTOR phosphorylation was accompanied by a significant decrease in phosphorylation of its downstream target P70S6K (at Thr^{389}; Fig. 8*B*). There were no significant changes in Akt/pAKT levels (Fig. 8*C*), suggesting that downregulation of mTOR signaling in *Acc2*-mutant hearts does not involve the AKT pathway.

DISCUSSION

The main findings of this study are *1*) a reduced heart size in *Acc2*-mutant mice, without impaired cardiac function; *2*) increased oxidation rates of both oleate and glucose in *Acc2*-mutant mouse heart; *3*) increased glucose uptake in *Acc2*-mutant mouse heart; and *4*) downregulation of PPARα and its target genes in the *Acc2*-mutant mouse.

Reduced heart size in Acc2-mutant mouse. The heart mass of the *Acc2*-mutant mouse was significantly reduced compared with wild-types (lower heart wt/body wt ratios). We confirmed this reduction in heart size by measuring the dry weight of hearts at the end of perfusion studies, which exhibited a ~25–30% reduction in size. Moreover, echocardiographic

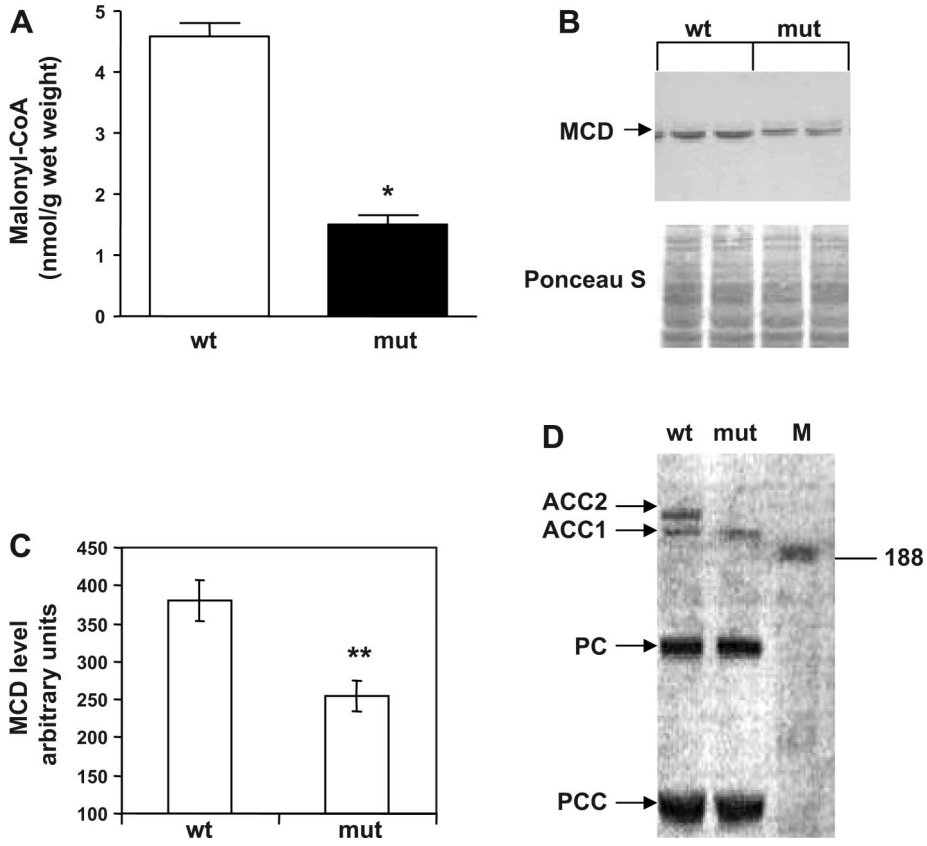

Fig. 2. Reduced malonyl-CoA, MCD, and ACC1 levels in *Acc2*-mutant hearts. *A*: Malonyl-CoA levels were measured (refer to METHODS) in hearts collected from 20-wk-old male mice ($n = 12$). *B*: MCD peptide levels were detected using μg of protein isolated from *Acc2*-mutant mice and compared with wild-types. *C*: densitometric analysis of MCD peptide levels. $*P = 0.0001$ and $**P = 0.001$ vs. wild-type. *D*: 30 μg protein of isolated mitochondria from heart and *Acc2*-mutant mice were subjected to electrophoresis gel separation and proteins were detected with avidin peroxidase. The arrows indicate the position of biotinylated proteins, i.e., ACC1; ACC2; PC, pyruvate carboxylase; PCC, propionyl-CoA carboxylase.

analysis performed showed that LV mass and LV wall diameter were significantly reduced in mutant vs. wild-type mice. However, echocardiography also revealed that contractile function was not altered in the *Acc2*-mutant mouse heart (Table 1).

It is unclear why the heart size of the mutant mouse is reduced and what the precise regulatory mechanisms are. Here, we propose that high FA oxidation rates by the *Acc2*-mutant heart deplete myocardial diacylglycerol and phosphatidic acid content, thereby leading to reduced phosphorylation of mTOR and its downstream targets, i.e., p70S6K. This is in agreement with previous work showing that phosphatidic acid binds to the FRB domain of mTOR resulting in its activation (16). Phosphorylation of mTOR on Ser^{2481} was significantly reduced in mutant hearts, suggesting a decrease in autophosphorylation and decreased activity of mTOR. Reduced mTOR phosphorylation was accompanied by a significant decrease in phosphorylation of its downstream target P70S6K (at Thr^{389}). The autophosphorylation site at Ser^{2481} is surrounded by bulky hydrophobic residues which are similar to a bulky hydrophobic site found in P70S6K (10, 28). Furthermore, a recent study showed that pretreatment of steridogenic luteal cells with rapamycin abolished phosphorylation at the Thr^{389} site and only partially reduced phosphorylation on Thr^{421}/Ser^{424}, suggesting a correlation between mTOR activity and phosphorylation of P706SK at the Thr^{389} site (7). We therefore propose that reduced mTOR signaling/activity will eventually result in the decreased heart size observed in the *Acc2*-mutant mouse.

Increased oxidation rates of exogenous oleate and glucose and higher glucose uptake in Acc2-mutant mouse hearts. Because we previously reported markedly reduced malonyl-CoA levels in the *Acc2*-mutant mouse heart (4), we predicted increased myocardial FAO rates. Here, we found that myocardial malonyl-CoA levels were markedly reduced in mutant mice, and cardiac FAO rates accordingly increased compared with wild-types. In agreement, we previously reported elevated FAO rates in isolated soleus muscle, hepatocytes, and adipocytes due to lower malonyl-CoA levels found in the *Acc2*-mutant mouse (4, 5, 27). Although malonyl-CoA levels were reduced in mutant hearts, a residual amount nonetheless remained. We propose that this may be mainly due to lower MCD levels (also a PPARα target gene) and remaining ACC1 expression.

A major concern is the question of the effects of constitutively increased fat oxidation in the heart because more than 70% of cardiac energy production results from fat oxidation (9, 39), and originally fuel competition between fat and carbohydrate was observed in the heart (29). Moreover, it is well known that diabetic heart is characterized by increased fat oxidation and reduced glucose metabolism (21, 22, 30). The *Acc2*-mutant mice had a normal life span and did not exhibit obvious contractile impairment, which is supported by our current echocardiographic studies showing normal heart function. Intriguingly, we found that myocardial glucose oxidation rates in mutant mice were increased despite higher oleate oxidation rates. This increase in glucose oxidation appears to be mainly due to enhanced glucose uptake (Fig. 6). In accor-

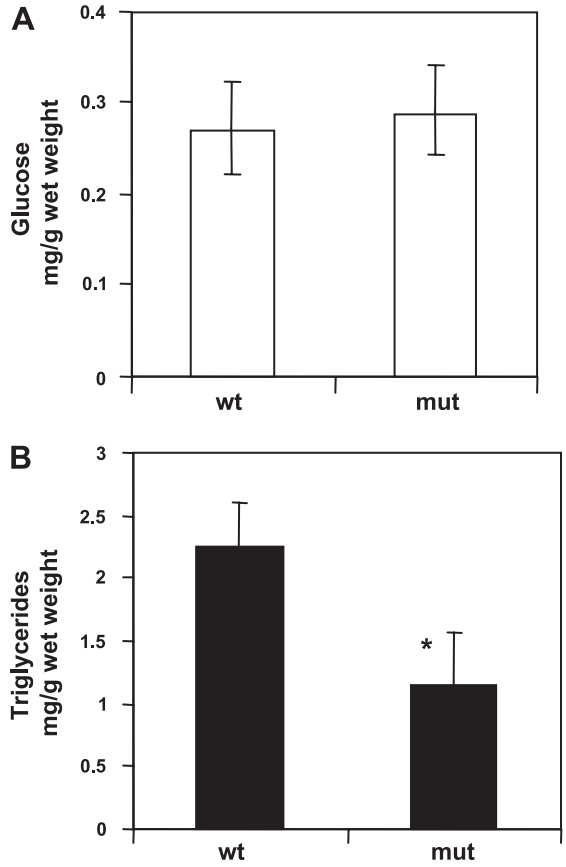

Fig. 3. Glycogen and triglyceride levels in wild-type and *Acc2*-mutant hearts. Glycogen (*A*) and triglyceride (*B*) levels were determined (refer to METHODS) in hearts from mutant and wild-type hearts ($n = 5$). Values are depicted as means ± SE. *$P = 0.007$ vs. wild-type.

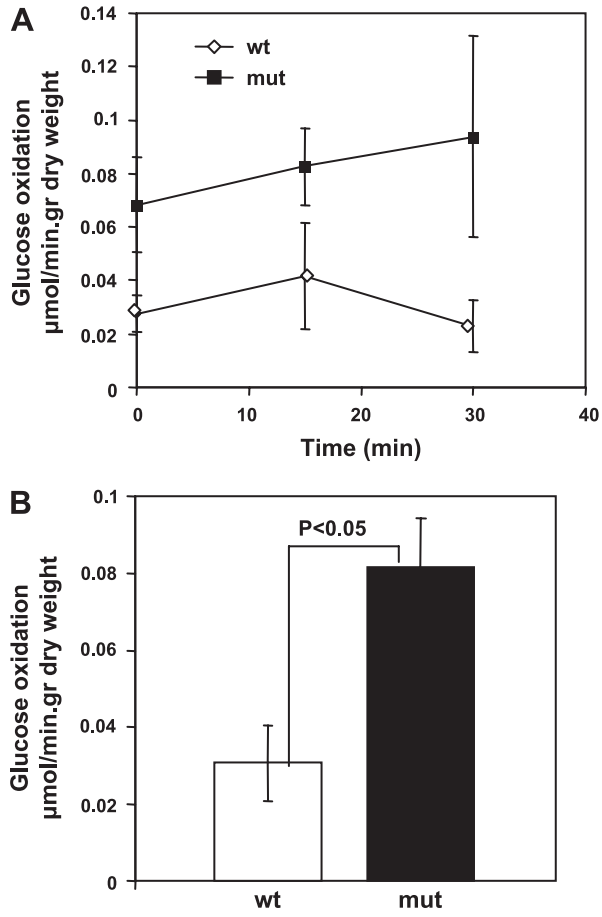

Fig. 5. Ex vivo cardiac glucose oxidation rates. Glucose oxidation was assessed in Langendorff perfused hearts during 30 min of aerobic perfusion in the presence of 0.4 mM oleate, 5 mM glucose, and 40 µU/ml insulin as substrates. *A*: rate of glucose oxidation. *B*: average values of rates from *A*. Values depicted are means ± SE ($n = 5$) for perfusate collected at 15-min intervals (refer to *A*). Statistical analysis was performed using ANOVA.

dance, we previously reported that adipose tissues of *Acc2*-mutant mice also displayed increased rates of glucose oxidation (4, 27). Moreover, our recently published study reported that *Acc2*-mutant mice displayed marked increases in insulin-stimulated whole body glucose uptake, glycolysis, and skeletal muscle glucose uptake (12). This is unexpected since the glucose-FA cycle predicts that increased FAO rates should result in a corresponding reduction in glucose oxidation rates (29).

The amount of oxygen needed for complete oxidation of one mol of oleate and one mol of glucose is 24 and 6 mol,

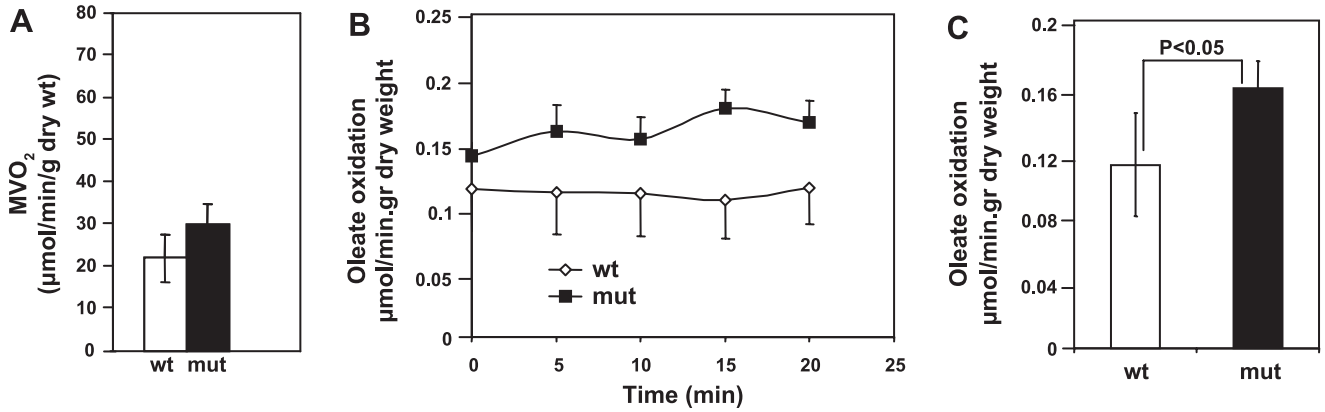

Fig. 4. Ex vivo cardiac $M\dot{V}O_2$ and oleate oxidation rates. Substrate oxidation was assessed in Langendorff perfused hearts during 20 min of aerobic perfusion in the presence of 0.4 mM oleate, 5 mM glucose, and 40 µU/ml insulin as substrates. Values depicted are means ± SE ($n = 5$) for perfusate collected at 5-min intervals. *A*: myocardial oxygen consumption. *B*: rate of oleate oxidation. *C*: average rates of oleate oxidation in *B*. Statistical analysis was performed using ANOVA.

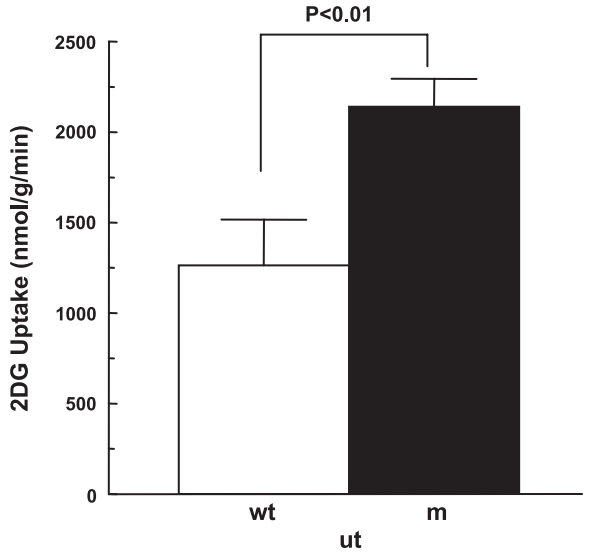

Fig. 6. Increased glucose uptake in hearts of *Acc2*-mutant mice. Glucose uptake in hearts was assessed by means of hyperinsulinemic-euglycemic clamps. Acc2 depletion significantly improved heart glucose uptake. Data are expressed as mean values ± SE ($n = 9$).

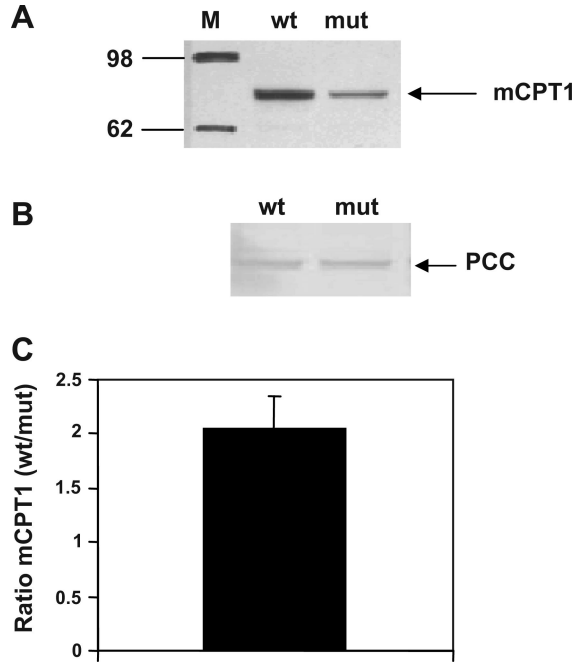

Fig. 7. Representative Western blot of mCPT1 peptide levels. Western blot analysis of purified mitochondria and crude extracts (METHODS) were separated by 4–12% NuPAGE MES gels. *A*: 30 μg protein of isolated mitochondria from heart and *Acc2*-mutant mice were subjected to electrophoresis gel separation. An antibody raised against rat muscle-type CPT1 was used to detect mouse mCPT1 by ECL ($n = 7$). *B*: PCC peptide levels indicated as a control for loading in blot *A*. *C*: densitometric analysis was performed on mCPT1 blots using standard laboratory techniques and mCPT1 levels are given as wild-type/mutant ratio.

respectively. The combined oxidation of exogenous glucose and oleate (~600 nmol $CO_2 \cdot min^{-1} \cdot g^{-1}$ dry wt) is lower than the value for oxygen consumption (20–30,000 nmol $O_2 \cdot min^{-1} \cdot g^{-1}$ dry wt). We propose that this may be due to increased breakdown of endogenous (triglycerides) and/or other exogenous fuel substrates (e.g., lactate, ketone bodies) that make a large contribution to the overall energy metabolism of mutant hearts. In agreement with this concept, we found that triglyceride levels were reduced in hearts of the *Acc2*-mutant mice. We also previously found that plasma β-hydroxybutyrate levels were significantly increased in the fed and fasted state of *Acc2*-mutant mice (12). In addition, glycogen levels were similar in wild-type and *Acc2*-mutant hearts, suggesting that exogenous glucose supplied is oxidized rather than being stored as glycogen. Together, our data suggest that *Acc2*-mutant hearts preferentially oxidize exogenous oleate and glucose, while endogenous fuel substrates such as triglycerides also make a greater contribution to overall oxidation rates compared with wild-types. However, it is important to note that we are comparing oxidation rates of exogenous fuel substrates (supplied in perfusate) and that this may not necessarily correspond with the absolute myocardial oxidation rates of these substrates. Moreover, serum-free FA concentrations are in the nanomolar range; hence, cardiomyocytes rely on hydrolysis of circulating lipoproteins by lipoprotein lipase as the main source for FA supply.

Table 2. *Transcript levels of cardiac glucose and fatty acid metabolic genes in WT and Acc2-mutant mice*

	WT	*Acc2*-Mutant
PPARα	0.43±0.03	0.3±0.02*
mCPT1	308±24	217±36*
MCAD	170±12	150±6
PGC-1α	0.3±0.04	0.23±0.04
GLUT 4	0.4±0.03	0.32±0.04
GLUT 1	0.01±0.001	0.013±0.001
PDK-4	10.6±1.6	3.27±1.2*

Values are given as means ± SE. *$P < 0.05$ vs. WT. Total RNA was isolated from WT and *Acc2*-mutant mouse hearts ($n = 4$) and indicated transcript levels were measured by real-time quantitative RT-PCR. mRNA levels for each gene were normalized to cyclophilin.

Reduced expression of PPARα and target genes in the Acc2-mutant mouse. To gain further insight into these findings, we determined the expression of several cardiac metabolic genes. We found that myocardial transcript levels of PPARα, a well-described FA-sensing transcriptional modulator, were significantly reduced in the *Acc2*-mutant mouse. Gene expression of two other PPARα target genes, i.e., MCAD and mCPT1, displayed downward trends, although this did not reach statistical significance. However, protein expression of mCPT1 was significantly reduced in the *Acc2*-mutant mouse.

Consistent with our ex vivo glucose oxidation data, transcript levels of PDK-4, a PPARα target gene, were markedly reduced in mutant mice. However, p-Akt peptide levels were not significantly altered in *Acc2*-mutant mice. A number of reasons could potentially explain our finding of increased glucose oxidation in this model. *1*) Reduced phosphorylation of the PDH complex by lower PDK-4 levels may override the feedback inhibition of FAO products. *2*) The activity of pyruvate dehydrogenase may be upregulated. *3*) Other factors that may affect glucose oxidation, for example, the intramitochondrial free Ca^{2+} concentration and/or pyruvate availability, may be increased. *4*) There may be crosstalk between malonyl-CoA and the PDH complex, with chronically lowered malonyl-CoA leading to PDH activation. *5*) Although GLUT1 and GLUT4 gene expression levels were not significantly altered, we can-

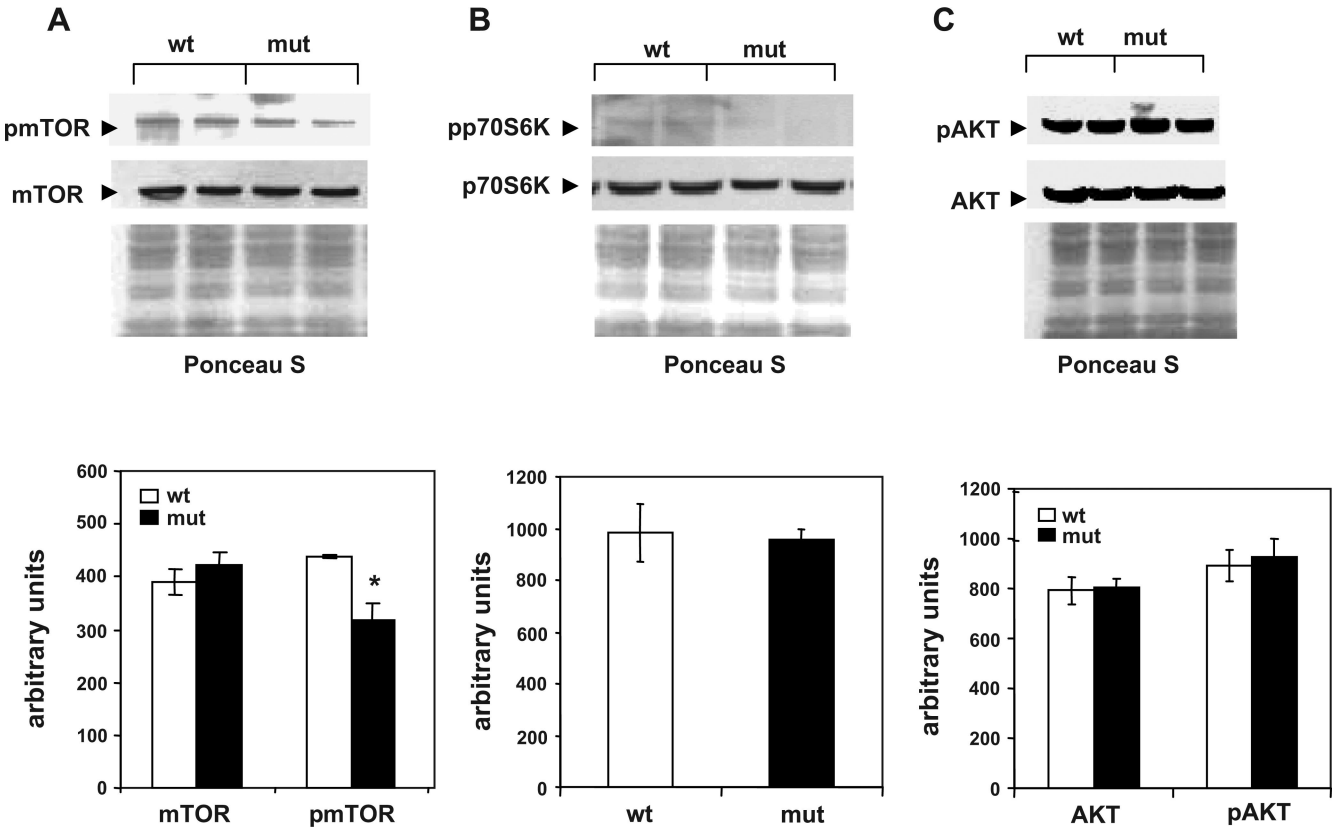

Fig. 8. Representative Western blots of mTOR, P70S6K, and Akt in *Acc2*-mutant hearts. Western blot analysis of protein extracts (METHODS) was separated by 4–12% NuPAGE MES gels. *A*: mTOR and pmTOR Ser^{2481} and corresponding densitometric analysis. *B*: P70S6K and pP70S6K Thr^{389} and densitometric analysis for P70S6K; the level of pP70S6K was very low in mutant heart extracts. *C*: Akt and pAKT Ser^{473} peptide levels and corresponding densitometric analysis. Ponceau staining shows equal loading. $*P = 0.01$ vs. wild-type.

not exclude the possibility of increased GLUT translocation from the sarcolemma to plasma membrane, explaining enhanced myocardial glucose uptake. *6*) Since lack of ACC2 promotes FAO, this would lead to decreased intracellular FA metabolites and less inhibition of insulin-mediated glucose uptake. Although we did not observe altered p-Akt phosphorylation in mutant hearts, this does not rule out improved insulin sensitivity in this instance.

We propose that the lower PPARα and mCPT1 expression observed may be a compensatory mechanism to prevent excessively high myocardial FAO rates in the *Acc2*-mutant mouse strain. If such a control mechanism was indeed lacking, we predict that excessively high FAO rates could for example result in increased uncoupling of mitochondrial oxidative phosphorylation and reduced cardiac mitochondrial energy production. In agreement with this concept, a recent study investigating myocardial substrate metabolism of an MCD-deficient mouse found increased levels of PPARα gene expression associated with unchanged FA and glucose oxidation rates compared with controls (15). Previously, we found reduced plasma free FA (FFA) levels for *Acc2*-mutant compared with wild-type mice (4). This should therefore result in attenuated FA-induced activation of PPARα and its target genes. Thus by lowering both ligand supply and the expression of FA metabolic genes, we believe that excessively high rates of FAO are prevented in the *Acc2*-mutant heart (35). In support, Young et al. (42) previously reported the downregulation of PPARα gene expression in streptozotocin-induced diabetic rats, suggesting that conditions associated with chronic elevation of cardiac FAO may result in decreased PPARα levels. Likewise, reduced PPARα mRNA levels in hearts of Zucker diabetic fatty rats were associated with elevated plasma FFA and triglyceride levels (43).

Limitations. The ex vivo glucose oxidation rates reported in this study are lower than what have previously been reported from our laboratory and other studies (20, 33). The perfusion data in the current study roughly translate to glucose oxidation contributing ~20% of the energy production of wild-type hearts. We believe that this may be a strain-specific phenomenon related to the particular mouse strain we employed in this study. Also, the perfusion data were generated using a nonworking heart system with low mechanic force and therefore the metabolic profile obtained using this model may not necessarily reflect what occurs in vivo. Thus, although we carried out in vivo analyses of cardiac function, our findings would have been further strengthened by the inclusion of ex vivo heart functional analyses.

In conclusion, we report increased exogenous myocardial energy substrate utilization and lower levels of endogenous fuels (triglycerides) in *Acc2*-mutant hearts, associated with a reduction in heart size but normal cardiac function. We propose that attenuated mTOR signaling may be responsible for reduced heart size in mutant mice. The fact that mutant hearts functioned normally despite the lack of a pivotal

metabolic regulator (i.e., ACC2) is intriguing, although underlying mechanisms are still unknown at this stage. Nonetheless, the study shows that ACC2 inhibition remains an attractive therapeutic target, despite continuously high myocardial FAO rates.

ACKNOWLEDGMENTS

We thank R. Salazar, P. Kordari, and S. Sen for technical assistance, C. R. Wilson and M. Burgmaier for advice, and R. A. Tate for editorial help.

GRANTS

This study was supported in parts by grants from the Hefni Technical Training Foundation and the National Institutes of Health Grant GM-63115 (to S. J. Wakil); National Heart, Lung, and Blood Institute Grants RO1-HL-073162-01 and T32-HL-07591 to H. Taegtmeyer; the South African MRC, National Research Foundation, Fulbright Commission and Ernest Oppenheimer Memorial Trust to M. F. Essop; and R01-DK-40936, U24-DK-76169, and a Distinguished Clinical Investigator Award from the American Diabetes Association (to G. I. Shulman).

REFERENCES

1. **Abu-Elheiga L, Jayakumar A, Baldini A, Chirala SS, Wakil SJ.** Human acetyl-CoA carboxylase: characterization, molecular cloning, and evidence for two isoforms. *Proc Natl Acad Sci USA* 92: 4011–4015, 1995.
2. **Abu-Elheiga L, Almarza-Ortega DB, Baldini A, Wakil SJ.** Human acetyl-CoA carboxylase 2. Molecular cloning, characterization, chromosomal mapping, and evidence for two isoforms. *J Biol Chem* 272: 10669–10677, 1997.
3. **Abu-Elheiga L, Brinkley WR, Zhong L, Chirala SS, Woldegiorgis G, Wakil SJ.** The subcellular localization of acetyl-CoA carboxylase 2. *Proc Natl Acad Sci USA* 97: 1444–1449, 2000.
4. **Abu-Elheiga L, Matzuk MM, Abo-Hashema KA, Wakil SJ.** Continuous fatty acid oxidation and reduced fat storage in mice lacking acetyl-CoA carboxylase 2. *Science* 291: 2613–2616, 2001.
5. **Abu-Elheiga L, Oh W, Kordari P, Wakil SJ.** Acetyl-CoA carboxylase 2 mutant mice are protected against obesity and diabetes induced by high-fat/high-carbohydrate diets. *Proc Natl Acad Sci USA* 100: 10207–10212, 2003.
6. **Abu-Elheiga L, Matzuk MM, Kordari P, Oh W, Shaikenov T, Gu Z, Wakil SJ.** Mutant mice lacking acetyl-CoA carboxylase 1 are embryonically lethal. *Proc Natl Acad Sci USA* 102: 12011–12016, 2005.
7. **Arvisais EW, Romanelli A, Hou X, Davis JS.** AKT-independent phosphorylation of TSC2 and activation of mTOR and ribosomal protein S6 kinase signaling by prostaglandin F2alpha. *J Biol Chem* 281: 26904–26913, 2006.
8. **Bianchi A, Evans JL, Iverson AJ, Nordlund AC, Watts TD, Witters LA.** Identification of an isozymic form of acetyl-CoA carboxylase. *J Biol Chem* 265: 1502–1509, 1990.
9. **Bing RJ, Siegel A, Ungar I, Gilbert M.** Metabolism of the human heart. II. Studies on fat, ketone and amino acid metabolism. *Am J Med* 16: 504–515, 1954.
10. **Burnett PE, Barrow RK, Cohen NA, Snyder SH, Sabatini DM.** RAFT1 phosphorylation of the translational regulators p70 S6 kinase and 4E-BP1. *Proc Natl Acad Sci USA* 95: 1432–1437, 1998.
11. **Chandler CE, Wilder DE, Pettini JL, Savoy YE, Petras SF, Chang G, Vincent J, Harwood HJ Jr.** CP-346086: an MTP inhibitor that lowers plasma cholesterol and triglycerides in experimental animals and in humans. *J Lipid Res* 44: 1887–1901, 2003.
12. **Choi CS, Savage DB, Abu-Elheiga L, Liu ZX, Kulkarni A, Distefano A, Hwang YJ, Reznick RM, Codella R, Zhang D, Cline GW, Wakil SJ, Shulman GI.** Continuous fat oxidation in acetyl-CoA carboxylase 2 knockout mice increases total energy expenditure, reduces fat mass, and improves insulin sensitivity. *Proc Natl Acad Sci USA* 104: 16480–16485, 2007.
13. **Debard C, Laville M, Berbe V, Loizon E, Guillet C, Morio-Liondore B, Boirie Y, Vidal H.** Expression of key genes of fatty acid oxidation, including adiponectin receptors, in skeletal muscle of type 2 diabetic patients. *Diabetologia* 47: 917–925, 2004.
14. **Depre C, Shipley GL, Chen W, Han Q, Doenst T, Moore ML, Stepkowski S, Davies PJA, Taegtmeyer H.** Unloaded heart in vivo replicates fetal gene expression of cardiac hypertrophy. *Nat Med* 4: 1269–1275, 1998.
15. **Dyck JR, Hopkins TA, Bonnet S, Michelakis ED, Young ME, Watanabe M, Kawase Y, Jishage K, Lopaschuk GD.** Absence of malonyl coenzyme A decarboxylase in mice increases cardiac glucose oxidation and protects the heart from ischemic injury. *Circulation* 114: 1721–1728, 2006.
16. **Fang Y, Vilella-Bach M, Bachmann R, Flanigan A, Chen J.** Phosphatidic acid-mediated mitogenic activation of mTOR signaling. *Science* 294: 1942–1945, 2001.
17. **Goodwin GW, Taylor CS, Taegtmeyer H.** Regulation of energy metabolism of the heart during acute increase in heart work. *J Biol Chem* 273: 29530–29539, 1998.
18. **Harris SP, Bartley CR, Hacker TA, McDonald KS, Douglas PS, Greaser ML, Powers PA, Moss RL.** Hypertrophic cardiomyopathy in cardiac myosin binding protein-C knockout mice. *Circ Res* 90: 594–601, 2002.
19. **Hassid WZ, Abraham S.** Chemical procedures for analysis of polysaccharides. *Methods Enzymol* 3: 34–35, 1959.
20. **How OJ, Aasum E, Severson DL, Chan WY, Essop MF, Larsen TS.** Increased myocardial oxygen consumption reduces cardiac efficiency in diabetic mice. *Diabetes* 55: 466–473, 2006.
21. **Lopaschuk GD.** Abnormal mechanical function in diabetes: relationship to altered myocardial carbohydrate/lipid metabolism. *Coron Artery Dis* 7: 116–123, 1996.
22. **Lopaschuk GD, Belke DD, Gamble J, Itoi T, Schonekess BO.** Regulation of fatty acid oxidation in the mammalian heart in health and disease. *Biochim Biophys Acta* 1213: 263–276, 1994.
23. **Lopez-Casillas F, Bai DH, Luo XC, Kong IS, Hermodson MA, Kim KH.** Structure of the coding sequence and primary amino acid sequence of acetyl-coenzyme A carboxylase. *Proc Natl Acad Sci USA* 85: 5784–5788, 1988.
24. **McGarry JD, Brown NF.** The mitochondrial carnitine palmitoyltransferase system. From concept to molecular analysis. *Eur J Biochem* 244: 1–14, 1997.
25. **McGarry JD, Stark MJ, Foster DW.** Hepatic malonyl-CoA levels of fed, fasted and diabetic rats as measured using a simple radioisotopic assay. *J Biol Chem* 253: 8291–8293, 1978.
26. **McGarry JD, Mills SE, Long CS, Foster DW.** Observations on the affinity for carnitine, and malonyl-CoA sensitivity, of carnitine palmitoyltransferase I in animal and human tissues. Demonstration of the presence of malonyl-CoA in nonhepatic tissues of the rat. *Biochem J* 214: 21–28, 1983.
27. **Oh W, Abu-Elheiga L, Kordari P, Gu Z, Shaikenov T, Chirala SS, Wakil SJ.** Glucose and fat metabolism in adipose tissue of acetyl-CoA carboxylase 2 knockout mice. *Proc Natl Acad Sci USA* 102: 1384–1389, 2005.
28. **Peterson RT, Beal PA, Comb MJ, Schreiber SL.** FKBP12-rapamycin-associated protein (FRAP) autophosphorylates at serine 2481 under translationally repressive conditions. *J Biol Chem* 275: 7416–7423, 2000.
29. **Randle PJ, Garland PB, Hales CN, Newsholme EA.** The glucose fatty-acid cycle. Its role in insulin sensitivity and the metabolic disturbances of diabetes mellitus. *Lancet* 1: 785–789, 1963.
30. **Rodrigues B, McNeill JH.** The diabetic heart: metabolic causes for the development of a cardiomyopathy. *Cardiovasc Res* 26: 913–922, 1992.
31. **Saggerson ED, Carpenter CA.** Carnitine palmitoyltransferase and carnitine octanoyltransferase activities in liver, kidney cortex, adipocyte, lactating mammary gland, skeletal muscle and heart. *FEBS Lett* 129: 229–232, 1981.
32. **Samuel VT, Choi CS, Phillips TG, Romanelli AJ, Geisler JG, Bhanot S, McKay R, Monia B, Shutter JR, Lindberg RA, Shulman GI, Veniant MM.** Targeting foxo1 in mice using antisense oligonucleotide improves hepatic and peripheral insulin action. *Diabetes* 55: 2042–2050, 2006.
33. **Sano M, Izumi Y, Helenius K, Asakura M, Rossi DJ, Xie M, Taffet G, Hu L, Pautler RG, Wilson CR, Boudina S, Abel ED, Taegtmeyer H, Scaglia F, Graham BH, Kralli A, Shimizu N, Tanaka H, Makela TP, Schneider MD.** Menage-a-trois 1 is critical for the transcriptional function of PPARgamma coactivator 1. *Cell Metab* 5: 129–142, 2007.
34. **Schaefer A, Klein G, Brand B, Lippolt P, Drexler H, Meyer GP.** Evaluation of left ventricular diastolic function by pulsed Doppler tissue imaging in mice. *J Am Soc Echocardiogr* 16: 1144–1149, 2003.

35. **Schrauwen P, Hesselink MK.** Oxidative capacity, lipotoxicity, and mitochondrial damage in type 2 diabetes. *Diabetes* 53: 1412–1417, 2004.
36. **Takai T, Yokoyama C, Wada K, Tanabe T.** Primary structure of chicken liver acetyl-CoA carboxylase deduced from cDNA sequence. *J Biol Chem* 263: 2651–2657, 1988.
37. **Thampy KG.** Formation of malonyl coenzyme A in rat heart. Identification and purification of an isozyme of Acetyl-CoA carboxylase from rat heart. *J Biol Chem* 264: 17631–17634, 1989.
38. **Tsujita Y, Kato T, Sussman MA.** Evaluation of left ventricular function in cardiomyopathic mice by tissue Doppler and color M-mode Doppler echocardiography. *Echocardiography* 22: 245–253, 2005.
39. **Wisneski JA, Gertz EW, Neese RA, Mayr M.** Myocardial metabolism of free fatty acids. Studies with ^{14}C-labeled substrates in humans. *J Clin Invest* 79: 359–366, 1987.
40. **Youn JH, Buchanan TA.** Fasting does not impair insulin-stimulated glucose uptake but alters intracellular glucose metabolism in conscious rats. *Diabetes* 42: 757–763, 1993.
41. **Young ME, Razeghi P, Cedars AM, Guthrie PH, Taegtmeyer H.** Intrinsic diurnal variations in cardiac metabolism and contractile function. *Circ Res* 89: 1199–1208, 2001.
42. **Young ME, Patil S, Ying J, Depre C, Ahuja HS, Shipley GL, Stepkowski SM, Davies PJ, Taegtmeyer H.** Uncoupling protein 3 transcription is regulated by peroxisome proliferator-activated receptor (alpha) in the adult rodent heart. *FASEB J* 15: 833–845, 2001.
43. **Zhou YT, Grayburn P, Karim A, Shimabukuro M, Higa M, Baetens D, Orci L, Unger RH.** Lipotoxic heart disease in obese rats: implications for human obesity. *Proc Natl Acad Sci USA* 97: 1784–1789, 2000.

available at www.sciencedirect.com
ScienceDirect
journal homepage: www.elsevier.com/locate/biochempharm

C75 is converted to C75-CoA in the hypothalamus, where it inhibits carnitine palmitoyltransferase 1 and decreases food intake and body weight

Paula Mera [a,b,1], *Assia Bentebibel* [a,1], *Eduardo López-Viñas* [b,c], *Antonio G. Cordente* [a], *Chandrashekaran Gurunathan* [a], *David Sebastián* [a], *Irene Vázquez* [a], *Laura Herrero* [a,b], *Xavier Ariza* [d], *Paulino Gómez-Puertas* [b,c], *Guillermina Asins* [a,b], *Dolors Serra* [a,b], *Jordi García* [d], *Fausto G. Hegardt* [a,b,*]

[a] *Department of Biochemistry and Molecular Biology and IBUB (Institute of Biomedicine University of Barcelona), Spain*
[b] *CIBER "Fisiopatología de la Obesidad y la Nutrición" (CB06/03), Instituto de Salud Carlos III, School of Pharmacy, University of Barcelona, E-08028 Barcelona, Spain*
[c] *Centro de Biología Molecular "Severo Ochoa" (CSIC-UAM), Cantoblanco, E-28049 Madrid, Spain*
[d] *Department of Organic Chemistry and IBUB, School of Chemistry, University of Barcelona, E-08028 Barcelona, Spain*

ARTICLE INFO

Article history:
Received 16 October 2008
Accepted 20 November 2008

Keywords:
Fatty-acid metabolism
Anti-obesity drugs
C75
CPT1 carnitine palmitoyltransferase
FAS fatty-acid synthase

ABSTRACT

Central nervous system administration of C75 produces hypophagia and weight loss in rodents identifying C75 as a potential drug against obesity and type 2 diabetes. However, the mechanism underlying this effect is unknown. Here we show that C75-CoA is generated chemically, *in vitro* and *in vivo* from C75 and that it is a potent inhibitor of carnitine palmitoyltranferase 1 (CPT1), the rate-limiting step of fatty-acid oxidation. Three-D docking and kinetic analysis support the inhibitory effect of C75-CoA on CPT1. Central nervous system administration of C75 in rats led to C75-CoA production, inhibition of CPT1 and lower body weight and food intake. Our results suggest that inhibition of CPT1, and thus increased availability of fatty acids in the hypothalamus, contribute to the pharmacological mechanism of C75 to decrease food intake.

© 2008 Elsevier Inc. All rights reserved.

1. Introduction

The brain plays an important role in the evaluation and control of energy homeostasis. Blood concentrations of glucose and fatty acids are sensed by neurons of the hypothalamus, which adjusts feeding behaviour and monitors fatty-acid metabolism. Several laboratories have attempted to design anti-obesity drugs and modulate fatty-acid metabolism to inhibit food intake. C75 is a synthetic inhibitor of fatty-acid synthase (FAS) [1] and has been proposed as an anti-obesity agent since its administration decreases food intake and body weight in rodents [2–5]. C75 can alter the metabolism of neurons in the hypothalamus, where an increase in the level of malonyl-CoA due to FAS inhibition serves as a secondary

* *Corresponding author*. Tel.: +34 934024523; fax: +34 934024520.
E-mail address: fgarciaheg@ub.edu (F.G. Hegardt).

[1] Both authors contributed equally to this study.

Abbreviations: ARC, arcuate nucleus; CPT, carnitine palmitoyltransferase; CrAT, carnitine acetyltransferase; FAS, fatty-acid synthase; wt, wild-type.

0006-2952/$ – see front matter © 2008 Elsevier Inc. All rights reserved.
doi:10.1016/j.bcp.2008.11.020

Please cite this article in press as: Mera P, et al. C75 is converted to C75-CoA in the hypothalamus, where it inhibits carnitine palmitoyltransferase 1 and decreases food intake and body weight. Biochem Pharmacol (2009), doi:10.1016/j.bcp.2008.11.020

messenger of nutrient status, thereby mediating the suppression of food intake [6,7]. Hypothalamic levels of long-chain fatty acyl-CoA (LCFA-CoA) also signal nutrient availability and control food intake [8].

Malonyl-CoA signals the availability of lipid and carbohydrate fuels [9] and acts as a physiological inhibitor of the enzyme carnitine palmitoyltransferase 1 (CPT1). CPT1 catalyzes the first step in the transport of LCFA from the cytoplasm to the mitochondria, and is the rate-limiting step in β-oxidation. Mammalian tissues express three CPT1 isoforms: CPT1A, CPT1B and CPT1C which differ in their sensitivity to malonyl-CoA and tissue distribution [10,11]. CPT1A and CPT1C are expressed in the brain. CPT1A is located in the mitochondrial membrane and CPT1C is expressed in the endoplasmic reticulum of neurons where although it has CPT1 activity, it does not participate in mitochondrial fatty-acid oxidation [12]. Interestingly, our group has generated a mutant form of CPT1A insensitive to malonyl-CoA (CPT1A M593S), and a mutant form of carnitine acetyltransferase (CrAT) that swaps its preference from short to LCFA-CoA (CrAT D356A/M564G). These mutants have allowed us to examine the structural requirements of substrates and inhibitors [13–15].

The inhibition of FAS by C75 produces an accumulation of malonyl-CoA which is difficult to reconcile with the activation of CPT1 reported by others [2,16–18]. To unravel this paradox the mechanism of action of C75 needs to be examined. We recently demonstrated that C75 is converted *in vitro* to C75-CoA, a potent inhibitor of CPT1 [19]. CPT1 activity was also inhibited in mitochondria from pancreas-, muscle-, and kidney-derived cell lines incubated with C75, which indicates that C75-CoA is produced in these cells. This inhibition was followed by a decrease in fatty-acid oxidation. The role of CPT1 in heart, liver and pancreatic β-cells makes it a potential target in the treatment of diabetes, obesity, and other human diseases.

Here we show that C75-CoA, and not C75, directly inhibits CPT1 activity. We also show that C75-CoA is formed in the hypothalamus in a dose-dependent way, where it inhibits CPT1 activity and decreases food intake and body weight. These results indicate that direct inhibition of CPT1 by C75-CoA in the hypothalamus could control body weight and feeding behaviour.

2. Materials and methods

2.1. Materials

L-[Methyl-^{3}H]carnitine hydrochloride was purchased from Amersham Biosciences (GE Healthcare, Europe, Barcelona, Spain). Yeast culture media products were from Difco™ Laboratories (Detroit, MI). Bradford solution for protein assays was from Bio-Rad Laboratories (Barcelona, Spain). RPMI 1640 was from Gibco-Invitrogen Corporation (Barcelona, Spain). C75, C_{17}-CoA, defatted bovine serum albumin (BSA), palmitoyl-CoA, malonyl-CoA, and other chemicals were from Sigma–Aldrich (Madrid, Spain). Acyl-CoA synthetase from *Pseudomonas* sp. was from Sigma (Madrid, Spain). Etomoxir was provided by H.P.O. Wolf (GMBH, Allensbach, Germany).

2.2. Animals

Sprague-Dawley female rats (210–230 g) were bred in our laboratory. Animals were maintained under a 12 h dark/light cycle with free access to food (2014, Harlan) and water. All experimental protocols were approved by the Animal Ethics Committee at the University of Barcelona, in accordance with current legislation.

2.3. Cannulation surgery

Chronic (i.c.v.) cannulae were stereotaxically implanted into lateral ventricle under ketamine (Imalgene, 90 mg/kg) and xylazine (Rompun, 11 mg/kg) anesthesia. The coordinates were 1.0 mm posterior to bregma, 1.4 mm lateral of the sagittal sinus and 6.2 mm ventral to the dura mater. Rats received subcutaneous injection of buprenorphine (0.05 mg/kg) for analgesia.

2.4. Stereotaxic microinjection

Rats were anesthetized as previously described and immobilized in a stereotaxic apparatus. Injections were given bilaterally into the ARC nucleus of the hypothalamus (2.7 mm posterior to bregma, 0.2 mm lateral of the sagittal sinus and 9.8 mm ventral to the dura mater). 30 min after the injection rats were sacrificed and hypothalamus was dissected.

2.5. Treatments

After 1 week of postsurgical recovery, cannula placements were verified by assessing a feeding response to ghrelin [20]. I.c.v. injection (5 μL) of etomoxir (190 μg), C75 (40 μg) or vehicle (RMPI 1640) were performed with a microliter syringe (Hamilton). For feeding experiments, rats received single injections of vehicle or compound dissolved in vehicle 30 min before the light was turned off. We measured intakes of chow, corrected for spillage, at 1, 2, 4 and 22 h. Body weight was measured after 22 h. For the activity experiments three rats were microinjected (ARC) with 2 μL of RPMI 1640 medium as a control or with 2 μL of C75 dissolved in the same medium at 33 mM final concentration. For the LC–MS/MS analysis, two rats were microinjected (ARC) with 2 μL of RPMI 1640 medium as control or with 2 μL of C75 dissolved in the same medium at 15, 30 or 60 mM final concentration. 30 min after injection rats were killed and hypothalamus was excised and stored at −80 °C for acyl-CoA extraction.

2.6. C75-CoA and acyl-CoAs extraction and quantification

Acyl-CoAs were extracted as described elsewhere [21], with some modifications. All procedures were performed at 0–4 °C. Hypothalamus from control- and C75-microinjected rats was thawed and 1 mL of 100 mM KH_2PO_4 pH 4.9 was added. 16 nmol of heptadecanoyl-CoA (C_{17}-CoA), as an internal standard, was added to all samples, which were then sonicated for 20 s. One millilitre of n-propanol was added and the emulsions were sonicated for a further 20 s, left on ice for 20 s, and sonicated again for 20 s. To this solution, 0.125 mL

Please cite this article in press as: Mera P, et al. C75 is converted to C75-CoA in the hypothalamus, where it inhibits carnitine palmitoyltransferase 1 and decreases food intake and body weight. Biochem Pharmacol (2009), doi:10.1016/j.bcp.2008.11.020

of saturated $(NH_4)_2SO_4$ was added, followed by 2 mL of 100% acetonitrile, and the mixture was then vortexed for 5 min at 4 °C. The tubes were then centrifuged for 5 min at 2100 × *g* at 4 °C. The supernatant was removed and passed through a sterile 0.2 μm filter (Millipore). The filtrate was lyophilized and re-dissolved in the same mobile phase (buffer B: 10% acetonitrile in 10 mM ammonium acetate buffer (pH 5.3)) used for the LC–MS/MS analysis. C_{17}-CoA and C75-CoA were used as standards to produce the calibration curves from which we quantified production of C75-CoA *in vivo*. The straight lines obtained had a regression coefficient of 99%.

2.7. Liquid chromatography–mass spectrometry (LC–MS/MS)

LC analyses were performed using a Perkin Elmer series 200 equipped with a quaternary pump and thermostatted autosampler. An XBridge (Waters) C_{18} column (50 mm × 2.1 mm, 3.5 μm) was used at room temperature and the volume injected was 15 μL. The mobile phases were buffer A, 50% acetonitrile in 10 mM ammonium acetate buffer (pH 5.3); buffer B, 10% acetonitrile in 10 mM ammonium acetate buffer (pH 5.3) and C, 100% acetone. The column was equilibrated with 15% buffer A for 10 min, and then the eluting gradient was as follows: 15% buffer A to 90% buffer A in 5.5 min, then 90% buffer A to 50% buffer A, 5% C to 45% C in 15.5 min, and 50% buffer A, 45% C in 25 min. The flow rate was 0.4 mL/min.

MS and MS/MS experiments were performed on an API 3000 triple-quadrupole mass spectrometer equipped with a Turbo Ionspray source. All the analyses were performed in positive mode with the following settings: capillary voltage, +3000 V; nebulizer gas (N_2), 10 (arbitrary units); curtain gas (N_2), 12 (arbitrary units); collision gas (N_2), 4 (arbitrary units); declustering potential, +30 V; focusing potential, +200 V; entrance potential, +10 V; collision energy, +40 V; collision cell exit potential, +15 V. Drying gas (N_2) was heated to 300 °C and introduced at a flow-rate of 6000 $cm^3\ min^{-1}$. Full scan data acquisition was performed scanning from *m/z* 500 to 1200 in profile mode and using a cycle time of 2 s with a step size of 0.1 u and a pause between each scan of 2 ms. In order to achieve maximum sensitivity, samples were injected in multiple reaction monitoring mode (MRM) by monitoring the 1022.5/515.6 and the 1020.7/513.5 transitions, obtained through product ion scan experiments with the C75-CoA and C_{17}-CoA standard, respectively. To calculate the C75-CoA concentration in the samples, 15 μL of increasing concentrations of C75-CoA and C_{17}-CoA from 10 to 5000 nM was injected. The areas of the resulting peaks were used to produce the calibration curve. The C_{17}-CoA was used as internal standard to calculate the percentage of recovery in the acyl-CoA extraction.

2.8. Enzymatic synthesis of C75-CoA and etomoxiryl-CoA

C75 was converted first, *in vitro*, to its CoA derivative by long-chain acyl-CoA synthetase in the presence of CoA, as described previously [19]. The unreacted CoA from the C75-CoA activation solution (1 mL) was removed by incubation for 30 min at 4 °C with 1.25 mL of SulfoLink Coupling Gel (Pierce Biotechnology), as carnitine acyltransferase activity is inhibited by CoA [22]. C75-CoA synthesized in this enzymatic reaction was used as a standard for LC–MS/MS analysis. The conversion of etomoxir to etomoxiryl-CoA was nearly complete, as deduced from the fluorometric assay of the remaining free CoA, as described elsewhere [23].

2.9. Non-enzymatic synthesis of C75-CoA

In the second experiment, a solution of C75 and CoA (pH 8.4) was stirred in the absence of acyl-CoA synthetase. The structure and relative stereochemistry of the C75-CoA adduct was determined by NMR. CoA sodium salt hydrate (8.6 mg), and $Na_3PO_4{\cdot}12H_2O$ (7.6 mg) were added to a solution of (±)-C75 (2.5 mg) in D_2O (0.8 mL) in an NMR tube. The structure of the C75-CoA adduct was fully determined by ^1H and ^{13}C NMR, gCOSY and gHSQC experiments.

2.10. Expression of rat CrAT and CPT1 in Saccharomyces cerevisiae

Plasmids pYESCrAT^{wt} [14], pYESCrAT$^{D356A/M564G}$ [15], pYESLCPT^{wt} [24], pYESLCPT^{M593S} [13] containing CrAT wt, CrAT D356A/M564G mutant, CPT1A wt and CPT1A M593S mutant, respectively, were expressed in yeast cells, and mitochondrial cell extracts were prepared as previously described [24]. An *S. cerevisiae* strain devoid of COT and CPT1 activity and lacking the endogenous *CAT2* gene (FY23Δ*cat2* (MATa trp1 ura3 Δ*cat2*::LEU2)) was used as an expression system [25].

2.11. Determination of carnitine acyltransferase activity

Mitochondrial-enriched fractions were obtained by differential centrifugation [26], with minor modifications. All protein concentrations were determined using the Bio-Rad protein assay with bovine serum albumin as a standard.

Two methods were used for the assay of carnitine acyltransferase: a radiometric method [24] and an endpoint fluorometric method [14,23]. The radiometric assay was used in all cases, unless otherwise indicated.

2.11.1. Radiometric method

The forward reaction of carnitine acyltransferase activity was assayed in mitochondrial-enriched fractions obtained from yeast (5 μg protein for CrAT D356A/M564G and 3–4 μg protein for CPT1A) and from rat hypothalamus (100 μg protein for CPT1). Enzyme activity was assayed for 4 min at 30 °C in a total volume of 200 μL. The substrates were 400 μM L-[methyl-^{3}H]-carnitine, and 50 μM myristoyl-CoA (for CrAT D356A/M564G) or palmitoyl-CoA (for CPT1A). Drugs were preincubated with the enzyme for 1–5 min depending on the assay. Drug concentrations ranging from 0.01 to 60 μM were used to calculate the IC_{50}. Enzyme assays were carried out to deduce the effects of the free acid (C75) versus the CoA ester (C75-CoA), that is, the potency of C75-CoA as inhibitor relative to C75 as an activator. In this case, CPT1A wt overexpressed in yeast (8 μg protein) was preincubated for 5 min with increasing concentrations of C75 (5–100 μM), C75-CoA (5–50 μM) with or without 100 μM C75 at each C75-CoA concentration. Enzyme activity was compared to the control (DMSO). In all cases, the molar ratio of acyl-CoA to albumin was kept at 5:1 to

Please cite this article in press as: Mera P, et al. C75 is converted to C75-CoA in the hypothalamus, where it inhibits carnitine palmitoyltransferase 1 and decreases food intake and body weight. Biochem Pharmacol (2009), doi:10.1016/j.bcp.2008.11.020

avoid the presence of free acyl-CoA and its deleterious detergent effects and to prevent the formation of micelles.

2.11.2. Fluorometric method

The forward reaction of carnitine acyltransferase activity was assayed for 8 min at 30 °C in a solution containing 0.1 mM acyl-CoA, 1.5 mM EDTA, 1.5 mM L-carnitine, and 40 mM Hepes buffer, pH 7.8, in a total volume of 600 μL. Acetyl-CoA was used as substrate for CrAT wt. Reactions were started by the addition of 5 μg of yeast-expressed protein. Increasing concentrations of C75-CoA, etomoxiryl-CoA or malonyl-CoA were independently incubated with yeast-overexpressed mitochondrial CrAT wt. Parallel (blank) assays were run in the absence of L-carnitine.

2.12. Construction of rat CrAT and CPT1A models

A model of rat CrAT wt enzyme was constructed by homology modelling using as templates the structures deposited in the Protein Data Bank (PDB) corresponding to human (1NM8) [27], and mouse CrAT (1NDB, 1NDF and 1NDI) [28], essentially as described elsewhere [14]. CrAT D356A/M564G was modelled by the same procedures using rat CrAT wt as template. CPT1A was also modelled using as templates the structures of mouse carnitine octanoyltransferase (1XL7, 1XL8) [29] and carnitine palmitoyltransferase 2 (PDB entry 2H4T) [30], essentially as described elsewhere [31,32]. The quality of the models was checked using the WHAT-CHECK routines [33] from the WHAT-IF program [34] and the PROCHECK validation program from the SWISS-MODEL server facilities [35]. To optimize geometries and release local constraints or inappropriate contacts, the modelled structures were energy minimized with the implementation of the GROMOS 43B1 force field in the program DeepView [36], using 500 steps of steepest descent minimization followed by 500 steps of conjugate-gradient minimization.

2.13. In silico molecular docking

Structural models of the molecular docking of the inhibitors C75-CoA and malonyl-CoA to the active site of the receptor proteins CPT1A, and CrAT mutant D356A/M564G were performed using the suite of programs included in the Autodock 3.0 package [35], as described elsewhere [14].

2.14. Statistical analysis

Data are represented as mean ± S.E.M. Student *t*-test was used for statistical analysis. Different experimental groups were compared with a one-way ANOVA followed by Turkey's test for comparisons post hoc. A probability level of $P < 0.05$ was considered significant.

3. Results

3.1. Synthesis and chemical characterization of C75-CoA by NMR

We have shown that C75-CoA can be synthesized from C75 and CoA in the presence of acyl-CoA synthetase from *Pseudomonas* sp. [19]. Here we show that the MS spectrum of C75-CoA gave an $[M + H]^+$ ion at *m/z* 1022.5, corresponding to the protonated molecule of C75-CoA. This ion corresponded to the formation of the C75-CoA molecule by conjugation of the CoA group without the loss of a water molecule. The product showed the following: a fragmentation ion at *m/z* 515.6, which was assigned to the C75-pantethenoic group, and an ion at *m/z* 428.1, which corresponds to adenosine 3′-diphosphate (Supplemental Fig. S1).

We hypothesised that the –SH group in CoA would be sufficiently nucleophilic to add to the electrophilic methylene group in C75 without any external agent (acyl-CoA synthetase) in an alkaline medium in which the thiol group is partially deprotonated. We mixed both reagents, C75 and HSCoA in a deuterated water solution at pH 8.4 (Fig. 1A) and the mixture was analyzed by ^{1}H NMR, comparing the results with the unreacted C75 and CoA. The peaks assigned to the methylene group (black triangle) progressively decreased and a new signal at ~2.9 ppm appeared due to the formation of the new saturated methylene group (white triangle) (Fig. 1B). These changes were fast (30 min). In a parallel experiment at neutral pH the same transformation was observed, albeit much more slowly (data not shown).

The structure and relative stereochemistry of the C75-CoA adduct shown in Fig. 1C were determined by one- and two-dimensional ^{1}H and ^{13}C NMR techniques in order to assign every signal (gCOSY and gHSQC experiments) [37]. In particular, the *trans–trans* relative configuration on the lactone ring shown in Fig. 1C is well established on the basis of the observed coupling constants (*J*), especially $J_{d,e}$. These coupling constants depend on the dihedral angle (H–C–C–H) of the protons involved and give information about their relative position. When we compared the coupling constants of the lactone ring moiety of our adduct with those reported [38,39] for the related compounds I and II (Fig. 1C) high correlation with II was observed, suggesting the same relative configuration.

As described above, we used two methods to obtain C75-CoA. In one, a solution of C75 and CoA was incubated in the presence of acyl-CoA synthetase. In the other, the adduct was synthesised in the absence of the enzyme. We aimed to determine whether the structural and inhibitory properties of the C75-CoA adducts depended on the presence of acyl-CoA synthetase in their synthesis. Two analytical tests were applied. First, a comparative mass/mass spectroscopy analysis showed that the C75-CoA synthesised in the presence of the enzyme (Supplemental Fig. S1) had the same ion fragmentation profile as that synthesised in the absence of the enzyme (data not shown). Second, we assayed their capacity to inhibit CPT1, obtaining identical results for both adducts (Fig. 1D). We conclude that the two adducts synthesized in the presence or absence of the enzyme have identical structure and properties.

3.2. Effect of C75 and C75-CoA on CPT1 activity

To examine the controversial effect of C75 on CPT1 activity we incubated yeast mitochondria with increased concentrations of C75 (Fig. 2A). The results reported indicate that free C75 alone is neither an activator nor an inhibitor of CPT1. We also

Please cite this article in press as: Mera P, et al. C75 is converted to C75-CoA in the hypothalamus, where it inhibits carnitine palmitoyltransferase 1 and decreases food intake and body weight. Biochem Pharmacol (2009), doi:10.1016/j.bcp.2008.11.020

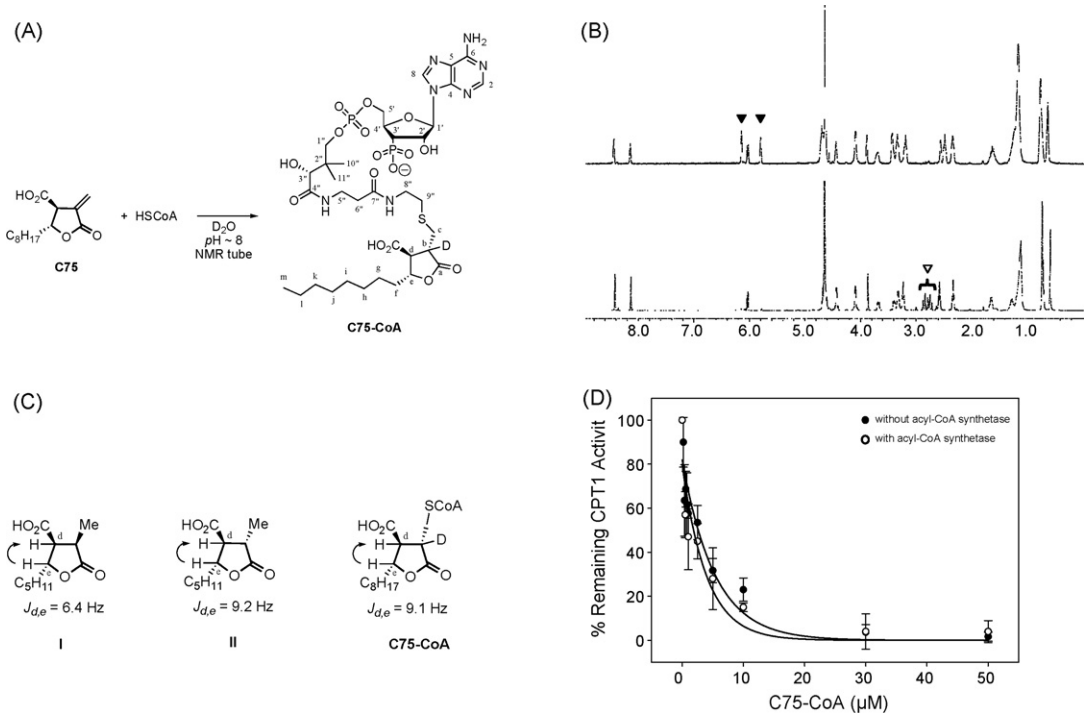

Fig. 1 – NMR structural studies. (A) Incubation of a ~1:1 mixture of C75 and CoA in D_2O (with 10% of DMSO-d6 in order to increase the solubility of C75). Peaks assigned to the methylene group (black triangles), peaks assigned to the saturated methylene groups (white triangles). (B) ^1H NMR (300 MHz) of a ~1:1 mixture of C75 and CoA in D_2O at pH ~8 at time 0 min (upper panel) and ^1H NMR (400 MHz) of a ~1:1 mixture of C75 and CoA in D_2O at pH ~8 after 30 min (lower panel). (C) Comparison of coupling constants (*J*) of C75-CoA adduct lactone ring with those reported early for related compounds I and II. (D) Comparison between the CPT1 inhibitory properties of C75-CoA synthesized in absence (●) and in presence (○) of acyl-CoA synthetase.

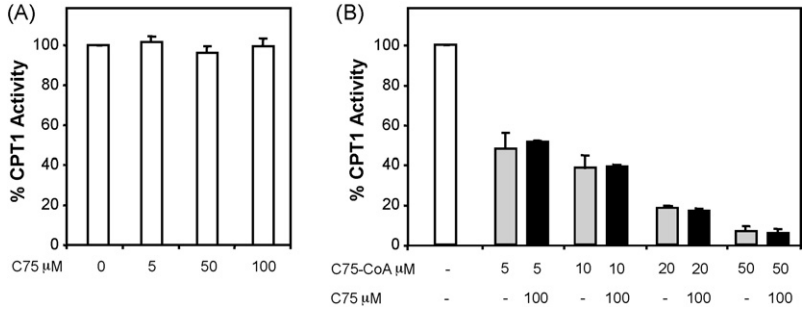

Fig. 2 – CPT1A wt overexpressed in yeast is inhibited by C75-CoA in presence of C75. (A) Mitochondrial fractions from yeast overexpression CPT1A wt were preincubated for 5 min with increasing concentrations of C75 and activity was measured. (B) Comparative CPT1A wt activity of mitochondrial fractions from yeast, incubated with increasing concentrations of C75-CoA and in presence or absence of a fixed concentration of C75 (100 μM). Data are represented as a percentage of the control value in the presence of DMSO and the results are the average of three independent experiments.

performed kinetic inhibitory experiments in which, in addition to increasing concentrations of C75-CoA, a fixed concentration of C75 (100 μM) was added to the mixture. CPT1 inhibition was not counteracted by the fixed amount of free C75 at any concentration of C75-CoA. In other words, even at the highest C75 concentrations, the free product did not overcome the inhibition by C75-CoA (Fig. 2B).

3.3. *Inhibitory effects of C75-CoA on yeast-expressed mutated CPT1A and CrAT*

To examine the structural requirements of the interaction between C75-CoA and CPT1 we carried out C75-CoA inhibitory experiments where we used specific acyltransferase mutants. We used CrAT D356A/M564G, which has a deep hydrophobic

Please cite this article in press as: Mera P, et al. C75 is converted to C75-CoA in the hypothalamus, where it inhibits carnitine palmitoyltransferase 1 and decreases food intake and body weight. Biochem Pharmacol (2009), doi:10.1016/j.bcp.2008.11.020

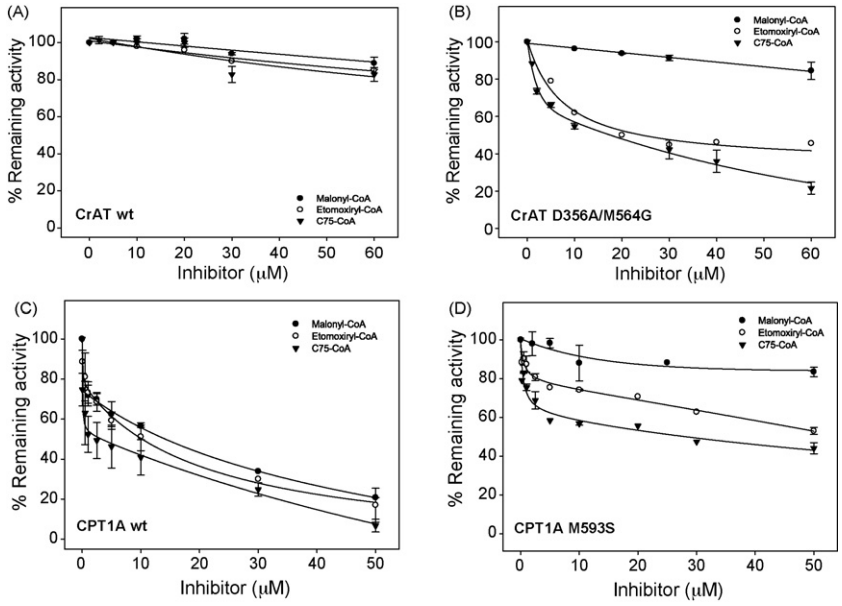

Fig. 3 – Effects of malonyl-CoA, etomoxiryl-CoA and C75-CoA on the activity of yeast-expressed wt CPT1A and CrAT, and the point mutants CPT1A M593S and CrAT D356A/M564G. Mitochondrial extracts from yeast expressing (A) CrAT wt, (C) CPT1A wt, and point mutants (B) CrAT D356A/M564G and (D) CPT1A M593S, were preincubated with increasing concentrations of malonyl-CoA (●), etomoxiryl-CoA (○) and C75-CoA (▼). Carnitine acyltransferase activity was measured, and data are expressed relative to control values in the absence of drugs (100%) as the mean of at least two independent experiments.

pocket for the binding of LCFA-CoAs instead of short acyl-CoAs and behaves like CPT1A in terms of acyl-CoA specificity [15]. We also used CPT1A M593S, which is active but insensitive to malonyl-CoA inhibition [13]. Experiments with etomoxiryl-CoA, a pharmacological inhibitor of CPT1, and malonyl-CoA, its physiological inhibitor, were carried out as controls.

C75-CoA and etomoxiryl-CoA inhibited CrAT D356A/M564G but had little effect on CrAT wt (Fig. 3A and B). At 60 μM of C75-CoA, the remaining CrAT activity was 83% for CrAT wt, and only 21% of the original level for CrAT D356A/M564G. For etomoxiryl-CoA, at a concentration of 60 μM, the remaining activity was 86% for CrAT wt, and 46% for the CrAT mutant. These results indicate that CrAT wt is insensitive to these drugs because the long aliphatic chain of C75-CoA and etomoxiryl-CoA does not fit in the shallow cavity of the wt enzyme, where only the acyl group of short-chain acyl-CoAs such as acetyl- and butiryl-CoA can enter. However, when this cavity was open and accessible to longer acyl-CoAs, as in the CrAT D356A/M564G mutant, the enzyme became sensitive to these inhibitors. In contrast, malonyl-CoA had little effect on mutant or wt CrAT (Fig. 3A and B). These results show that CrAT D356A/M564G, like the wt enzyme, does not contain the structural determinants needed for the initial interaction with malonyl-CoA and enzyme inhibition.

Next we compared the inhibitory effect of C75-CoA on CPT1A wt and CPT1A M593S. At 50 μM of C75-CoA, the remaining activity of the M593S mutant was about 45% of the original level (Fig. 3D), whereas the activity of the CPT1A wt was almost abolished (Fig. 3C). A similar effect was observed with etomoxiryl-CoA. Malonyl-CoA, as expected, inhibited CPT1A wt while the activity of the malonyl-CoA-insensitive enzyme (CPT1A M593S) was unaffected. The IC_{50} for C75-CoA and CPT1A M593S was 108-fold higher than that for CPT1A wt (25.9 μM *vs.* 0.24 μM). In the case of etomoxiryl-CoA the IC_{50} increased 31-fold compared with the wt enzyme (168 μM *vs.* 4.1 μM). This indicates that CPT1A inhibitors in addition to fitting in the hydrophobic pocked also need to interact with the malonyl-CoA site of CPT1A to produce potent inhibition.

3.4. *Molecular model of docking of C75-CoA into CPT1A wt, and CrAT D356A/M564G*

Since CPT1 has not yet been crystallized, we do not know the location of C75-CoA in the CPT1 crystal. Therefore, we used computational docking methods to identify a putative location of C75-CoA molecule in the 3D models of the catalytic core of CPT1A wt and of CrAT D356A/M564G. The model locates the C75-CoA molecule (Fig. 4A) in CTP1A wt in a position that coincides with the site of palmitoyl-CoA substrate [32], thus introducing the aliphatic chain into the hydrophobic cavity in the protein active centre. The carboxyl group in the head of the C75-CoA molecule is positioned at the equivalent locus for the carnitine substrate in the CPT1A wt models, partially filling it. This indicates that this inhibitor could hamper the correct positioning of the carnitine substrate. Moreover, the head of C75-CoA is also located near the catalytic His residue (His^{473}), which would impair the catalytic activity of CPT1A. The position of the carboxyl group on C75-CoA (Fig. 4A) is similar to that proposed for the dicarbonyl moiety of malonyl-CoA on CPT1A [32], which thus interferes with the correct positioning of carnitine substrate (Fig. 4C). This shared mode of action could be explained in part by the presence of a carboxyl group in carnitine, C75-CoA and malonyl-CoA molecules (Fig. 4D), putatively located in the active centre of the enzyme.

Please cite this article in press as: Mera P, et al. C75 is converted to C75-CoA in the hypothalamus, where it inhibits carnitine palmitoyltransferase 1 and decreases food intake and body weight. Biochem Pharmacol (2009), doi:10.1016/j.bcp.2008.11.020

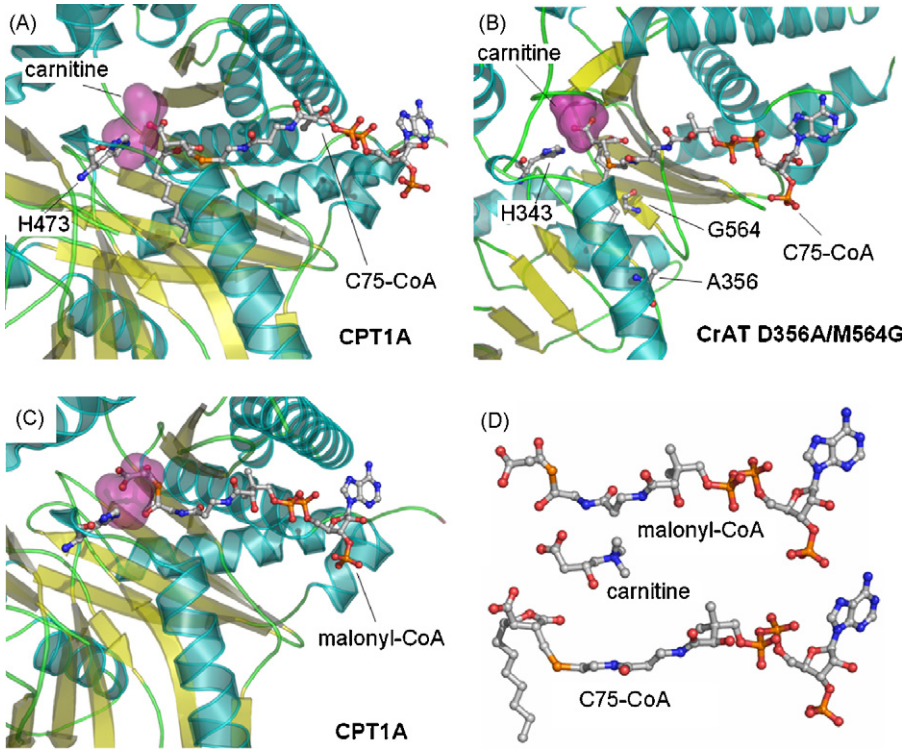

Fig. 4 – *In silico* docking of inhibitors to 3D models for the active centres of wt CPT1A and CrAT D356A/M564G mutant. (A) Predicted docked solution for C75-CoA molecule in the active centre of wt CPT1A. Location of catalytic residue His^{473} is indicated. Carboxylate group of C75-CoA partially occupies the volume corresponding to the carnitine substrate molecule (magenta). (B) Putative position for C75-CoA docking solution for C75-CoA in the active centre of CrAT D356A/M564G. The aliphatic chain of the inhibitor is located in the tunnel opened by mutated residues A356 and G564. The carboxylate group of C75-CoA is placed in the carnitine locus (magenta). Location of catalytic His^{343} is also indicated. (C) Docking of malonyl-CoA on CPT1A wt showing a similar positioning to C75-CoA, locating the dicarbonyl moiety in the space usually occupied by carnitine. (D) Molecular structures of malonyl-CoA, carnitine and C75-CoA, showing a similar arrangement of their corresponding carboxyl groups. Molecular representations were performed using PyMOL (DeLano Scientific, San Carlos CA).

An analogous model was constructed for the location of C75 in CrAT D356A/M564G mutant structure. The position of the C75 aliphatic chain moiety is similar to that proposed for stearoyl-CoA in the same enzyme derivative [15], in which the hydrocarbon chain is located in the cavity that opens up when Asp^{356} and Met^{564} are replaced by Ala and Gly, respectively (Fig. 4B). The carboxyl group at the head of C75 is located in the carnitine locus, close to the catalytic His^{343} residue as mentioned above for CPT1A.

3.5. *C75 is converted to C75-CoA in rat hypothalamus*

Since C75 has been proposed as a regulator of food intake through its action on the hypothalamus, we examined whether C75-CoA is produced in the hypothalamus following direct injection of C75. We injected 7.6, 15.2 and 30.4 μg of C75 in the arcuate (ARC) nucleus by stereotaxic surgery. Thirty minutes after injection the rats were killed and acyl-CoAs, including C75-CoA, were extracted from the hypothalamus. Analysis of the samples by LC–MS/MS showed a peak corresponding to C75-CoA (Fig. 5). The production of C75-CoA increased with the amount of C75 injected. Considering that in our conditions the average weight of the rat hypothalamus was 50 mg, the concentrations of C75-CoA produced in the hypothalamus after an injection of 7.6, 15.2 and 30.4 μg of C75 were 3.7, 15.9 and 25.1 nmol/g tissue, respectively.

3.6. *Central nervous system administration of C75 inhibits CPT1 activity and decreases food intake and body weight*

Having demonstrated the conversion of C75 into C75-CoA in the rat hypothalamus, we then studied the effect of a stereotaxic microinjection of C75 into the rat ARC nucleus on CPT1 activity. Hypothalamic mitochondrial fractions from rats injected with 16.8 μg of C75 were assayed for CPT1 activity and the value was compared to hypothalamic mitochondrial fractions from rats injected with RPMI medium. Activity was decreased by 46% in C75-treated rats (Fig. 6A).

Next we administered C75 in the lateral cerebral ventricle of the rat and measured food intake and body weight. Consistent with previous results [2–5], C75 produced a decrease in food intake and body weight (Fig. 6B and C). The anorectic action of etomoxir was seen at a later point (22 h).

Please cite this article in press as: Mera P, et al. C75 is converted to C75-CoA in the hypothalamus, where it inhibits carnitine palmitoyltransferase 1 and decreases food intake and body weight. Biochem Pharmacol (2009), doi:10.1016/j.bcp.2008.11.020

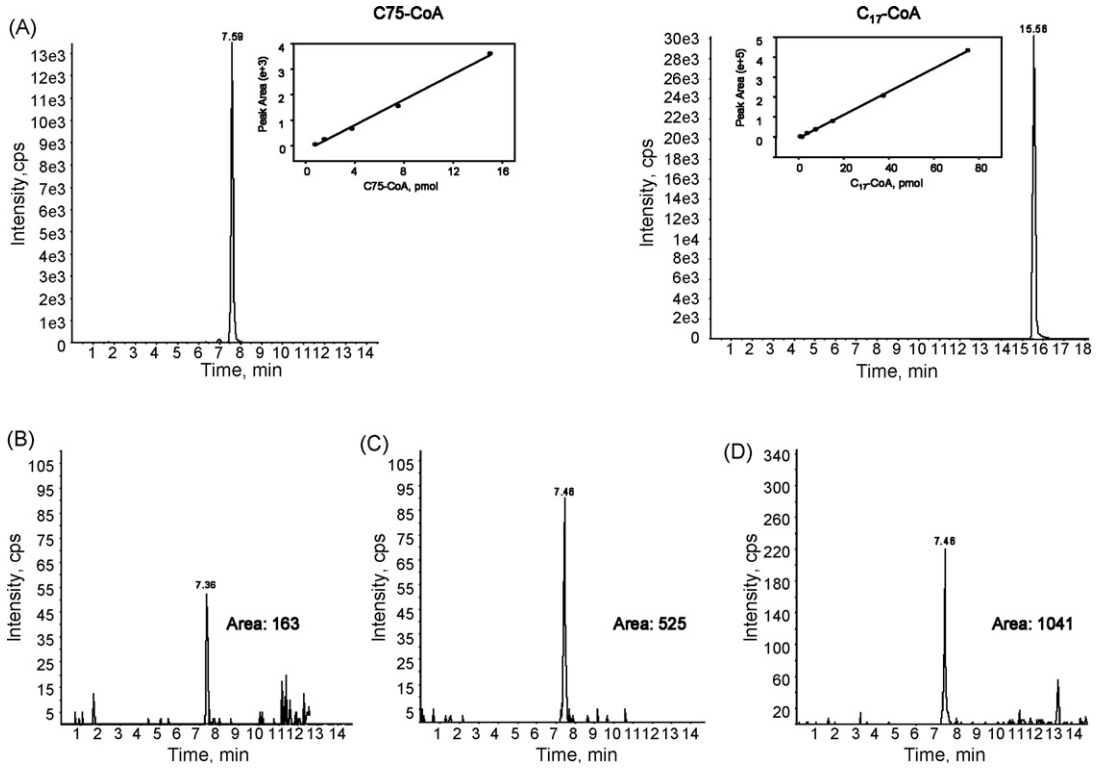

Fig. 5 – Analysis of the C75-CoA levels after hypothalamic C75 injections. (A) LC–MS/MS representative chromatograms of C75-CoA and C_{17}-CoA. Five concentrations of C75-CoA: 50, 100, 250, 500 and 1000 nM and seven concentrations of C_{17}-CoA: 50, 100, 250, 500, 1000, 2500 and 5000 nM were injected and the areas below the resulting peaks were calculated. The calibration curves are shown in insets. Representative LC chromatograms for C75-CoA obtained from rat hypothalamus after the injection in the hypothalamic ARC nucleus of 2 μL of C75 at various concentrations: (B) 15 mM, (C) 30 mM and (D) 60 mM. 30 min after injection rats were decapitated, and the hypothalamus was excised, immediately frozen and stored at −80 °C. Acyl-CoAs were extracted as described in Experimental Procedures, and C_{17}-CoA was used as internal standard. Peak areas are shown in arbitrary units.

4. Discussion

Energy balance is monitored by the hypothalamus, where inhibitors of FAS have been described to suppress food intake [40,41]. C75 acts on fatty-acid metabolism by inhibiting FAS activity. Inhibition of FAS produces accumulation of malonyl-CoA, which, as a physiological inhibitor of CPT1, prevents the oxidation of newly synthesized fatty acids. Moreover, C75 may activate CPT1 [2,18]. The effect of C75 on FAS is difficult to reconcile with the C75-activation of CPT1 as they have opposite effects: inhibition by malonyl-CoA and direct activation of CPT1. The simultaneous activation and inhibition of CPT1 by C75 appears paradoxical, and it has not been addressed satisfactorily. Kuhajda et al. suggested that C75 could modulate the inhibition of AMP-activated protein kinase (AMPK) which would lead to an increase in acetyl-CoA carboxylase (ACC) activity and a subsequent increase in malonyl-CoA levels [42]. This does not solve the paradox, since there would be an increase in malonyl-CoA (putatively inhibiting CPT1 activity) and a simultaneous activation of CPT1 produced by C75 itself (Fig. 7).

Here we attempt to explain the anorectic effects of C75 in terms of its inhibitory action on CPT1. Inhibition of CPT1 could prevent the oxidation of fatty acids of the ARC nucleus in the hypothalamus leading to a local accumulation of LCFA-CoAs. The increase in LCFA-CoA is a central signal of 'nutrient abundance' which in turn activates a chain of neuronal events, via up-regulation of anorexigenic genes and down regulation of orexigenic genes, that would promote a switch in fuel sources from carbohydrates to lipids and limit food intake [8]. The detailed mechanism of this up- or down-regulation has not been addressed yet. Likewise, central administration of fatty acid suppresses food intake. Here we demonstrated that C75 is transformed into C75-CoA in the hypothalamus where it inhibits CPT1 activity. We propose that this direct effect *in vivo* of C75-CoA on CPT1 would explain by itself the inhibition of CPT1 activity. However, FAS could be inhibited by C75 in the hypothalamus. Therefore, malonyl-CoA could be in excess, inhibiting CPT1, together with C75-CoA. The anorectic effects of C75 are similar to those produced by other CPT1 inhibitors such as ST1326 and tetradecylglycidic acid, and to those of a riboprobe that specifically cleaves CPT1A mRNA [8]. The CPT1 inhibitor etomoxir also decreased feeding and reduced body weight in rats supporting those previous results [8].

It was important to discern whether C75 was an inhibitor or an activator of CPT1. Our results indicate that C75 is neither an activator nor an inhibitor of CPT1 when incubated with

Please cite this article in press as: Mera P, et al. C75 is converted to C75-CoA in the hypothalamus, where it inhibits carnitine palmitoyltransferase 1 and decreases food intake and body weight. Biochem Pharmacol (2009), doi:10.1016/j.bcp.2008.11.020

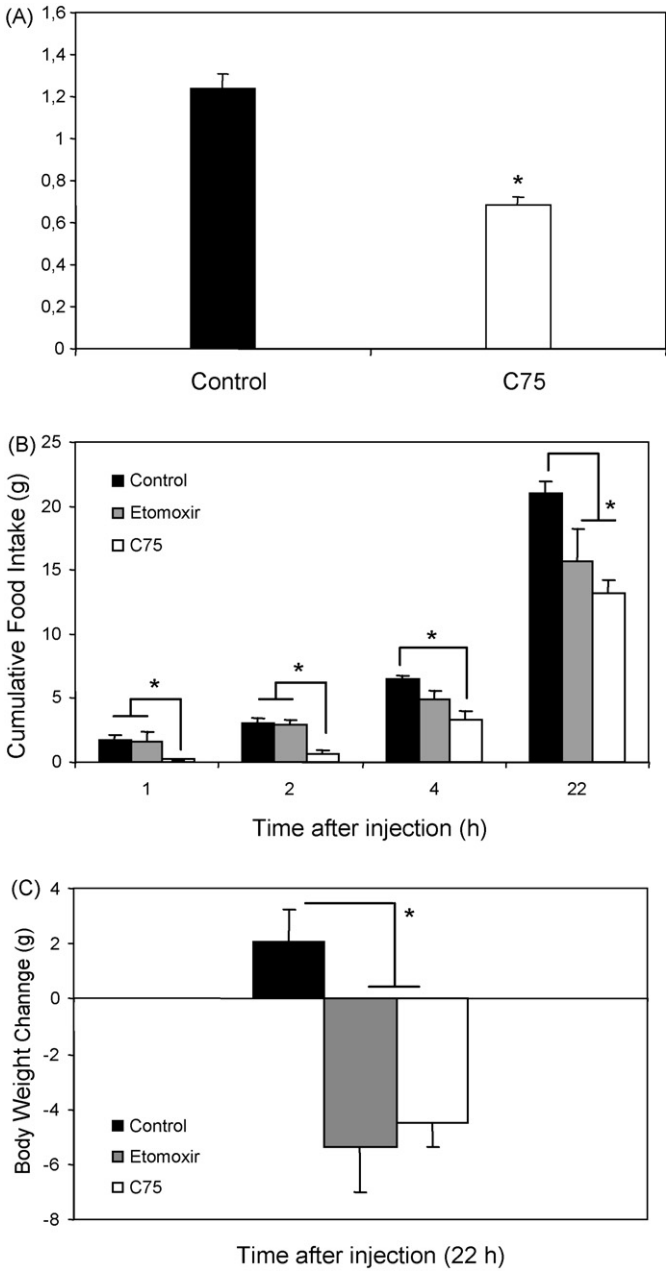

Fig. 6 – Central nervous system administration of C75 inhibits CPT1 activity and decreases food intake and body weight. (A) Determination of CPT1 activity after the injection of C75 in ARC nucleus. Control injections (n = 3; 2 μL of RPMI 1640 medium as a control, black bar). C75 injections (n = 3; 2 μL of C75 33 mM in RPMI 1640 medium, white bar). (B) Food intake measured in rats at 1, 2, 4 and 22 h after i.c.v. injection of C75 (white bars), etomoxir (grey bars) and control (RPMI medium, black bars). n = 5. (C) Body weight measured in rats at 22 h after i.c.v. injection of C75 (white bar), etomoxir (grey bar) and control (RPMI medium, black bar). n = 5. *$P < 0.05$.

yeast-expressed CPT1A. C75 did not overcome the inhibition caused by C75-CoA. This agrees with the observed net effect of inhibition of CPT1 activity. Results shown here and elsewhere [19] demonstrate that C75-CoA inhibits CPT1A *in vitro* more strongly than etomoxiryl-CoA (IC_{50} values are 0.24 μM and 4.1 μM, respectively).

The finding that C75 forms a CoA adduct before it can inhibit CPT1 is reminiscent of the case of etomoxir. McGarry and co-workers [43,44] showed that the CPT1 inhibitory molecules were neither tetradecylglycidic acid nor etomoxir themselves, but rather their CoA esters produced in the presence of acyl-CoA synthetase. The CoA group may direct and fix the drug molecule in the cavities of CPT1, as it does with the natural physiological inhibitor malonyl-CoA and with the substrate palmitoyl-CoA. The synthesis of C75-CoA is produced stereo specifically through the electrophilic methylene group of C75. Moreover, our finding that C75-CoA is produced in absence of acyl-CoA synthetase indicated that it could be synthesised in the hypothalamus, irrespective of whether it is expressed in hypothalamic neurons.

Our results indicate that C75-CoA is formed in the hypothalamus following stereotaxic injection of C75. Inhibition of hypothalamic CPT1 by C75-CoA *in vivo*, as seen in our experiments, is independent of the putative inhibition by malonyl-CoA, which may be formed after the action of C75 either on FAS or on AMPK. Hypothalamic CPT1 activity was determined in twice-washed mitochondria. Therefore, malonyl-CoA was unlikely to remain within CPT1, as this metabolite leaves CPT1 freely when mitochondria are washed. In contrast, C75-CoA, as it is a tight-binding inhibitor, remains bound to the enzyme after washing, which means that its inhibition is persistent [19]. Hence, C75-CoA not only inhibits CPT1 *in vitro*, but it also inhibits CPT1 activity in the hypothalamus after C75 has been converted to its CoA derivative.

That C75-CoA is an inhibitor of CPT1A is also supported by the docking analysis of the CPT1A model. Comparison of computer-calculated docking models shows that CoA is bound at the same site, whether it belongs to C75-CoA or malonyl-CoA, or palmitoyl-CoA. The carboxylic acid bound to the lactone of C75 protrudes into the carnitine site. The inhibitory mechanism of C75-CoA resembles that observed for malonyl-CoA (Fig. 4C) [32]. Several authors reported the competition between malonyl-CoA and carnitine [45,46]. The carboxylate group of malonyl-CoA and C75-CoA may partially mimic the interaction between the enzyme and the carboxylate group of carnitine, thus preventing the positioning of this substrate and inhibiting the catalytic activity of the enzyme. Several authors [47,48] suggest that the presence of two carbonyl groups in close juxtaposition in the malonyl-CoA molecule might be responsible for the interaction and the inhibitory effect on CPT1A. Because C75-CoA also has these two carbonyl groups, it may behave like malonyl-CoA. Indeed the docking models show that C75-CoA could bind to the malonyl-CoA site of the enzyme [32].

Moreover, the hydrocarbon chain of C75 is located at the same site as the hydrocarbon long-chain of palmitic acid. The kinetic experiments of inhibition of C75-CoA against palmitoyl-CoA [19] are confirmed by the docking studies, and both support the notion that C75-CoA is a strong inhibitor of CPT1A.

To assess the involvement of the hydrocarbon chain of C75-CoA positioning in the acyl group binding pocket, we carried

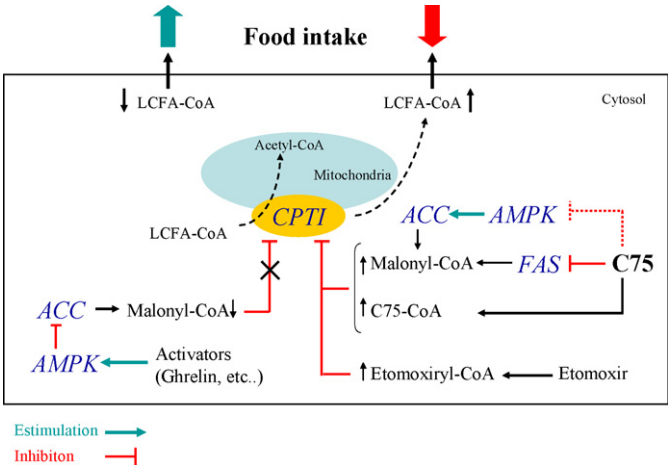

Fig. 7 – Model of action of C75 on hypothalamic fatty-acid metabolism. Energy balance is monitored by the hypothalamus. The accumulation of malonyl-CoA due to FAS-inhibition by C75 leads to a reduction in CPT1 activity. This would increase the cytosolic pool of LCFA-CoA and thus a decrease of food intake. In addition, C75 has been suggested to inhibit AMPK resulting in an activation of ACC and consequent increase of malonyl-CoA levels [42]. Here we have shown that C75 is converted into C75-CoA in the hypothalamus contributing to the direct inhibition of CPT1. Our experiments also demonstrate that other CPT1 inhibitors such as etomoxir produce similar effects decreasing food intake. On the other hand, AMPK-activators such as ghrelin [49] lead to ACC inactivation reducing malonyl-CoA levels and CPT1 inhibition. Thus, increased β-oxidation produces a reduction on LCFA-CoAs promoting food intake.

out C75-CoA inhibitory experiments with the new mutated protein, CrAT D356A/M564G. This protein has a deep hydrophobic pocket for the binding of long-chain instead of short-chain acyl-CoAs and shows CPT1-like behaviour in terms of acyl-CoA specificity, although unlike CPT1A, it is not inhibited by malonyl-CoA [15]. The inhibition by C75-CoA of the mutant CrAT D356A/M564G suggests that C75-CoA fits in the large hydrophobic pocket of this enzyme, as in CPT1A wt, and that the presence of this pocket is necessary for C75-CoA inhibition. However, CrAT D356A/M564G is not as sensitive as CPT1A wt to C75-CoA, since the IC_{50} for C75-CoA acting on CPT1A wt is 50-fold lower than that observed for the CrAT double mutant. These results indicate that factors other than the presence of a hydrophobic pocket contribute to the inhibitory potency of C75-CoA toward CPT1. CPT1A M593S, which is insensitive to malonyl-CoA inhibition, shows limited sensitivity towards C75-CoA, but its IC_{50} for C75-CoA is similar to that of CrAT double mutant (25.9 μM *vs.* 12.8 μM, respectively). Therefore, the lack of a ''malonyl-CoA-like'' interaction between CrAT double mutant or CPT1A M593S and the carbonyl groups in the polar head of C75-CoA might explain their limited sensitivity to the inhibitor.

We conclude that C75 is converted into C75-CoA and that it strongly inhibits CPT1 *in vitro* and *in vivo*. Docking and kinetic analysis revealed the molecular basis by which C75-CoA interacts with the enzyme and its substrates. We also show that C75-CoA is formed *in vivo* in the hypothalamus, where it inhibits CPT1. Here the inhibition of CPT1 could alter fatty-acid oxidation, thus putatively promoting down-regulation of orexigenic genes and up-regulation of anorexigenic genes, which induces restriction in food intake. These results point to the potential use of drugs to inhibit CPT1 activity, and control food intake in the treatment of obesity and diabetes.

Acknowledgements

We thank Jeus Perez-Clausell from the Department of Cell Biology, School of Biology, University of Barcelona, Felipe Casanueva's group from the Department of Molecular Endocrinology and Carlos Diéguez's group from the Department of Physiology, School of Medicine, University of Santiago de Compostela for their support in stereotaxis experiments, to Olga Jaúregui from the Scientific-Technical Services of the University of Barcelona for her technical assistance in the LC–MS/MS analysis. We also thank Biomol-Informatics SL (http://www.biomol-informatics.com) for bioinformatics consulting. This study was supported by Grant SAF2007-61926 and by grant CTQ2006-13249 from the Ministerio de Educación y Ciencia, Spain; by grant C3/08 from the Fondo de Investigación Sanitaria of the Instituto de Salud Carlos III; by the Activities Program among R&D groups of the Comunidad de Madrid in Biosciences (S-BIO-0260/2006-COMBACT) and by the Ajut de Suport als Grups de Recerca de Catalunya (2005SGR-00733), Spain. Financial support of ''Fundación Ramón Areces'' to CBMSO is also acknowledged. A.G.C. and D.S. were recipients of fellowships from the University of Barcelona, and A.B. and C.G. from the Ministerio de Educación y Ciencia, Spain.

Appendix A. Supplementary data

Supplementary data associated with this article can be found, in the online version, at doi:10.1016/j.bcp.2008.11.020.

Please cite this article in press as: Mera P, et al. C75 is converted to C75-CoA in the hypothalamus, where it inhibits carnitine palmitoyltransferase 1 and decreases food intake and body weight. Biochem Pharmacol (2009), doi:10.1016/j.bcp.2008.11.020

REFERENCES

[1] Kuhajda FP, Pizer ES, Li JN, Mani NS, Frehywot GL, Townsend CA. Synthesis and antitumor activity of an inhibitor of fatty acid synthase. Proc Natl Acad Sci USA 2000;97:3450–4.
[2] Thupari JN, Landree LE, Ronnett GV, Kuhajda FP. C75 increases peripheral energy utilization and fatty acid oxidation in diet-induced obesity. Proc Natl Acad Sci USA 2002;99:9498–502.
[3] Thupari JN, Kim EK, Moran TH, Ronnett GV, Kuhajda FP. Chronic C75 treatment of diet-induced obese mice increases fat oxidation and reduces food intake to reduce adipose mass. Am J Physiol Endocrinol Metab 2004;287:E97–104.
[4] Clegg DJ, Wortman MD, Benoit SC, McOsker CC, Seeley RJ. Comparison of central and peripheral administration of C75 on food intake, body weight, and conditioned taste aversion. Diabetes 2002;51:3196–201.
[5] Kumar MV, Shimokawa T, Nagy TR, Lane MD. Differential effects of a centrally acting fatty acid synthase inhibitor in lean and obese mice. Proc Natl Acad Sci USA 2002;99:1921–5.
[6] Loftus TM, Jaworsky DE, Frehywot GL, Townsend CA, Ronnett GV, Lane MD, et al. Reduced food intake and body weight in mice treated with fatty acid synthase inhibitors. Science 2000;288:2379–81.
[7] Hu Z, Cha SH, Chohnan S, Lane MD. Hypothalamic malonyl-CoA as a mediator of feeding behavior. Proc Natl Acad Sci USA 2003;100:12624–9.
[8] Obici S, Feng Z, Arduini A, Conti R, Rossetti L. Inhibition of hypothalamic carnitine palmitoyltransferase-1 decreases food intake and glucose production. Nat Med 2003;9:756–61.
[9] McGarry JD, Brown NF. The mitochondrial carnitine palmitoyltransferase system. From concept to molecular analysis. Eur J Biochem 1997;244:1–14.
[10] Esser V, Brown NF, Cowan AT, Foster DW, McGarry JD. Expression of a cDNA isolated from rat brown adipose tissue and heart identifies the product as the muscle isoform of carnitine palmitoyltransferase I (M-CPT I). M-CPT I is the predominant CPT I isoform expressed in both white (epididymal) and brown adipocytes. J Biol Chem 1996;271:6972–7.
[11] Price N, van der Leij F, Jackson V, Corstorphine C, Thomson R, Sorensen A, et al. A novel brain-expressed protein related to carnitine palmitoyltransferase I. Genomics 2002;80:433–42.
[12] Sierra AY, Gratacos E, Carrasco P, Clotet J, Urena J, Serra D, et al. CPT1c is localized in endoplasmic reticulum of neurons and has carnitine palmitoyltransferase activity. J Biol Chem 2008;283:6878–85.
[13] Morillas M, Gomez-Puertas P, Bentebibel A, Selles E, Casals N, Valencia A, et al. Identification of conserved amino acid residues in rat liver carnitine palmitoyltransferase I critical for malonyl-CoA inhibition. Mutation of methionine 593 abolishes malonyl-CoA inhibition. J Biol Chem 2003;278:9058–63.
[14] Cordente AG, Lopez-Vinas E, Vazquez MI, Swiegers JH, Pretorius IS, Gomez-Puertas P, et al. Redesign of carnitine acetyltransferase specificity by protein engineering. J Biol Chem 2004;279:33899–908.
[15] Cordente AG, Lopez-Vinas E, Vazquez MI, Gomez-Puertas P, Asins G, Serra D, et al. Mutagenesis of specific amino acids converts carnitine acetyltransferase into carnitine palmitoyltransferase. Biochemistry 2006;45:6133–41.
[16] Nicot C, Napal L, Relat J, Gonzalez S, Llebaria A, Woldegiorgis G, et al. C75 activates malonyl-CoA sensitive and insensitive components of the CPT system. Biochem Biophys Res Commun 2004;325:660–4.
[17] Aja S, Bi S, Knipp SB, McFadden JM, Ronnett GV, Kuhajda FP, et al. Intracerebroventricular C75 decreases meal frequency and reduces AgRP gene expression in rats. Am J Physiol Regul Integr Comp Physiol 2006;291:R148–54.
[18] Aja S, Landree LE, Kleman AM, Medghalchi SM, Vadlamudi A, McFadden JM, et al. Pharmacological stimulation of brain carnitine palmitoyl-transferase-1 decreases food intake and body weight. Am J Physiol Regul Integr Comp Physiol 2008;294:R352–61.
[19] Bentebibel A, Sebastian D, Herrero L, Lopez-Vinas E, Serra D, Asins G, et al. Novel effect of C75 on carnitine palmitoyltransferase I activity and palmitate oxidation. Biochemistry 2006;45:4339–50.
[20] Lopez M, Lelliott CJ, Tovar S, Kimber W, Gallego R, Virtue S, et al. Tamoxifen-induced anorexia is associated with fatty acid synthase inhibition in the ventromedial nucleus of the hypothalamus and accumulation of malonyl-CoA. Diabetes 2006;55:1327–36.
[21] Golovko MY, Murphy EJ. An improved method for tissue long-chain acyl-CoA extraction and analysis. J Lipid Res 2004;45:1777–82.
[22] Zierz S, Engel AG. Different sites of inhibition of carnitine palmitoyltransferase by malonyl-CoA, and by acetyl-CoA and CoA, in human skeletal muscle. Biochem J 1987;245:205–9.
[23] Hassett RP, Crockett EL. Endpoint fluorometric assays for determining activities of carnitine palmitoyltransferase and citrate synthase. Anal Biochem 2000;287:176–9.
[24] Morillas M, Gomez-Puertas P, Roca R, Serra D, Asins G, Valencia A, et al. Structural model of the catalytic core of carnitine palmitoyltransferase I and carnitine octanoyltransferase (COT): mutation of CPT I histidine 473 and alanine 381 and COT alanine 238 impairs the catalytic activity. J Biol Chem 2001;276:45001–8.
[25] Swiegers JH, Dippenaar N, Pretorius IS, Bauer FF. Carnitine-dependent metabolic activities in Saccharomyces cerevisiae: three carnitine acetyltransferases are essential in a carnitine-dependent strain. Yeast 2001;18:585–95.
[26] Rickwood D, Graham JM. Subcellular fractionation: a practical approach. Oxford: IRL Press at Oxford University Press; 1997.
[27] Wu D, Govindasamy L, Lian W, Gu Y, Kukar T, Agbandje-McKenna M, et al. Structure of human carnitine acetyltransferase. Molecular basis for fatty acyl transfer. J Biol Chem 2003;278:13159–65.
[28] Jogl G, Tong L. Crystal structure of carnitine acetyltransferase and implications for the catalytic mechanism and fatty acid transport. Cell 2003;112:113–22.
[29] Jogl G, Hsiao YS, Tong L. Crystal structure of mouse carnitine octanoyltransferase and molecular determinants of substrate selectivity. J Biol Chem 2005;280:738–44.
[30] Hsiao YS, Jogl G, Esser V, Tong L. Crystal structure of rat carnitine palmitoyltransferase II (CPT-II). Biochem Biophys Res Commun 2006;346:974–80.
[31] Morillas M, Lopez VE, Valencia A, Serra D, Gomez-Puertas P, Hegardt FG, et al. Structural model of carnitine palmitoyltransferase I based on the carnitine acetyltransferase crystal. Biochem J 2004;379:777–84.
[32] Lopez-Vinas E, Bentebibel A, Gurunathan C, Morillas M, de Arriaga D, Serra D, et al. Definition by functional and structural analysis of two malonyl-CoA sites in carnitine palmitoyltransferase 1A. J Biol Chem 2007;282:18212–24.
[33] Hooft RW, Vriend G, Sander C, Abola EE. Errors in protein structures. Nature 1996;381:272.
[34] Vriend G. WHAT IF: a molecular modeling and drug design program. J Mol Graph 1990;8:52–6. 29.

Please cite this article in press as: Mera P, et al. C75 is converted to C75-CoA in the hypothalamus, where it inhibits carnitine palmitoyltransferase 1 and decreases food intake and body weight. Biochem Pharmacol (2009), doi:10.1016/j.bcp.2008.11.020

[35] Goodsell DS, Morris GM, Olson AJ. Automated docking of flexible ligands: applications of AutoDock. J Mol Recognit 1996;9:1–5.
[36] Guex N, Peitsch MC. SWISS-MODEL and the Swiss-PdbViewer: an environment for comparative protein modeling. Electrophoresis 1997;18:2714–23.
[37] d'Ordine R, Paneth P, Anderson VE. 13C NMR and 1H-1H NOEs of Coenzyme-A: conformation of the pantoic acid moiety. Bioorg Chem 1995;23:169–81.
[38] Amador M, Ariza X, García J. A versatile stereoselective approach to paraconic acids. Heterocycles 2006;705–20.
[39] Ariza X, García J, López M, Montserrat L. A concise synthesis of (-)-methylenoactocin and (-)-phaseolinic acid from (6S,9S)-tetradec-7-yne-6,9-diol. Synlett 2001;120–2.
[40] Shimokawa T, Kumar MV, Lane MD. Effect of a fatty acid synthase inhibitor on food intake and expression of hypothalamic neuropeptides. Proc Natl Acad Sci USA 2002;99:66–71.
[41] Lane MD, Wolfgang M, Cha SH, Dai Y. Regulation of food intake and energy expenditure by hypothalamic malonyl-CoA. Int J Obes (Lond) 2008;32(Suppl. 4):S49–54.
[42] Kuhajda FP, Landree LE, Ronnett GV. The connections between C75 and obesity drug-target pathways. Trends Pharmacol Sci 2005;26:541–4.
[43] Weis BC, Cowan AT, Brown N, Foster DW, McGarry JD. Use of a selective inhibitor of liver carnitine palmitoyltransferase I (CPT I) allows quantification of its contribution to total CPT I activity in rat heart. Evidence that the dominant cardiac CPT I isoform is identical to the skeletal muscle enzyme. J Biol Chem 1994;269:26443–8.
[44] Declercq PE, Falck JR, Kuwajima M, Tyminski H, Foster DW, McGarry JD. Characterization of the mitochondrial carnitine palmitoyltransferase enzyme system. I. Use of inhibitors. J Biol Chem 1987;262:9812–21.
[45] McGarry JD, Mills SE, Long CS, Foster DW. Observations on the affinity for carnitine, and malonyl-CoA sensitivity, of carnitine palmitoyltransferase I in animal and human tissues. Demonstration of the presence of malonyl-CoA in non-hepatic tissues of the rat. Biochem J 1983;214:21–8.
[46] Bird MI, Saggerson ED. Interacting effects of L-carnitine and malonyl-CoA on rat liver carnitine palmitoyltransferase. Biochem J 1985;230:161–7.
[47] Cook GA, Mynatt RL, Kashfi K. Yonetani-Theorell analysis of hepatic carnitine palmitoyltransferase-I inhibition indicates two distinct inhibitory binding sites. J Biol Chem 1994;269:8803–7.
[48] Kashfi K, Mynatt RL, Cook GA. Hepatic carnitine palmitoyltransferase-I has two independent inhibitory binding sites for regulation of fatty acid oxidation. Biochim Biophys Acta 1994;1212:245–52.
[49] Lopez M, Lage R, Saha AK, Perez-Tilve D, Vazquez MJ, Varela L, et al. Hypothalamic fatty acid metabolism mediates the orexigenic action of ghrelin. Cell Metab 2008;7:389–99.

Please cite this article in press as: Mera P, et al. C75 is converted to C75-CoA in the hypothalamus, where it inhibits carnitine palmitoyltransferase 1 and decreases food intake and body weight. Biochem Pharmacol (2009), doi:10.1016/j.bcp.2008.11.020